The influence of *BCL6* on the *WNT* pathway in glioblastoma therapy resistance

By

Rosemary Margaret Alice Gordon-Schneider

A thesis submitted to the Victoria University of Wellington in fulfilment of the requirements for the degree of Master of Cell and Molecular bioscience

Supervisor: Melanie McConnell

Victoria University of Wellington

2018

Abstract

Glioblastoma is a devastating disease with a median survival of 18 months from diagnosis and a 5 years survival rate of only 10%. The gold standard of treatment for glioblastoma is surgical resection followed by chemotherapeutic treatment with Temozolomide, a DNA alkylating agent, and irradiation around the remaining tumour margins. These treatments are both designed to create DNA damage to the cancerous cells, causing the cell cycle to halt, and result in apoptosis. This treatment does extend patients life for a few months, however glioblastoma cells quickly become resistant to therapy, and disease is always fatal. The anti-apoptotic protein *BCL6*, confers resistance to apoptosis in response to DNA damage and has been shown to be upregulated in Glioblastoma in response to DNA damaging chemotherapy and irradiation. This upregulation has been hypothesised to increase resistance to these therapies. By minimizing resistance to the standard therapies, the outlook for sufferers of glioblastoma could be greatly improved. Dysregulation of the *WNT* pathway has also been shown to be very important in carcinogenesis of glioblastoma and is responsible for the diffuse nature of the tumour which makes total resection nearly impossible. An RNA-seq screen was carried out on a glioblastoma cell line in which *BCL6* was inhibited using the small molecule inhibitor FX1. This resulted in a change in expression of a large number of *WNT* related genes. This indicates that there is a link between *BCL6* and the *WNT* pathway. Changes in expression in the *WNT* genes *DKK1, WNT5a* and *WNT5b* were validated. Experiments were carried out to investigate the effects of chemotherapy and *BCL6* inhibition on both the canonical and non-canonical *WNT* pathways. It was found that *BCL6* has an influence of the level of activity of the canonical *WNT* pathway. It also influences migration, the cell cycle, and clonogenicity. Understanding this link between *WNT* and *BCL6* could be crucial in finding an effective treatment for glioblastoma.

Acknowledgements

Firstly, I'd like to thank my amazing supervisor, Melanie McConnell. You have been so great every step of the way from helping me troubleshoot experiments, to telling me that actually, I am doing a good job even though it might not feel like it. Thank you so much Melanie, without you, this would have been a much more stressful, much less rewarding experience.

I'd like to thank my nearly husband Remy. It has been a stressful time for you too and you've done an amazing job with putting up with me, making sure I have food, calming me down when I'm feeling anxious, reminding me that I can do it. I love you and I'm so glad that I get to keep you.

Dini, thank you so much for helping me with my data, helping me calm down when I'm freaking out, babysitting Tato, fixing Microsoft word when it crashed 2 days before my hand-in, and just being a really great friend. You're the best.

Mum and Dad, thank you for making me. You did a good job… Also, thanks for supporting me through this, financially and emotionally. You are the best parents ever and I feel so lucky to have you.

Christina, thanks for being such a great sister. You are the other half of me and you always get it.

Jeff, you have read every section and made sure I didn't sound completely stupid. I owe you big time!

Potato – Best. Cat. Ever.

Finally, thanks to everyone on AM level 3 who has helped me and been my friend. Calvey, Vim, Matt, Georgia, Rory, Phoebe, Katharina, Nikki, and everyone else.

Table of contents

Table of figures

List of Abbreviations

Amp	Ampicillin
BCL6	B-Cell Lymphoma 6
BSA	Bovine Serum Albumin
CI	Combination Index
CSC	Cancer Stem Cell
DAPI	4',6-diamidino-2-phenylindole
DLBCL	Diffuse Large B Cell Lymphoma
DMF	Dimethylformamide
DMSO	Dimethyl Sulfoxide
Dox	Doxorubicin
FCS	Foetal Calf Serum
FSC	Forward Scatter
GBM	Glioblastoma

GC	Germinal Centre
GFP	Green Fluorescent Protein
GSC	Glioblastoma Stem Cell
HRP	Horse Radish Protein
LB	Luria Broth
LT Dox	Long Term treatment with Doxorubicin
LT TMZ	Long Term treatment with Temozolomide
MMc	McConnell Lab group
PBS	Phosphate Buffered Saline
PBS-T	Phosphate Buffered Saline with Tween20
PCP	Planar Cell Polarity pathway
Puro	Puromycin
qRT-PCR	Quantitative Reverse Transcriptase Polymerase Chain Reaction
RNA-seq	RNA- sequencing
ROS	Reactive Oxygen Species

RPMI	Roswell Park Memorial Institute Medium 1640
SSC	Side Scatter
TC	Tissue Culture
TCGA	The Cancer Genome Atlas
TMZ	Temozolomide
WHO	World Health Organisation

1. Introduction

Glial cells

1.1.1. Glial cells

Glial cells are a type of brain cells, however the complete function of these cells has not been fully elucidated. A known function of glial cells is as a type of structural glue to hold the brain together. The word glia translates directly from ancient Greek to mean glue (García-Martín, Majewska, Guizzetti, Jäkel, & Dimou, 2017). These 'glue cells' make up approximately half of all cells in the brain (von Bartheld, Bahney, & Herculano-Houzel, 2016). Glial cells are highly heterogenous, with four different subsets: microglia, astrocytes, oligodendrocytes, and NG2-glia. Astrocytes make up the majority of the glial cell population and support neuronal function, whereas Oligodendrocytes regulate myelination and Microglia are the macrophages of the CNS (García-Martín et al., 2017).

Glioma

1.1.2.

Glioma are characterised by their likeness to, and origin from glial cells. Glioma can arise from any of the glial cell subtypes and due to this, and the wide variety of mutations that can result in the change from glial cell to glioma, they are very heterogenous both within and between tumours (Alcantara Llaguno & Parada, 2016). Glioma are characterised and graded by histological analysis. Low grade lesions (World Health Organisation (WHO) grades I and II) and high grade malignancies (WHO grade III and IV) are characterised by histological features including necrosis, pleiomorphic cells, abundant mitoses, and microvascular proliferation (Wen & Kesari, 2008). Grade IV, the most aggressive which has the poorest prognosis, is also known as Glioblastoma.

1.1.Glioblastoma

Glioblastoma multiforme (GBM) is the most common and malignant type of brain cancer making up 15% of all intercranial neoplasms. Glioblastoma is classified as a WHO grade IV glioma. Lower grade gliomas generally progress to a grade IV glioblastoma within 5-10 years (Zong, Verhaak, & Canoll, 2012). The average age at diagnosis of GBM is 64 years, however most tumours occur in people from 45 to 75 years (Stupp et al., 2005). The median survival for patients with GBM is 1 year from diagnosis, with the 5-year survival rate at 10% with treatment, however expected survival without treatment is a little as 3 months (Ramirez, Weatherbee, Wheelhouse, & Ross, 2013). This dismal life expectancy is largely due to the aggressive nature of GBM and the resistance of GBM to current treatments (Stupp et al., 2005). Glioblastoma presents as a solid tumour with highly diffuse borders. It is genetically heterogenous within and between tumours and can arise from a range of cell types such as neural stem cells, glial progenitor cells, or astrocytes (Zong et al., 2012). The heterogenous nature and quick resistance to treatment makes glioblastoma a difficult cancer to treat (Stupp et al., 2005). An effective treatment is desperately needed to increase the life expectancy and quality of life for people suffering from this devastating disease.

Glioblastoma subtypes

Commonly mutated genes have been discovered through analyses of human GBM samples by the Cancer Genome Atlas Research Network (TCGA). The most frequently mutated oncogenes and tumour suppressors are TP53, PIK3CA, PIK13R1 NF1, PTEN, RB1, EGFR, and RTK (TCGA, 2008). Mutations in these genes cause gene expression changes, copy number changes, or changes in DNA sequence. These pathways regulate the cell cycle, senescence, apoptosis, and proliferation all of which are important in GBM (Brennan et al., 2013). There are two common modifications associated with survival outcomes, the first of which is methylation of the O6-methyl-guanyl-methyl-transferase (MGMT) promoter. MGMT repairs O^6-methylguanine lesions caused by Temozolomide and therefore methylation of the promoter results in a decrease in repair of temozolomide induced lesions and a decrease in survival outcomes. The second modification is one in the isocitrate dehydrogenase-1 (IDH-1) gene. Mutation of this gene is associated with increased survival outcomes, however the mechanism for this is unknown (Combs et al., 2011).

Glioblastoma that develop *de novo* are classified as primary GBM, whereas tumours from a pre-existing lower grade glioma are secondary GBM. There are four glioma subtypes, classical, mesenchymal, neural, and proneural. Classical tumours have high levels of epidermal growth factor receptor (EGFR). Mesenchymal tumours have mutations in NF1, a tumour suppressor gene; PTEN and TP53 . Neural tumours have similar patterns of mutations to the other subgroups, however also express markers that are normal for neuronal cells such as NEFL, GABRA1, SYT1 and SLC12A5 (Verhaak et al., 2010). Proneural tumours are characterised by mutations in the *IDH1* and *PDGFRA* genes. *G-CIMP*$^+$ is also characteristic of this tumour subtype, however patients with this mutation generally have a survival advantage (Brennan et al., 2013). This subtyping is useful for predicting patient outcomes however it is still difficult to accurately predict outcomes with this method due to high levels of heterogeneity within tumours (Sottoriva et al., 2013).

1.1.2. Invasion

One of the characteristics of glioblastoma is diffuse borders due to the invasive nature of the GBM cells. This diffuse nature is due to the high levels of invasion of the cancerous GBM into neighbouring healthy brain tissues. Recurrence generally happens within 1-2 cm of the resection border (Hou, Veeravagu, Hsu, & Tse, 2006). The GBM cells lose polarity and adhesion; they also gain mobility and the ability to degrade the surrounding extracellular matrix (ECM), and gain a stem-cell like phenotype. These factors all contribute to the ability of a GBM cell to migrate into the space around pre-existing blood vessels, and into the space between neurons and glial cells in the brain parenchyma (Biasoli et al., 2014; Claes, Idema, & Wesseling, 2007). These invasive properties of GBM are key in recurrence after treatment (Paw, Carpenter, Watabe, Debinski, & Lo, 2015).

1.1.3. Management/treatment

First-line treatment involves surgical debulking of the tumour, followed by radiotherapy and chemotherapy generally using Temozolomide (TMZ) (Stupp et al., 2005). This method is often ineffective due to the invasive nature of GBM. The indistinct borders of the tumours make it near impossible to resect all the tumour cells without damaging the healthy brain tissue in the surrounding area. The remaining tumour is then treated with DNA damaging therapies, resulting in a short extension of life. Glioblastoma resistance to treatment and reoccurrence happens rapidly, leading to glioblastoma always being fatal (Lefranc et al., 2006).

Temozolomide

Temozolomide (5-Monomethyltriazenoimidazole-4-carboxamide) is a small lipophilic molecule, which acts as an alkylating agent that inhibits DNA synthesis by adding methyl groups to guanidine residues thereby crosslinking adjacent DNA strands (Agarwala & Kirkwood, 2000). TMZ is the first line chemotherapy drug used to treat many cancers including glioma and metastatic melanoma. TMZ can penetrate into all tissues including passing the blood brain barrier (H. S. Friedman, Kerby, & Calvert, 2000; J. Zhang, FG Stevens, & D Bradshaw, 2012). TMZ is administered as a prodrug that is stable in the low pH of the stomach and is lipophilic allowing it to exit the stomach and enter the blood vessels. Once in the blood vessels it is then activated by conversion to imidazole-4-carboxamide (MTIC), which spontaneously breaks down to the methyldiazonium ion at physiological pH. TMZ does not require enzymatic conversion for activation and has 100% bioavailability in a physiological system (Agarwala & Kirkwood, 2000).

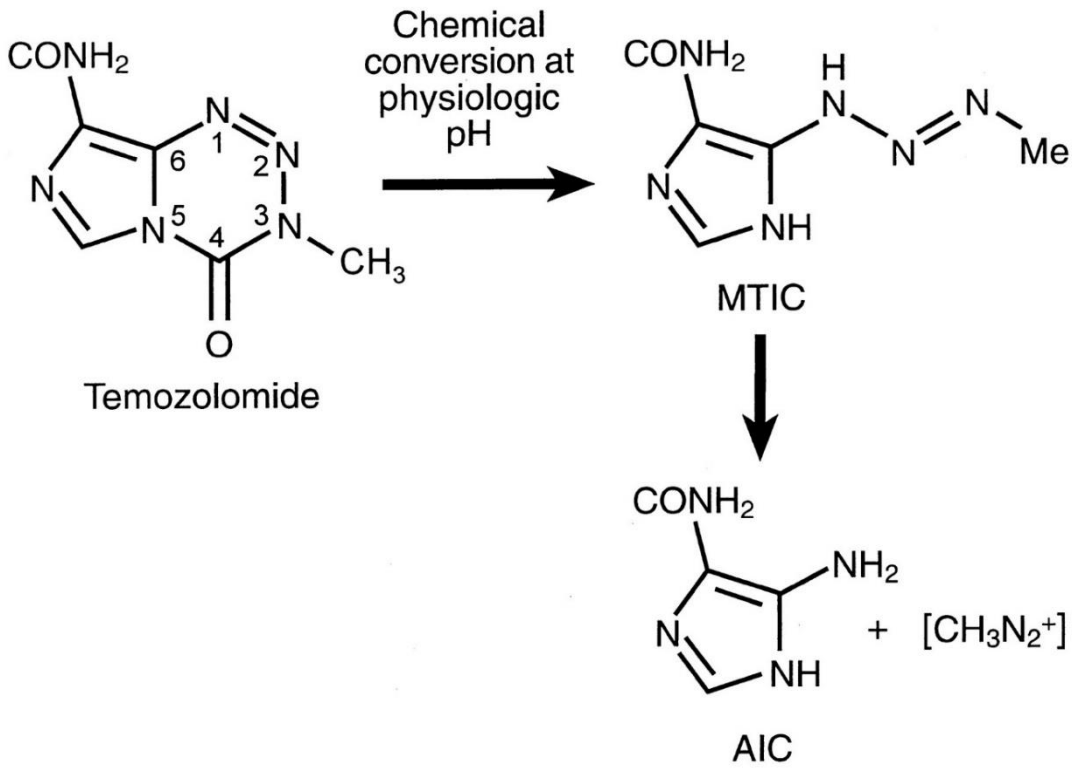

Figure 1 Temozolomide structure and conversion. Temozolomide conversion from inactive prodrug to active form, MTIC, then methyldiazonium ion at physiological pH. Figure adapted with publisher's permission (Agarwala & Kirkwood, 2000).

1.1.5. Doxorubicin

Over-coming the blood brain barrier (BBB) is one of the greatest challenges in finding new and effective treatments for GBM. While TMZ can cross the blood brain barrier, it does not completely eradicate GBM cells from the brain.

Doxorubicin (Dox) is an anthracycline chemotherapeutic used in the treatment of many cancers such as bladder, breast, lung, stomach, and ovarian. Dox has been shown to be very effective at treating GBM cells *in vitro* and *in vivo* using localized delivery methods (Lesniak, Upadhyay, Goodwin, Tyler, & Brem, 2005). Doxorubicin has two anti-tumourigenic functions: disrupts DNA synthesis and increases production of reactive oxygen species. In the former, Dox intercalates into DNA and affects topisomerase II activity by inhibting its ability to reseal unwound DNA after a double stranded break. This results in many double stranded breaks (DSBs) all along the chromosome, which lead to apoptosis of the cell (Thorn et al., 2011). In the latter anti-tumourigenic function, Dox increases the production of mitochondrial reactive oxygen species (ROS). Mitochondrial NADH-dehydrogenase reduces Dox to produce an unstable semiquinone. The semiquinone then donates an electron to oxygen forming of a superoxide radical (Davies & Doroshow, 1986). This leads to damage of DNA, proteins, and cell membranes (Thorn et al., 2011). Although Dox has been shown to be an effective chemotherapeutic, it cannot be used in the treatment of GBM. Dox is unable to pass the BBB rendering it useless in the fight against GBM in its current form (Zou et al., 2017). Considerable efforts are being made to aid the entry of Dox into the brain. Dox conjugation to short naturally derived vectors, D-penetratin or SynB1 increases Dox transport into the brain by 20% (Rousselle et al., 2000). Pre-treatment with morphine or ondansetron increases permeability of the BBB to Dox significantly (Sardi et al., 2013, 2014) The application of doxorubicin-loaded monosialoganglioside micelles can effectively penetrate the BBB (Zou et al., 2017). The development of these methods or others could result in a greater extension of life in GBM patients than current treatments can accommodate.

1.1.6. DNA Damage response

DNA damage happens to most of our cells every day, and the cells must repair this damage, or apoptose for the organism to remain functional. DNA damage can occur endogenously when a topoisomerase does not function correctly, or due to mitochondrially released ROS. DNA damage also occurs due to external factors such as UV radiation, ROS produced by inflammation, or carcinogenic chemicals. The cell requires a way to repair this damage, so it can continue to survive and pass on the correct genetic information. The DNA damage response (DDR) is a collection of mechanisms used to detect, signal the presence of, and repair DNA lesions (Jackson & Bartek, 2009). During the cell cycle, checkpoints test for DNA damage and halt the cell cycle to allow repairs to take place. DNA damage is sensed by the ataxia-telangiectasia mutated (ATM), ATM- and Rad3-Related (ATR) and DNA-dependent protein kinase (DNA-PKcs) kinases (Ray, Blevins, Wani, & Wani, 2016). These kinases regulate many proteins involved in the DDR. There are several mechanisms activated by these kinases directly and indirectly, which respond to the signal and initiate repair. Each kinase is suited to a different kind of DNA damage including mismatch repair (MMR), base excision repair (BER), single stranded break repair (SSBR), nucleotide excision repair (NER), and double stranded break repair (DSBR), which has two types – homologous, and non-homologous end joining (HEJ and NHEJ) (Maréchal & Zou, 2013). These mechanisms are essential to maintain genetic integrity and minimizing the mutation rate within cells.

1.1.7. Cancer stem cells

Cancer stem cells are tumour cells that have a stem cell phenotype and express stem cell markers. These cells have enhanced DNA repair and unlimited proliferatory potential, and can both self renew, and differentiate. This means that they are able to form new tumours when implanted into mouse models (Liebelt et al., 2016). Glioma derived stem cells (GSCs) have increased chemo- and radio- resistance compared to normal cells and are thought to be responsible for GBM recurrence (Bao et al., 2006). These cells have been found in high numbers inside GBM tumours, but also on the periphery of these tumours migrating into neighbouring tissues (Munthe et al., 2016). Peripheral GSCs are unlikely to be removed by surgical resection due to their invasion into the neighbouring healthy brain tissue and are therefore a recurrence waiting to happen (Bao et al., 2006; Lathia, Mack, Mulkearns-Hubert, Valentim, & Rich, n.d.; Stupp et al., 2005).

1.1.8. Resistance to treatment

The current therapies for the tumour borders post-resection are Temozolomide, and irradiation. These are both designed to result in severe DNA damage causing apoptosis of the remaining tumour cells. Resistance to these treatments in GBM is rapid, resulting in relapse of the tumour. Resistant cells show stem-like properties (Osuka & Meir, 2017). Due to the invasive nature of GBM, resection cannot remove all of the tumour cells without removing too much brain tissue. The presence of treatment resistant GBM stem cells in the periphery of the tumour (GSCs) means that further treatment with chemotherapy and radiation is ineffective at killing all of the cancerous cells (Munthe et al., 2016; Stupp et al., 2005). These remaining cells can proliferate and result in fast regrowth of the tumour. Discovering what pathways are involved in the resistance of GSCs to these treatments and targeting that pathway may result in better patient outcomes (Osuka & Meir, 2017; Ramirez et al., 2013).

1.2. The *WNT* pathway

The *WNT* family cysteine rich glycoproteins that are essential in many aspects of cell function, including cell proliferation, homeostasis, movement, polarity, and embryonic fate determination. *WNT* proteins are homologs of the wingless family of proteins in drosophila and the mom genes in C. elegans. *WNT*s are highly conserved and can be found in all metazoan animals (Schubert & Holland, 2013). *WNT*s are cysteine rich proteins approximately 350-400 amino acids in length with a signal secretion peptide at the N-terminal (Proffitt & Virshup, 2012). There are 19 known *WNT* proteins, which upon binding result in different cascades and outcomes within the cell (Logan & Nusse, 2004). There are three known signalling pathways that *WNT* genes are involved in: the canonical *WNT* pathway (β-catenin dependent) which regulates gene expression, and two non-canonical pathways: the planar cell polarity pathway (PCP pathway) which regulates cytoskeletal rearrangements; and the *WNT*/Ca^{2+} pathway for regulating Ca^{2+} levels within the cell (Komiya & Habas, 2008).

1.2.1. *WNT*-beta catenin pathway

The β-catenin dependent *WNT* pathway, also known as the canonical *WNT* pathway is the most well documented of the *WNT* pathways and is involved in many different processes within the cell. The canonical *WNT* pathway acts through the destruction or accumulation of β-catenin (Figure 2). When the *WNT* pathway is 'off', the β-catenin protein is bound by protein complex containing Axin, adenomatous polyposis coli (APC), casein kinase 1α (CK1α), and glycogen synthase kinase 3 (GSK3) (Zhang et al. 2012). This complex allows phosphorylation of β-catenin targeting it for ubiquitination followed by breakdown by the proteasome. The *WNT* pathway is turned 'on' upon binding of extracellular *WNT* proteins to the extracellular N-terminal of the Frizzled (Fz) receptor, a 7-transmembrane spanning protein. *WNT* also binds low-density-lipoprotein-related protein 5/6 (LRP5/6). Once these two proteins have bound *WNT*, Axin is recruited to the membrane and binds the cytoplasmic tail of LRP5/6. This binding

is catalysed by phosphorylation of LRP5/6 by either CK1α or GSK3 (Macdonald et al. 2010). The Dishevelled protein (Dsh) is then activated by binding the cytoplasmic tail of Fz and phosphorylation by CK1, CK2, metastasis associated kinase, protein kinase C, and Par1. Dsh once activated prevents the degradation of β-catenin, which then builds up in the cytoplasm. Accumulation of β-catenin in the cytoplasm induces translocation of this protein into the nucleus. In the nucleus β-catenin acts as a co-activator of transcription by binding TCF/LEF, which then turns on transcription of the *WNT* pathway activated genes (Komiya & Habas, 2008; Macdonald, Tamai, & He, 2010). Genes regulated by this pathway are known to be involved in cell fate in embryonic development, cell proliferation, cell polarity, and adult cell homeostasis. Dysregulation of this pathway can result in congenital malformations, cancer and osteoporosis (Macdonald et al., 2010).

1.2.2. The β-catenin independent *WNT* pathways

The β-catenin independent arms of the *WNT* pathway are not as well studied and understood as the β-catenin dependent arm but are still important in the contribution of the *WNT* pathway

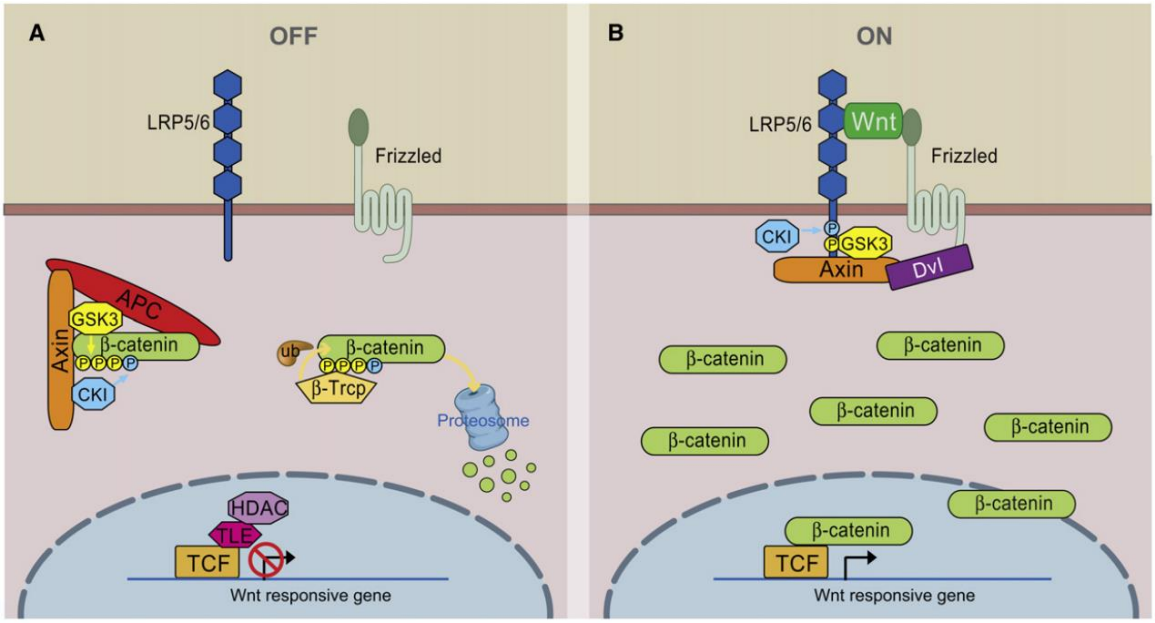

Figure 2 The canonical Wnt pathway. (Macdonald et al., 2010)

to GBM.

The planar cell polarity pathway (PCP) functions by the binding of *WNT* to FZ and either receptor tyrosine kinase-like orphan receptor (ROR), related-to-tyrosine-kinase (RYK), or protein tyrosine kinase 7 (PTK7) coreceptors. The *WNT*/Fz complex is then internalised resulting in activation of GTPases Rho and Rac, c-jun-n-terminal kinase (JNK), and Rho-kinase (ROCK). This results in the control of cell motility and cell polarity (Vladar, Antic, & Axelrod, 2009).

The Ca^{2+} pathway is also β-catenin independent. *WNT* binds Fz and coreceptor ROR1/2. Dvl binds the cytoplasmic tail of Fz, then forms a complex with Axin and GSK3. This complex phosphorylates ROR1/2 which acts on phospholipase C (PLC). PLC acts on membrane bound phospholipid, phosphatidyl inositol 4,5-biphosphaste resulting in the production of inositol-triphosphate (IP_3) and DAG. IP_3 releases Ca^{2+} from the endoplasmic reticulum (ER). This increase in cytoplasmic Ca^{2+} concentration activates DAG, which in turn activates protein kinase C (PKC). PKC activates nuclear factor kappa-light-chain-enhancer of activated B cells (NFκB) and cAMP response element-binding protein (CREB) which translocate to the nucleus and activate transcription (De, 2011). These pathways are important in regulation of cell functions and activation of each is decided by the binding of specific *WNT* proteins.

PORCN

PORCN is an essential protein for *WNT* pathway function. PORCN is a membrane bound o-acyltransferase on the ER. It is responsible for the palmitoylation of *WNT* proteins and their export out of the ER. Without this function, *WNT* proteins would be unable to leave the ER and the *WNT* pathway would be unable to function. Embryonic PORCN deficiency has been shown to result in a disease called focal dermal hypoplasia, which is an X-linked dominant disease characterised by abnormal development of ecto- and mesodermal tissues (Grzeschik et al., 2007). IWP-2 is a small molecule inhibitor of *WNT* designed to stop the production of the *WNT* protein through the inhibition of PORCN (Chen, 2009). IWP-2 has been successfully used in many studies to inhibit the *WNT* pathway (Chai et al., 2012; Chen et al., n.d.; Hao et al., 2012).

1.2.4. *WNT* in the cell cycle

It is well known that the canonical *WNT* pathway regulates the expression of genes involved in proliferation including C-myc and cyclin D (Davidson, 2010; Komiya & Habas, 2008). However, a new link between the *WNT* pathway and the cell cycle has been discovered. The mitotic CDK14/cyclin Y complex phosphorylates LRP6 and promotes canonical *WNT* signalling (Davidson et al., 2009; D. Liu, Guest, & Finley, n.d.; Mao et al., 2001). The CDK14/cyclin Y complex is involved in the G2/M phase of the cell cycle (D. Liu et al., n.d.).

β-catenin is essential for centromere separation during mitosis (Bahmanyar et al., 2008) and levels have been discovered to cycle with the cell cycle, peaking during the G2/M phase (Olmeda, Castel, Vilaró, & Cano, 2003). Canonical *WNT* activation has also been shown to cycle along with β-catenin through the use of a *WNT* reporter assay (Figure 3) (Davidson & Niehrs, 2010). The interactions between the *WNT* pathway and the cell cycle are yet to be fully understood but from the information we do have, it can be concluded that the relationship between the two is a complex one.

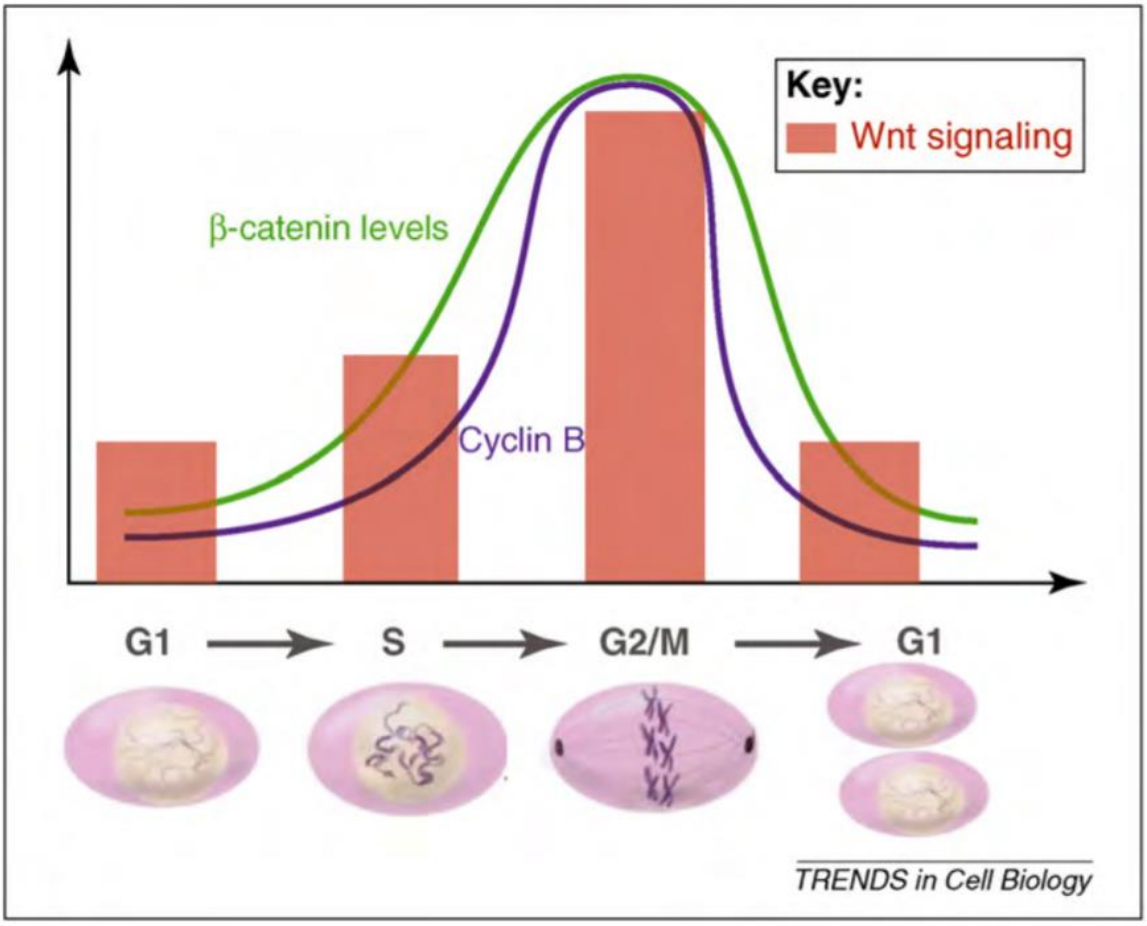

Figure 3 β-catenin levels, canonical WNT activation, and cyclin B levels all oscillate in time with the cell cycle. Figure reproduced with permission of the publisher. (Davidson, 2010)

1.2.5. *WNT* in GBM

The *WNT* pathway plays a crucial role in proliferation, death, migration, and cell fate decision. (Y. Lee, Lee, Ahn, Lee, & Nam, 2016). Many studies have suggested that this dysregulation of *WNT* and promotion of stemness promotes GBM growth and invasiveness (Y. Liu et al., 2012; Pulvirenti et al., 2011; Reya & Clevers, 2005; J. Wang, Ma, & Cooper, 2013; K. Zhang, Zhang, Han, Pu, & Kang, 2012). Mutations in APC–a, the negative regulator of canonical *WNT*, leading to the hyperactivation of this pathway are common. Mutations in β-catenin, APC, and AXIN1 have also been identified as processes leading to cancerous phenotypes (Bowman & Nusse, 2011). Dickkopf (DKK) acts as an endogenous inhibitor of *WNT* signalling, and when epigenetically deactivated, can no longer regulate *WNT* activation (Foltz et al., 2010). Many other *WNT* inhibitor genes have been found to have epigenetic silencing in gliomas (Anastas & Moon, 2013). *DKK1* hypermethylation is found in 50% of secondary GBM (Foltz et al., 2010). These aberrant changes in *WNT* signalling ultimately lead to the gain of tumourigenic properties and allow GBM to continue to grow and migrate in an unregulated manner. This makes the *WNT* pathway a highly promising target for therapeutic interventions (Reya & Clevers, 2005).

1.3. B-cell lymphoma 6

BCL6 is a zinc finger transcription factor. It is a dimeric protein with an N-terminal BTB/POZ domain which binds co-repressors essential for it to function as a transcriptional repressor including BCoR, SMRT, and NCoR. The C-terminal has zinc finger domains allowing for DNA binding. This terminal domain binds HDACs and ETO proteins. The N-terminal functions in proliferation, survival, and DNA damage checkpoints (Cardenas et al., 2017; Miles, Crockett, Lim, & Elenitoba-Johnson, 2005). Targeting this N-terminal would inhibit *BCL6* from carrying out these functions that are important in carcinogenesis (Cardenas et al. 2016).

B cell lymphoma 6 (*BCL6*) is normally expressed in developing B and T cells and protects the cells from DNA-damage induced apoptosis during maturation. In these immune cells, *BCL6* is essential for pre-B-cell self-renewal and for establishing the polyclonal B cell repertoire (Katia Basso & Dalla-Favera, 2012; Duy et al., 2010; Toyama et al., 2002). *BCL6* is a transcriptional repressor that targets many genes, including DNA-damage-sensing genes (i.e. ATR, TP53, ARF) and cell cycle checkpoint genes (i.e. PTEN and some CDK genes) (Hatzi & Melnick, 2014). *BCL6* is aberrantly expressed in a variety of cancers such as diffuse large B cell lymphoma (DLBCL), breast cancer, leukaemia, colorectal cancer and gastric cancer. *BCL6* is upregulated in glioma and as a prognostic marker, predicts poor patient outcomes. Expression of *BCL6* is essential in the viability of GBM cells and the inhibition of *BCL6* causes loss of malignancy and senescence (Xu et al., 2017). Treatment with DNA damaging chemotherapeutics further upregulates *BCL6* expression which could result in more aggressive resistance to treatment, and reoccurrence (Fabre et al. 2017).

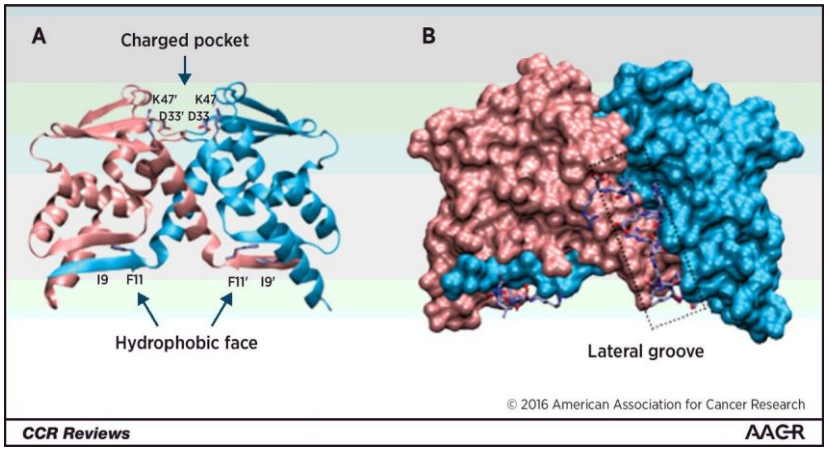

Figure 4 Structure of the BCL6 protein (A). BCL6 is a protein dimer. The BCL6 small molecule inhibitor, FX1 targets the BTB/POZ domain in the lateral groove shown above (B). Figure reproduced with permission of the publisher (Cardenas et al., 2017).

An *in silico* functional group mapping approach (SILCS) was used to map important binding sites on the *BCL6* protein and design small molecule inhibitors with a higher affinity to these binding sites than their endogenous co-repressors. FX1 was shown to have a 10-fold higher binding affinity for an essential region of the lateral groove of *BCL6*, the BTB/POZ binding

domain than any endogenous co-repressor and treatment with FX1 caused regression of DLBCL in mice (Cardenas et al., 2016).

BCL6 has been shown to regulate cell cycle arrest, apoptosis, differentiation and activation in B-cells. Literature directly linking *BCL6* and the *WNT* pathway is sparse however there are many genes that have been identified as targets of *BCL6* that are involved in the *WNT* pathway (K Basso, 2009).

1.3.1. Investigating the influence of *BCL6* on the *WNT* pathway in the survival of Glioblastoma

Glioblastoma is a horrendous disease with a mortality rate of 100%. There are many different mutations that can contribute to the development and tumourigenicity of this cancer and knowing which mutations a patient has can help to predict the aggressiveness of their tumour and how long a patient may have. Mutations in the *BCL6* gene have been associated with poor patient outcomes and have been shown to be essential to GBM survival (Xu et al., 2017).. Mutations in *WNT* genes are common in many cancers and have been identified as important in the development and characteristics of GBM. An RNA-seq study was carried out to identify changes in gene expression in response to DNA damaging chemotherapy, and to the inhibition of *BCL6* in GBM cells. Many *WNT* genes were affected by these treatments. A link between *BCL6* and *WNT* in GBM has been suggested (K Basso, 2009). This prior discovery of a link bewteen *WNT* and *BCL6* along with the RNA-seq identified connection suggest that there is a need for more research to elucidate the influence of *BCL6* on the *WNT* pathway in regards to GBM and if this can be harnessed to reduce resistance of GBM cells to chemothearapy.

1.4. Research Aims

Due to literature linking *BCL6* with the *WNT* pathway; *BCL6* with GBM; and *WNT* with GBM; and the *WNT* pathway expression changes discovered in previous RNA-seq data from GBM treatment with the *BCL6* inhibitor FX1, it is likely that *BCL6* has an influence on the *WNT* pathway in GBM. Confirming this influence will contribute to the understanding of how *BCL6* works within GBM and produce a clearer understanding of how *BCL6* can be used as a therapeutic target in treatment for GBM.

There are three aims addressed in this project:

- Validate RNA-seq identified changes in expression of *BCL6*, *DKK1*, *WNT5a*, and *WNT5b* in response to treatment with chemotherapeutics, and inhibition of *BCL6*.
- Assess changes in intracellular *WNT* activity in Glioma cell lines in response to treatment with chemotherapeutics and inhibition of *BCL6*.
- Assess the effect of chemotherapy and *BCL6* inhibition on *WNT*-related cell functions.

2. Methods

2.1. Cell Culture

LN18 cells are a grade IV glioma cell line obtained from ATCC®, initially established from a right temporal lobe glioma in a 61-year-old male (Diserens et al., 1981). This cell line was chosen as it is fast growing and has previously been used as a model for human glioma in work on *BCL6* within this lab group.

T98G cells are a grade IV glioblastoma obtained from ATCC® but initially established from a glioblastoma removed from a 61-year-old male Caucasian. This cell line is fast growing and readily transfectable. T98G cells are a good in-vitro model for glioblastoma. (Stein, 1979).

Raji cells were purchased from ATCC® and were cryogenically stored. Raji cells are a non-adherent B lymphocyte cell isolated from an 11-year-old male with Burkitt's lymphoma in the left maxilla (Pulvertaft, 1964). These cells have been shown to have high endogenous *BCL6* expression and were therefore a good cell line to use as a positive control (Fabre et. al., 2017 Appendix).

Cellular functions are unlikely to match between *in vitro* and *in vivo* GBM cells. Due to the length of time cells are cultured for and the immortalization process, variability in transcriptional regulation between cell lines and primary cultures occurs. Cell lines are however easy to use, and produce consistent results so are therefore a good primary model (Jones, Bigner, Schold, Eng, & Bigner, 1981; Miller et al., 2017).

Cells were cultured in RPMI1640 (Life Technologies) supplemented with 5% FCS. Cells were grown in 75 cm^2 tissue culture flasks (TC treated culture flask, CELLSTAR®) at 37°C with 5% CO_2 in air atmosphere in a humidified incubator (Sanyo Electric Co., Ltd.). Cell confluence was assessed using a phase-contrast inverted microscope (Olympus IXS1, Olympus, Tokyo, Japan). When cell confluence reached 70%, growth medium was removed, cells were rinsed with

Dulbecco's Phosphate Buffered Saline (PBS) (Life Technologies), then treated with 0.05% Trypsin-EDTA (TE) (Life Technologies) for 3 minutes at 37°C before the TE was deactivated using fresh growth medium, then a fraction of the cells were resuspended in fresh growth medium.

For long term storage, $2x10^6$ cells suspended in 1 mL of RPMI-1640 medium (Life Technologies) containing 50% foetal calf serum (FCS) (Life Technologies) and 8% dimethyl sulfoxide (DMSO) were placed into a 2 mL cryotube (Greiner). These cryovials were then placed into CoolCell® Cell Freezing Containers then stored at -80°C overnight before being placed into liquid nitrogen. Cells were regularly tested for mycoplasma contamination by PCR screening. Cells were cultured under sterile conditions in a Logic Labconco® Biological safety cabinet (Total Lab Systems Ltd., New Zealand), and equipment was sterilized with both 70% ethanol and UV light before commencing cell culture.

2.2. Treatments

2.2.1. DMSO

Dimethyl sulfoxide (Me_2SO or DMSO) is a widely used solvent for increasing solubility of compounds. Drug solubility in water or PBS can often be much lower than necessary to achieve the desired effect. By dissolving a compound in DMSO before diluting it in a water based medium for cell culture, the solubility can be dramatically increased with only a small amount of solvent present in the final solution (Lipinski, 2008).

DMSO is also useful as a cryoprotectant when freezing cells (Castro et al., 2011; Egli et al., 2003). Concentrations of up to 10% while freezing cells have been shown to vastly improve viability of cells upon revival by minimizing effects of formation of intracellular ice (Mazur, Leibo, & Chu, 1972).

While DMSO is essential to a wide variety of in-vitro and in-vivo work, it has also been shown to be quite toxic at higher concentrations. At low concentrations (0.01-0.001%) proliferation has been shown to be slightly increased, while at higher concentrations (0.5-3%), viability has been shown to be decreased. The safest concentration to use while culturing cells is 0.1% (Singh, Mckenzie, & Ma, 2017).

2.3. Treatment conditions

Cells were treated for 24 hours before analysis. Treatments were used at specific concentrations for this study. Doxorubicin (Dox) was used at 3 μM as this is a concentration that has been successfully used within the MMc lab group and elicits the desired response. Dox is highly soluble and dissolves well in PBS at a concentration of 10 mM.

Temozolomide (TMZ) was used at a concentration of 400 μM. A higher concentration would have been desirable to elicit a more severe effect however, TMZ has poor solubility in both

PBS and DMSO making it difficult to work with and could only be dissolved in PBS at a concentration of 2.6 mM. Any higher concentration would result in the PBS carrier diluting out the RPMI growth medium. TMZ is soluble up to 50 mM in DMSO therefore the highest working concentration that could be used in medium without the DMSO negatively affecting the cells would be 50 µM. A higher ratio of PBS to medium as opposed to DMSO to medium is acceptable when treating cells due to off target effects from the carrier.

FX1 was dissolved in DMSO at a concentration of 25 mM. FX1 was used to treat cells at a concentration of 25 µM resulting in a DMSO concentration in RPMI of 0.1% which has been shown to be the concentration of DMSO showing the least effects on cell growth and viability (Singh et al., 2017). It was discovered during this project that the FX1 stocks, which were a new batch from our supplier, had significantly different activity from the batch used in previous work. Assays performed by Marie-Sofie Fabre showed that in order to gain similar effects to the previous batch, a concentration of 60 µM needed to be used. This resulted in the concentration of DMSO being 0.24% - more than double the desired concentration of DMSO. To account for this, a DMSO control of 0.24% was used to compare and normalise results to this higher concentration.

IWP-2 was dissolved in DMSO at 8 mM therefore to working concentration used was 4 µM making the DMSO concentration applied to the cells an acceptable 0.05%.

PBS and DMSO were used as carrier controls at the corresponding concentration to the compounds being used in each experiment.

Cells were also treated with a low dose of either Dox or TMZ every two days for fourteen days to mimic chemotherapeutic treatment in a human. Dox was used at 15 nM and TMZ was used at 10 nM.

2.4.Preparation of Plasmid DNA

A *WNT* reporter plasmid developed by Roel Nusse, 7TGC (Addgene plasmid # 24304) was kindly given to us by Prof Ari Melnick (Weill Cornell Medical College). The plasmid contains 7 TFP binding sites, an mCherry transfection reporter with an SV40 promoter, an eGFP *WNT* activation reporter, and selection markers of ampicillin (amp) and puromycin (puro) on a pRRLSIN.cPPT.PGK-GFP.WPRE backbone. The plasmid map can be seen in Figure 5.

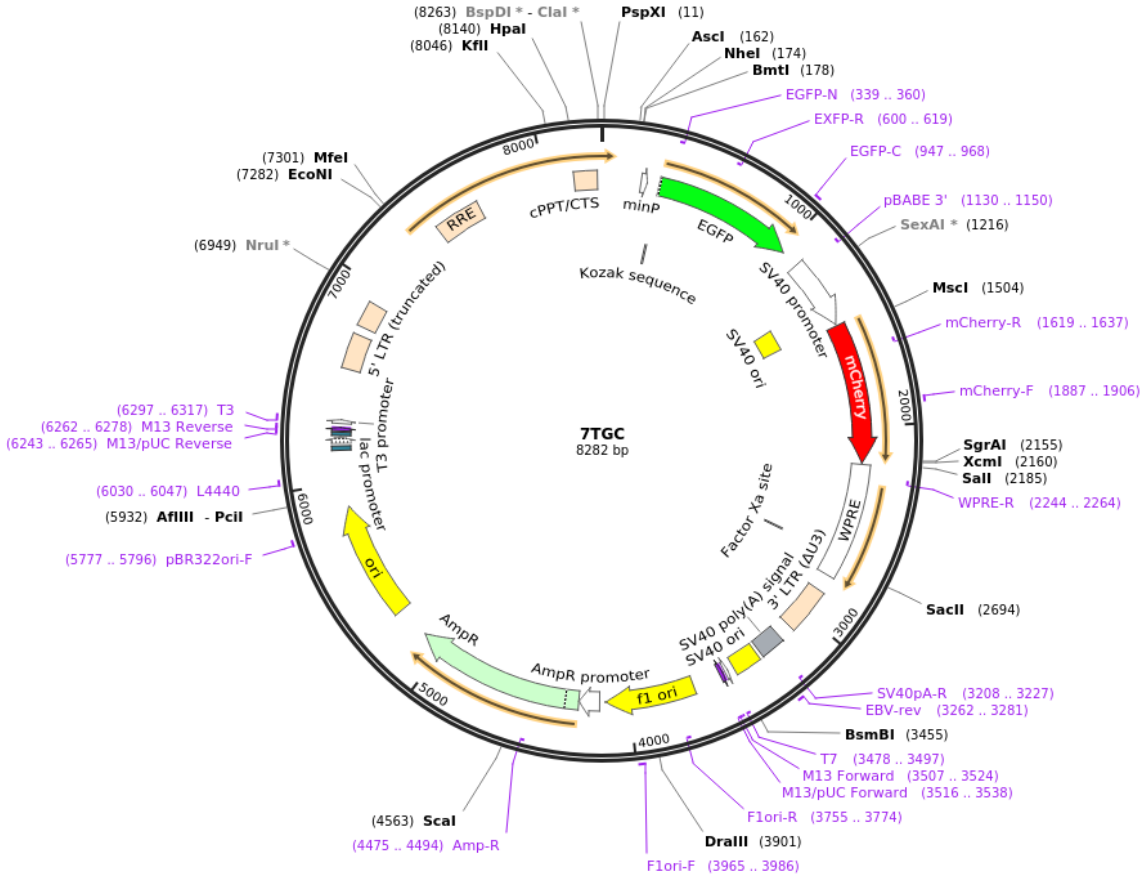

Figure 5 7TGC plasmid map. Addgene plasmid: # 24304.

The plasmid was transformed into One Shot® TOP10 Competent E. coli according to the manufacturer's protocol. Luria Broth (LB) agar plates (1% Bacto-tryptone, 5% Bacto-yeast extract 1% NaCl, 1% agar) containing 100 µg/mL of ampicillin (Sigma-Aldrich, Auckland, New Zealand) were used for antibiotic selection. After incubation for 16 hours at 37°C, single positive colonies from each were selected and inoculated into 400 mL of sterile liquid LB broth

supplemented with 100 µg/mL of ampicillin. The cultures were incubated for 16 hours at 37°C while shaking at 220 rpm (Bioline Shaking Incubator, Edwards Instrument Company, Australia). The cultures were then centrifuged at 5000 g for 10 min (SORVALL RC 6+ Ultrafuge, ThermoScientific). Plasmid purification was then carried out using a NucleoBond® Xtra Maxi Plus kit (Macherey-Nagel) as per the manufacturer's protocol. The final concentration of the plasmid was measured using an ND-1000 Nanodrop spectrophotometer (ThermoFisher Scientific). Quality of the sample was assessed by A260/280 and A260/230 ratios.

2.5. Transfection Optimization

2 mL of LN18 cells were seeded into a 6 well tissue culture treated plate at a concentration of 1×10^5 cells/mL and left to adhere overnight. Varying combinations of DNA concentrations and DNA to ViaFect ratios were applied to cells as per figure 6. Cells were then analysed for transfection efficiency via fluorescence microscopy.

2.6. Transfection

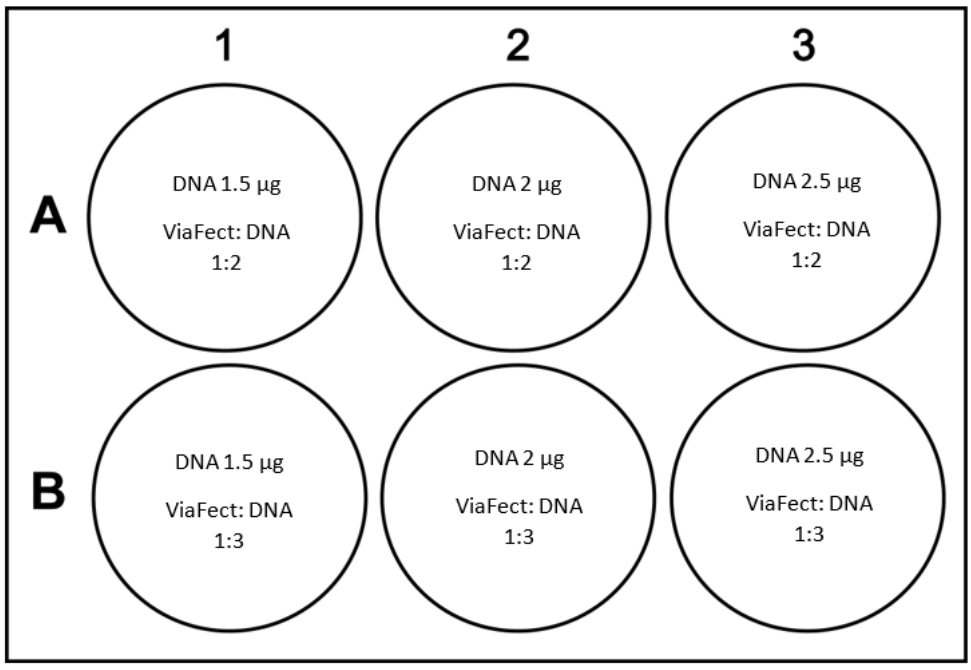

Figure 6 ViaFect transfection optimisation

Cells were seeded into a 6-well tissue culture treated plate at $1x10^5$ cells/mL and left to adhere overnight. 2 µg of DNA and 6 µL of ViaFect™ was combined and made up to 300 µL with supplemented RPMI medium per well needed. This solution was incubated at room temperature for 20 minutes to allow for the transfection complexes to form, before the growth medium was replaced, and the transfection mix was added. The cells were incubated with the transfection complexes for 24 hours. The cells were viewed under a fluorescent microscope to confirm expression of the transfected fluorophore and therefore transfection.

Stable cell line

2.6.1.

An attempt at creating a stably transfected LN18 cell line containing the 7TGC plasmid was made. LN18 cells were incubated with varying concentrations of puromycin, from 1 µg/mL to 10 µg/mL to find the minimal concentration at which cells were no longer viable in the absence of the plasmid carrying the puro resistance gene but remained alive in the presence of that plasmid. This concentration was then applied to transfected cells to select for cells which had maintained the plasmid and have therefore gained resistance to puromycin.

2.7. MTT Proliferation Assay

Cells were seeded into a 96-well tissue culture treated microplate at 2500 cells per well. Cells were left to adhere for 24 hours before addition of drug. After a 3-day incubation with the drug, 3-(4,5-dimethylthiazol-2-yl)-2,5-diphenyltetrazolium bromide (MTT) was applied and incubated at 30°C for 2 hours. The resulting formazan crystals were then solubilised using a solution of 10% SDS, 45% DMF by volume in Milli-Q water, pH adjusted by acetic acid to 4.50 (MTT Solubiliser). Cells were left in MTT solubiliser overnight at 30°C before being measured using a spectrophotometric multi-well plate reader (Enspire 2300, Perkin Elmer, Waltham, MA). Background absorbance of a well containing all components except cells was subtracted from the absorbance of test wells and control wells. Absorbance of test wells was divided by the absorbance of control wells then multiplied by 100 to get a percentage of growth inhibition in comparison to the untreated control.

2.8. Clonogenic Assay

Cells were seeded into 6-well tissue culture treated plates at a concentration of $1x10^5$ and left overnight to adhere. Drug was applied and incubated for 24 or 48 hours before cells were detached using TE, counted six times using a haemocytometer to ensure accurate cell counts, and seeded into 10 cm tissue culture treated dishes in numbers from 50 cells per plate to 400 cells per plate in all treatment groups except Dox which required higher seeding densities to achieve any colonisation and therefore numbers from 500 cells per plate to 16,000 cells per plate were seeded. Cells were incubated for 10-14 days in a 30°C incubator with 5% CO_2 in air atmosphere in a humidified incubator to allow proliferation. Cells were then fixed using a 6% neutral buffered formalin solution on a rocker for an hour before being stained with a solution of 0.4% methylene blue in 50% methanol, 50% distilled water overnight. Plates were imaged using an inverted fluorescent microscope (Olympus IXS1, Olympus, Tokyo, Japan) and analysed using FIJI software. Images were 'thresholded' using the 'Li' setting on the software, then colonies were identified as particles of sizes >10, then counted. Plating efficiency was calculated by dividing the number of colonies by the number of cells initially seeded and compared between treatment groups.

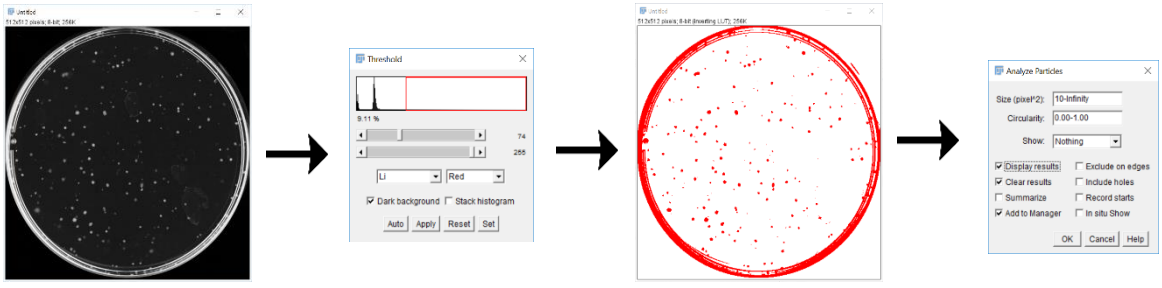

Figure 7 FIJI analysis of Clonogenic assay plates.

2.9. Flow cytometry

The BD FACSCanto™ II is located at Victoria University and was therefore the most logical option for use in flow cytometrical analysis however, it lacked a 561 nM laser needed to excite the mCherry fluorophore in the *WNT* reporter plasmid. The BD LSRFortessa™ flow cytometer at the Malaghan Institute of Medical Research (MIMR) was therefore utilised for experiments with the *WNT* reporter plasmid including transfection efficiency and the *WNT* reporter assay, while the BD FACSCanto™ II was used for cell cycle analysis.

2.10. Reporter assay

Cells were transfected using the protocol described in section 2.4, then after 24hrs treated for another 24 hours before cells were lifted using TE and resuspended in FACs buffer (PBS with 2% FCS and 0.05% sodium azide). Cells were stored on ice until data collection. Cells were stained with 1µg/mL of DAPI (Life Technologies) to select for intact cells. Fluorescence data was then collected using a BD LSRFortessa™ flow cytometer. Controls of mCherry-only transfected cells, GFP-only transfected cells, untransfected cells, and untransfected cells stained with DAPI were used to ensure correct compensation calculation for any spectral crossover between the fluorophores through the BD FACSDIVA™ software.

For collection, cells were gated first, using side scatter – area (SSC-A) versus forward scatter width (FSC-W) to remove any doublets from the analysis. Live cells were then selected for using Forward Scatter – Area (FSC-A) versus UV 450 50 C-Area laser (UV-A) and selecting only DAPI negative cells. From the live cells, mCherry expressing cells were selected by SSC-A versus G 610 20 B-Area (mCh-A). From these cells, GFP expressing cells were selected by SSC-A versus G 601 20 B-A (GFP-A) and 10,000 cells were counted.

Data was analysed using FlowJo® software. Single cells and then live cells were selected as above. The selected cells were displayed GFP-A versus mCh-A and a quadrant gate was

applied to calculate the number of GFP expressing cells out of the total number of transfected cells.

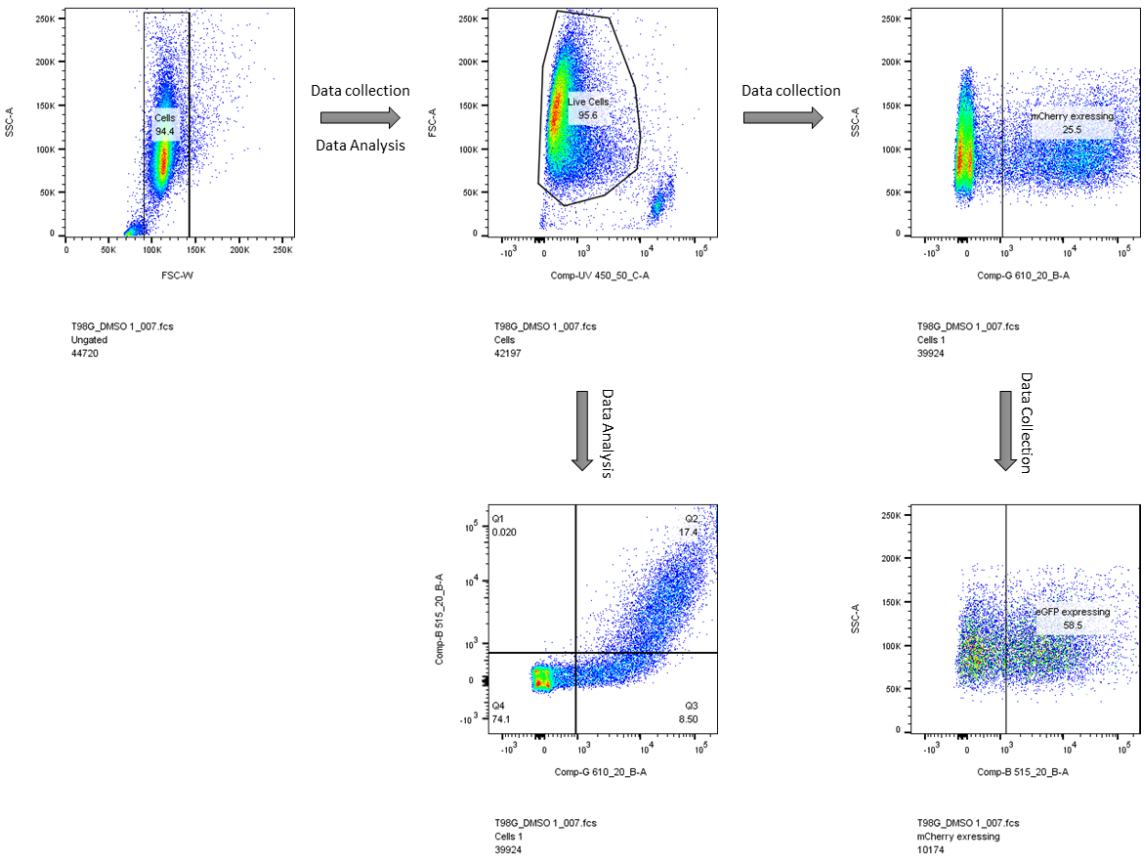

Figure 8 Gating strategy for flow cytometrical collection and analysis of 7TGC reporter assay

2.11. Confocal microscopy

Cells were seeded into tissue culture treated 35 mm Nunc™ Glass Bottom Dishes (ThermoFisher). Cells were transfected as described in section 2.6. Cells were then treated for 24 hours before NucBlue™ Live ReadyProbes™ Reagent (ThermoFisher) was added.

Cells were imaged using an Olympus FluoView FV1000 confocal laser-scanning microscope using a 100x oil-immersion objective. A 405 nm laser was used to image cell nuclei stained with DAPI (4', 6-Diamidine-2'-phenylindole dihydrochloride) (ThermoFisher), using the Dichrome DAPI 425-460 nm filter set. A 559 nm laser was used to image the mCherry cytoplasmic fluorescent protein, using the bandpass 575-675 nm filter set. A 473 laser was utilised to image the cytoplasmic eGFP protein using a 485-545 nm filter set. The imaging mode was set to sequential.

Images were analysed using FIJI as shown in Figure 9. Images were imported, and channels were split. Each image was changed to an 8-bit image then thresholded using the Li setting. Images were watershed to separate any touching cells, then particles were counted. Particles counted in the DAPI channel were used as a total cell count. Particles counted in the mCherry channel were considered to be all transfected cells within the frame. Particles counted in the green channel were considered to be all cells that have *WNT* activation. The ratio of eGFP expressing cells to mCherry expressing cells was compared between treatment and control groups.

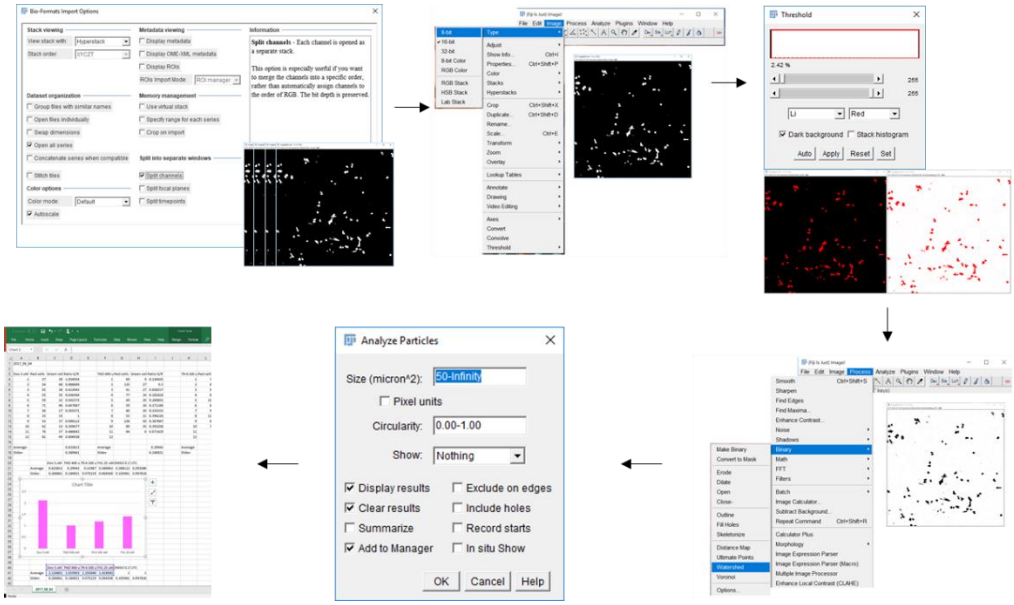

Figure 9 Fiji analysis of confocal images.

2.12. Cell cycle analysis

Cells were treated for 24 hours before being lifted using TE, and rinsed 2x in PBS. Cells were resuspended in DPBS and added dropwise to ice-cold 100% ethanol while vortexing to fix with a final EtOH concentration of 70%. Cells were stored in the ethanol for 1 hour before being rinsed in DPBS 2x then resuspended in FACS buffer with 250 mg/mL RNase (ThermoFisher) and 10 µg/mL of PI (ThermoFisher) and incubated for 30 minutes at 37°C. Cell cycle was then analysed by flow cytometry using the BD FACSCanto II.

Cells were gated by PI-W vs. PI-A to remove any doublets and debris. Cell cycle phases were then gated using cell count vs. PI-A as shown in Figure 10.

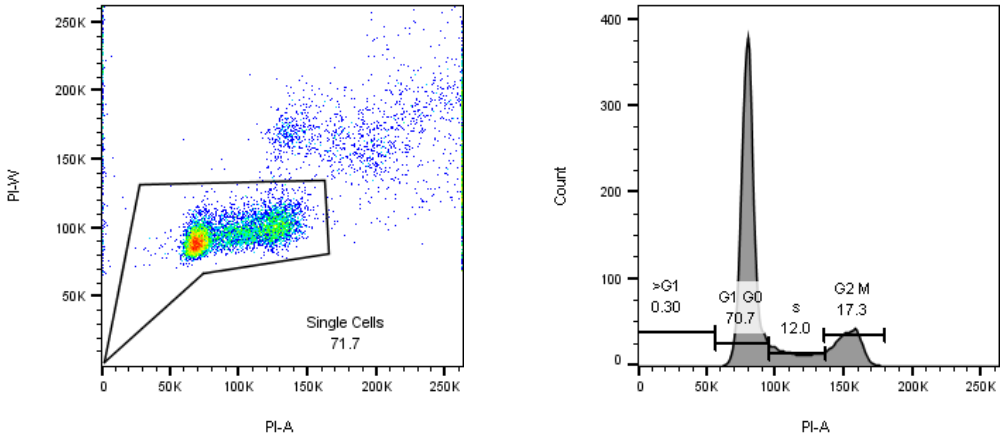

Figure 10 Gating strategy for cell cycle analysis

2.13. qRT-PCR

2.13.1. RNA extraction

Cells were lifted from the treatment plate using TE, then rinsed two times with PBS before being pelleted and snap-frozen and stored at -80°C for later extraction.

These frozen pellets were later lysed, and RNA was extracted using a Zymo Quick-RNA™ MiniPrep kit as per the manufacturer's protocol. Cells were lysed, cell debris was removed using a column. The flow through containing the nucleic acid was precipitated using 100% EtOH then loaded into a binding column followed by treatment with DNase for 20 minutes. RNA prep buffer was run through the column, then wash buffer before RNA was eluted using DNase/RNase free water. Extracted RNA was immediately quantified by using a Nanodrop spectrophotometer. The 260/280 and 260/230 nm ratios were assessed to ensure RNA purity.

2.13.2. Reverse transcription

RNA concentrations were normalised by dilution of all samples to the concentration of the sample with the lowest amount of RNA. RNA was then reverse transcribed into cDNA using a Takara PrimeScript™ RT Master Mix (Perfect Real Time) kit as per the manufacturer's instructions. The Takara PrimeScript™ RT Master Mix contains both oligo dT and random hexamers so the benefits of both types of primer can be achieved. The RT master mix reduces handling and error as it contains RTase, RNase inhibitor, random hexamers, oligo dT primer, dNTP mix and reaction. Oligo dT primers allow cDNA synthesis from full length copies of poly-adenylated mRNA. Random hexamers are added as they allow reverse transcription of all RNA including rRNA, tRNA, and snRNA.

2.13.3. qPCR

A KAPA SYBR® FAST qPCR Master Mix (2X) Kit was used as per the manufacturer's protocol however, reactions were scaled down to 10 µL per reaction. QuantiTect Primer Assays from Qiagen were used as they are well tested and have been reliably used within our lab group for many years. Little information is provided on the sequence of these primers due to intellectual property. Primer assays for *BCL6*, *DKK1*, *WNT5a* and *WNT5b* were used. qPCRs were run on a CFX96 Touch™ Real-Time PCR Detection System. Melt curves were used for each qRT-PCR to ensure that single products were produced with each primer. No-template controls and no reverse transcriptase controls were used for each gene to ensure that there was no DNA contamination in any of the qPCR constituents and that the primers did not dimerise resulting in a false positive signal.

PCR products were run on an agarose gel to confirm that there was a single PCR product for each primer, and that the products were the expected size. 5 µL of product from each gene, and 5 µL from each control sample was combined with 1 µL of loading dye and loaded into a 1% agarose TAE gel containing 1x RedSafe™. 5 µL of Invitrogen™ TrackIt™ 100 bp DNA Ladder was put into a well at either end of the gel which was then run at 100 volts for 1 hour. The gel was then imaged using a GE Typhoon FLA 9000 Gel Imaging Scanner.

2.14. Western Blotting

Cells were treated in either unsupplemented RPMI or RPMI supplemented with 5% FCS for 24 hours. Cells from each sample (approximated 1 x 10^6 cells) were then pelleted by centrifugation at 400 g for 3 minutes. The supernatant was aspirated off, samples were washed in PBS 2 times then frozen at -80°C for later use.

Cell pellets were resuspended in crude lysis buffer (70 mM NaCl, 20 mM Tris, 0.1% IGEPAL with Halt™ Protease Inhibitor Cocktail) by pipetting up and down 20 times to ensure complete lysis. Cells were then incubated on ice for 1 hour before centrifugation at 14,000 x g for 5 minutes to remove cell debris. The supernatant was then taken, and protein concentration was quantified using a Qubit™ Fluorometer. Protein concentration was then normalized, and samples were boiled with Laemmli buffer (200 mM Tris-Cl (pH 6.8), 400 mM DTT, 8% SDS, 0.4% bromophenol blue, 40% glycerol) for 5 minutes. 50 µg of protein was loaded into each well of a 10% acrylamide resolving gel (8 mL ddH_2O, 5 mL 1.5M Tris pH 8.8, 200 µL 10% SDS, 6.66 mL Bis Acrylamide, 100 µL 10% ammonium persulphate, 10 µL TEMED) with a 4% stacking gel (6.1 mL ddH_2O, 2.5 mL 0.5M Tris pH 6.8, 100 µL 10% SDS, 1.33 mL Bis Acrylamide, 50 µL 10% ammonium persulphate, 10 µL TEMED) alongside one well containing 5 µL PageRuler™ Plus Prestained Protein Ladder (Thermo Scientific). The gel placed in a tank and covered in running buffer (14.4 g Glycine, 3 g Tris, 1 g SDS, ddH2O to 1L) then run at 160 V for 1 hour. The gel was then transferred to a polyvinylidene difluoride (PVDF) membrane (Bio-Rad) (depolarized with 100% methanol (MeOH)) at 20 V overnight in transfer buffer (14.4 g Glycine, 3 g Tris, 200 mL MeOH, ddH2O to 1L).

The membrane was blocked for two hours in 5% BSA PBS-T (PBS with 0.1% Tween® 20 (Sigma Aldrich®) with 5% bovine serum albumin (BSA) (ICP Biologicals)). The membrane was then incubated overnight at 4°C in BSA PBS-T with a 1:500 dilution of primary antibody (Anti Bcl-6 mouse monoclonal IgM antibody (D-8): sc-7388; anti α-tubulin mouse monoclonal IgG: sc-8035 (Qiagen)). The membrane was then rinsed 5 times in PBS-T for 5 minutes on a rocker before incubation for 2 hours in BSA PBS-T with a 1:1000 dilution of secondary antibody

(Goat anti-mouse IgG HRP: sc-2005 (Qiagen)). The membrane was then rinsed in PBS-T 10 times for 5 minutes on a rocker. The HRP antibody was developed using Western Lightning Ultra chemiluminescence substrate as per the manufacturer's instructions (PerkinElmer). Imaging was carried out using a GE Amersham Imager 600.

2.15. Wound Healing Assay

Condition Optimization

2.15.1.

A wound healing assay was used to analyse the effect different treatments had on the migratory ability of both LN18 and T98G cells. To ensure that migration, not replication was being measured, cells were incubated in unsupplemented RPMI. The resulting cell cycle block was analysed by flow cytometry.

2.15.2. Cell Cycle Analysis

Cells were incubated in RPMI containing either 5% or 0% FCS for 24 hours before being lifted and resuspended in PBS. The cell cycle prep and analysis were carried out as described in section 2.1.

2.15.3.

Final Protocol

Cells were seeded into 24 well plates at 1.5 x 10^5 cells per ml, with 500 µL per well in unsupplemented RPMI. Cells were left to adhere overnight. This results in a monolayer of cells covering the bottom of the well. Cells were the treated in unsupplemented RPMI for 24 hours

before a wound was made using a 200 µl pipette tip in the apparatus shown in Figure 11. This wound making apparatus ensured relatively reproducible wounds in the monolayer.

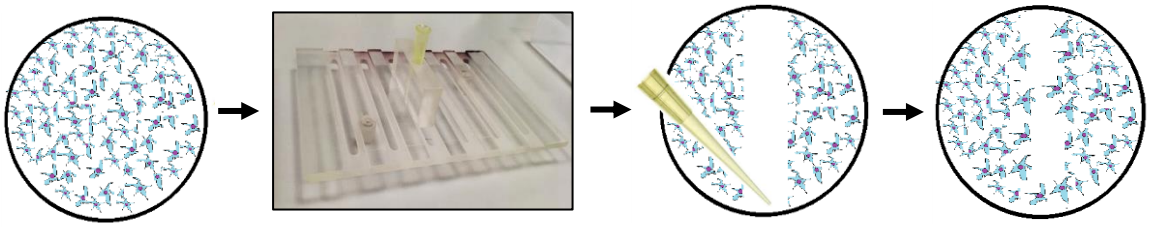

Figure 11 Migration assay workflow. Cells were grown to confluency, a wound was made using a pipette tip, wounds were imaged at t= 0 and t= 17 and the migration was measured.

Cells were then rinsed twice with PBS before being treated again in RPMI supplemented with 0.1% FCS. Wounds were then imaged using a phase-contrast inverted microscope (Olympus IXS1, Olympus, Tokyo, Japan), before being incubated for 17 hours at 37°C, then imaged again. Images were analysed using FIJI as shown in Figure 12. The area of the scratch was measured using the FIJI MRI wound healing tool. The area gained was calculated by taking away the area of the scratch at t17 from the area of the scratch at t0.

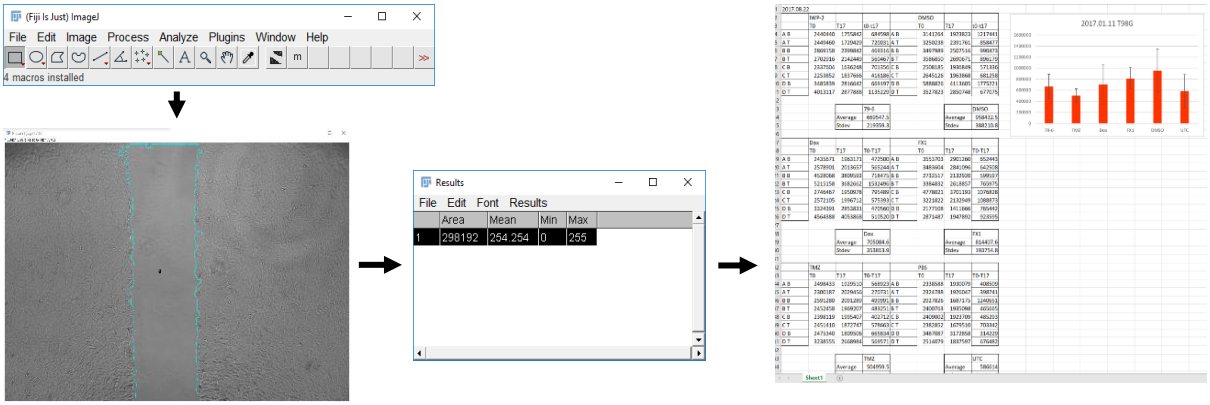

Figure 12 FIJI analysis of migration assay. The FIJI MRI wound healing plug-in was used to measure wound size.

3. b Results I: Changes in gene expression in response to inhibition of *BCL6*

An RNA-sequencing (RNA-seq) experiment to investigate the transcriptional changes in a glioblastoma cell line in response to Dox and FX1 was carried out by Nicole Jones for her PhD work. LN18 cells were treated with the chemotherapeutic drug doxorubicin, or with the small-molecule inhibitor of *BCL6*, FX1 for 24 hours and numbers of RNA-transcript were measured to identify changes in gene expression relative to baseline. Investigating the changes in gene expression will help in understanding how *BCL6* works within a glioblastoma cell.

The expression of multiple *WNT*-related genes were examined in cells treated with the *BCL6* inhibitor FX1 due to reports that the *WNT* signalling pathway is a direct target of *BCL6* in lymphoma. Several *WNT*-related genes were identified as having altered expression when cells were treated with FX1 or Dox suggesting that there may be a link between therapy, *BCL6* expression and *WNT* signalling.

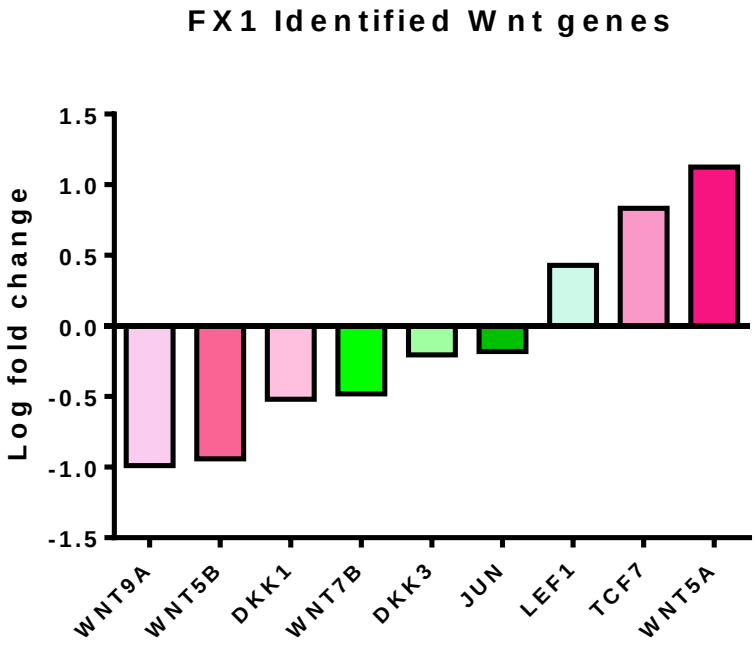

gene	WNT5A	WNT5B	TCF7	DKK1	WNT9A	LEF1	DKK3	WNT7B	JUN
padj	3.29E-17	2.98E-11	4.05E-08	4.38E-06	0.00073	0.02146	0.03192	0.04935	0.09318

Figure 13 WNT genes identified to have expression changes in response to FX1 taken from RNA-seq data produced by Nicole Jones and analysed by Sam Lee. Colour scale represents adjusted p-value (padj). Low to high is shown in a scale from pink to green. Data reproduced with permission from the researchers.

Criteria for selection were a fold change log 0.5 or greater, and an adjusted p-value lower than 0.05. The genes *DKK1, WNT5a* and *WNT5b* were chosen for validation by qPCR as they had a change in expression of an acceptable magnitude while also having adjusted p-values low enough that the fold changes were significant.

RNA-seq data from the Dox treated LN18 cells showed upregulation or downregulation in many *WNT* and *WNT*-associated genes (Figure 14). The genes *DKK1*, *WNT5b*, DKK3, Jun, *WNT*9A showed changes in expression in both datasets.

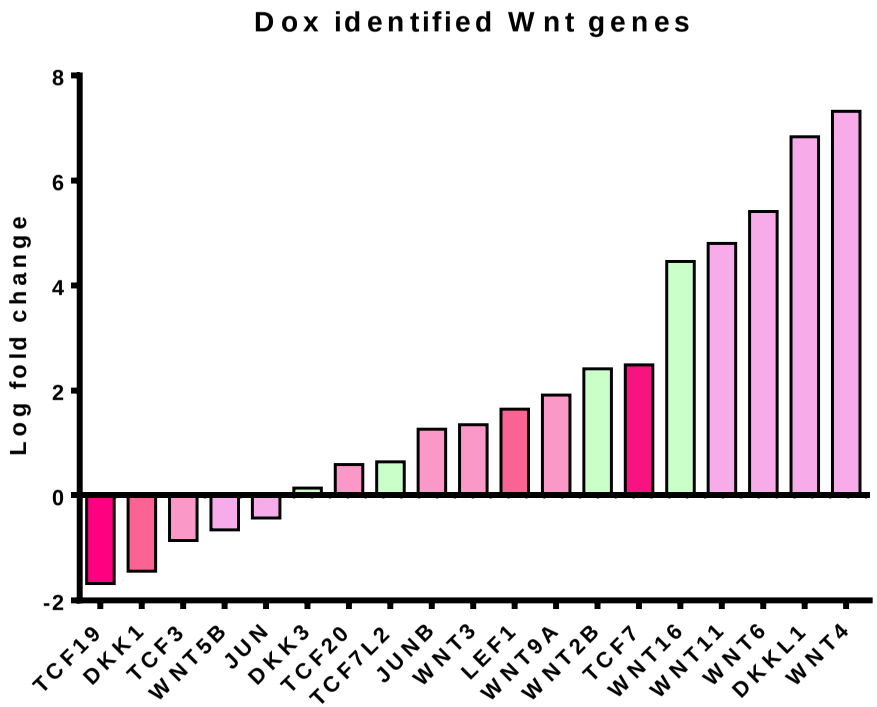

TCF19	TCF7	DKK1	LEF1	WNT3	TCF20	WNT9A	JUNB	TCF3	WNT11	WNT4	DKKL1	JUN	WNT5B	WNT6	WNT2B	TCF7L2	WNT16	DKK3
1.70E-87	2.18E-83	1.17E-42	2.41E-29	2.95E-15	6.69E-15	9.29E-15	1.44E-12	2.54E-10	4.56E-09	7.20E-08	5.91E-07	6.32E-07	1.69E-06	6.10E-05	0.003473	0.004916	0.006418	0.068213

Figure 14 WNT genes identified to have expression changes in response to Dox taken from RNA-seq data produced by Nicole Jones and analysed by Sam Lee. Colour scale represents adjusted p-value. Low to high is shown in a scale from pink to green. Data reproduced with permission of the researchers.

3.1. Validation of changes in gene expression in response to *BCL6* inhibition and chemotherapy

Quantitative reverse transcriptase polymerase chain reaction (qRT-PCR) was used to validate changes in gene expression identified in a previously conducted RNA-sequencing (RNA-seq) experiment (Jones et al, in preparation). Because the *WNT* genes *DKK1, WNT5a, and WNT5b* were found to have significant changes in expression in the RNA-seq data they were chosen to be validated. Two cell lines were used throughout to ensure all phenotypes were reproducible in different glioma cell lines, LN18 and T98G. *HPRT-1* was used as a housekeeping gene as amplification did not change under the chosen treatment conditions.

The genes described above were tested for expression changes in response to treatment with chemotherapy drugs Dox and TMZ, and the *BCL6* inhibitor, FX1. As a control for therapy effect, *BCL6* was also measured.

Cells were treated for 24 hours with 25 μM FX1, 3 μM Doxorubicin (Dox), and 400 μM Temozolomide (TMZ). These doses were the same as the doses used in Nicole Jones' RNA seq experiment described above. Cells were also treated in a manner mimicking chemotherapeutic doses in human cancer patients by treating with a low dose of either Dox, 15 nM or TMZ 10 nM every two days for fourteen days (LT Dox and LT TMZ). These doses were chosen from unpublished data generated by Marie-Sophie Fabre. RNA was extracted from these cells and changes in abundance of RNA transcripts was measured.

Melt curves and qPCR products

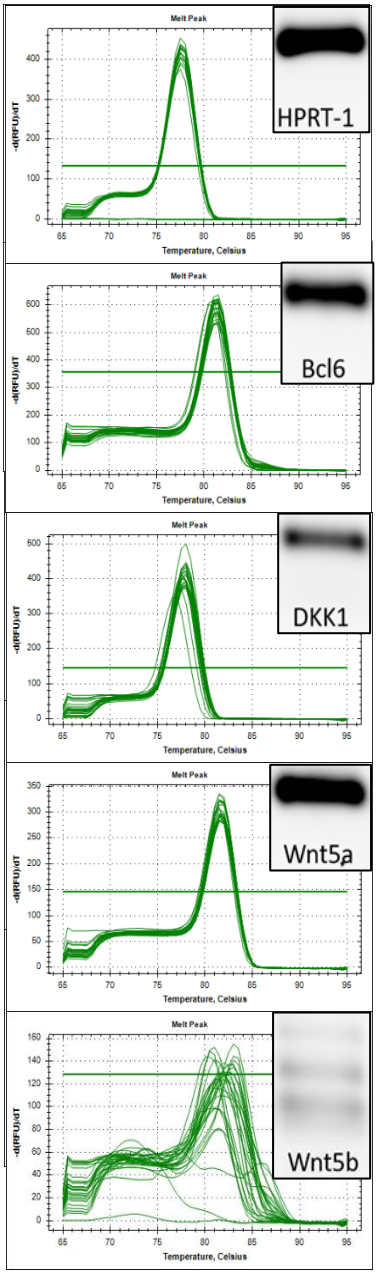

Figure 15 qPCR melt curves from the qPCR data and gene products from an agarose gel. N=3 technical replicates

A good primer should be specific for a gene and amplify only one gene product. PCR products were run on a gel to test that there would only be one band for each sample, but the exact size of each expected band was unknown. Due to intellectual property, no information on the sequence of these primers, or the PCR products is available.

Single bands were seen in the DNA gel run with the PCR products for the genes *HPRT-1, BCL6, DKK1*, and *WNT5a*. The melt curves produced by these PCRs corresponded well with the products seen in the DNA gels. A good melt curve should show a single peak at a single temperature for each gene. A second peak in the melt curve indicates another product being formed that has different melting temperature to the intended product. Melting temperatures can be affected product size, or by GC content as the melting temperature of purines is higher than that of pyrimidines. The melt curves for *HPRT-1, BCL6, DKK1*, and *WNT5b* all show relatively clean melt curves with only one peak. Each of these experiments were carried out with three biological replicates, each with three technical replicates.

Multiple bands were seen in the lane containing the PCR products of *WNT5b*. These DNA gels were run three times with different qPCR replicates used in each to confirm the presence of these erroneous products. The *WNT5b* melt curve showing multiple peaks and the agarose

gel showing multiple bands both suggest that multiple products were formed by this primer pair.

3.1.2. Baseline gene expression

Baseline gene expression in LN18 and T98G cells was measured and compared between cell lines. The expression of *BCL6, DKK1, WNT5a*, and *WNT5b* at a baseline level was measured and normalised to the housekeeping gene, *HPRT-1*. Baseline expression *of BCL6, DKK1*, and *WNT5b* were at similar levels in both cell lines (Figure 16). There was a substantial difference in baseline expression of *WNT5a* indicating differences in genetic regulation between the two cell lines.

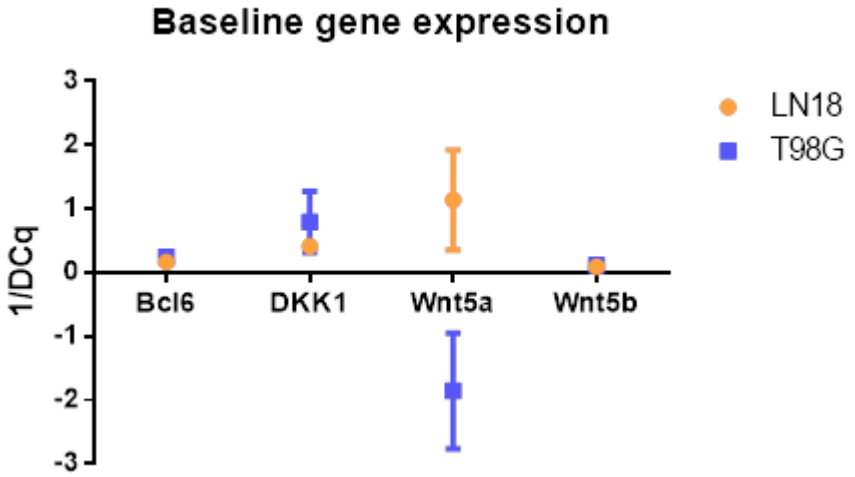

Figure 16 Baseline gene expression of BCL6, DKK1, WNT5a, and WNT5b in LN18 and T98G cells expressed as 1/DCq.

3.1.3. *BCL6* expression in response to treatment

Because expression of the oncogenic protein, *BCL6* has been shown to be upregulated in response to chemotherapy and radiation resulting in increased resistance to treatment (Fabre, Jones et. al. in revision appendix section 9.2). qRT-PCR was used to validate this response in T98G cells and LN18 cells. qRT-PCR was carried out with 3 technical replicates for each treatment, and 3 biological replicates of each treatment. Data presented are averages of the biological replicates, normalised to their respective carriers

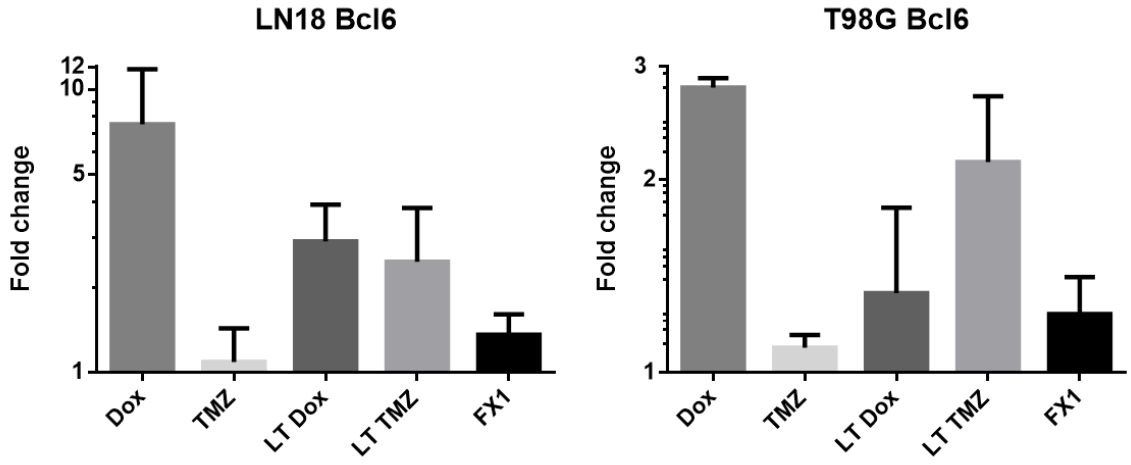

Figure 17 BCL6 gene expression in response to treatment. N=3 biological replicates with 3 technical replicates. Error bars represent the SEM. No statistical significance was found.

A 7.5-fold increase in expression was observed in LN18 cells and a 2.8-fold increase in T98G cells in response to Dox treatment. This is a notable increase in *BCL6* expression and was consistent in both LN18 cells and T98G cells indicating a potential link between Dox treatment and an increase in *BCL6* expression.

Long term Dox treated cells showed a 2.5-fold increase in *BCL6* expression in LN18 cells, and a 1.3-fold expression increase in T98G cells. This moderate increase in *BCL6* expression is consistent in both LN18 and T98G cells lines and could indicate a link between Dox treatment and *BCL6* expression, similar to the short-term treatment (Fabre et. al. 2017, Appendix section 9.2).

Treatment with TMZ showed a minor increase in *BCL6* expression with a 1.08-fold increase in LN18 cells, and a 1.09-fold increase in T98G cells. This is a modest and statistically insignificant increase in *BCL6* expression. It is unlikely that this treatment has any real effect on the expression of *BCL6.*

Long term TMZ treated cells showed a 2.5-fold increase in LN18 cells and a 2.1-fold increase in T98G cells. This is a notable increase in *BCL6* expression and corresponds with previous findings by Fabre et. al. who observed that TMZ, Dox and IR all increased *BCL6* expression level.

With FX1 treatment *BCL6* expression increased 1.35-fold in LN18 cells and 1.23-fold in T98G cells.

3.1.4. *DKK1* expression in response to treatment

The *DKK1* protein is an endogenous inhibitor of *WNT* signalling (Niida et al., 2004). It was shown in the RNA-seq data that *DKK1* expression decreased in response to FX1 treatment and decreased in response to Dox treatment. TMZ was not tested in the RNA-seq data, neither was long-term treatment of either Dox or TMZ. The long-term treatment may give a more accurate idea of expression in response to chemotherapeutic treatment in humans as it is a more accurate representation of the drug delivery in the system of a human body.

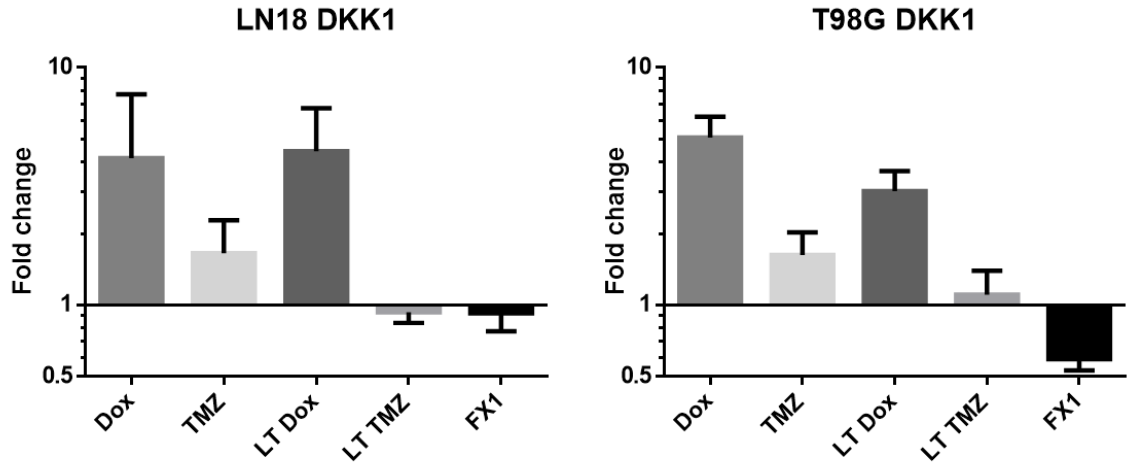

Figure 18 DKK1 gene expression in response to treatment.

N=3 biological replicates with 3 technical replicates. Error bars represent the SEM. These results were found to be statistically insignificant.

Dox treatment resulted in a 4.2-fold *DKK1* expression increase in LN18 and a 5-fold increase in T98G cells (Figure 18). This is converse to what was observed in the RNA-seq data however, this response was consistent between the two cells lines and between replicates.

Similarly, long-term treatment with Dox resulted in a 4.5-fold increase in *DKK1* expression in LN18 cells and a 3-fold increase in T98G cells. This increase in expression is also consistent

between the two cell lines and shows that under more clinically relevant settings with long term treatment, there is a consistent increase in *DKK1* expression.

TMZ treatment in LN18 cells resulted in a 1.7-fold increase in *DKK1* expression, and a 1.1-fold increase in expression in T98G cells. This modest increase in *DKK1* expression is seen in both cells lines however the effect might prove to be more significant if a higher concentration of TMZ were to be used to treat the cells.

Long-term treatment with TMZ showed a 0.9-fold decrease in expression in LN18 cells and a 1.1-fold increase in T98G cells indicating little to no change in expression in either cell line.

Treatment with FX1 showed a decrease in expression of *DKK1* in both T98G and LN18 cells with a 0.9-fold change and a 0.6-fold change respectively. This is consistent with the RNA-seq results which showed a 0.5-fold change in *DKK1* expression in response to FX1 treatment. The qRT-PCR results are consistent between the two cell lines.

3.1.5. *WNT5a* expression in response to treatment

WNT5a is a glycoprotein involved in the non-canonical *WNT* pathway. In the RNA-seq data, *WNT5a* expression was found to be downregulated when *BCL6* was inhibited. No change in expression was observed when cells were treated with Dox. Again, long term treated Dox and TMZ were not tested by RNA-seq.

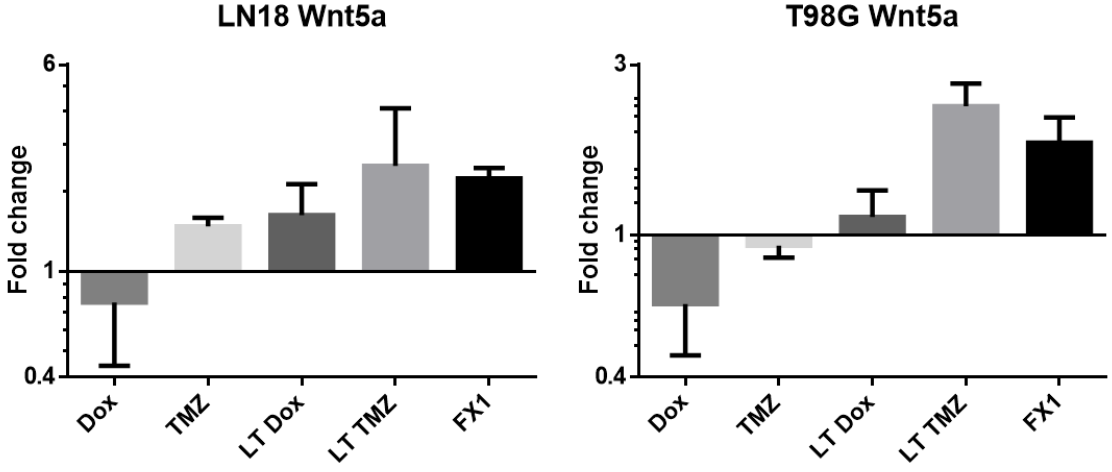

Figure 19 WNT5a gene expression in response to treatment. N=3 biological replicates with 3 technical replicates. Error bars represent the SEM. These results were found to be statistically insignificant.

Dox treatment resulted in a downregulation of *WNT5a* in LN18 cells and T98G cells with 0.76-fold and 0.64-fold changes respectively. This was not seen in the RNA-seq data but *WNT5a* is downregulated in both cell lines making it likely to be a relevant change in gene expression. The fold-change of *WNT5a* expression in LN18 cells was 1.6-fold, and 1.1-fold in the T98G cells. TMZ treatment showed a 1.5-fold change in LN18 cells and a 0.9-fold change in T98G cells. This opposing up- and down- regulation of expression in the gene *WNT5a* could indicate that the systems of *WNT* regulation within the two cells lines differ. The long-term treatment of TMZ on both the LN18 and T98G cells resulted in an upregulation if *WNT5a* with fold changes of 2.5 and 2.3 respectively. The effect of long term TMZ treatment resulted in a larger increase of *WNT5a* expression than in the short term TMZ treatment. When *BCL6* was inhibited by FX1, there was a reproducible increase in the expression of *WNT5A* in both glioma cells lines with a 2.2-fold increase in LN18 cells and a 1.8-fold increase in T98G cells.

This is interesting as it has had an inverse effect to the short term Dox on *WNT5A* expression. Again, this is consistent with the hypothesis that *BCL6* induced by therapy is driving gene expression.

WNT5b expression in response to treatment

3.1.6.

WNT5b is a *WNT* ligand involved in non-canonical *WNT* signalling. When treated with FX1, *WNT5b* expression was found to be upregulated in the RNA-seq data. *WNT5b* has two different transcript variants resulting from alternative splicing (NCBI gene ID:81029).

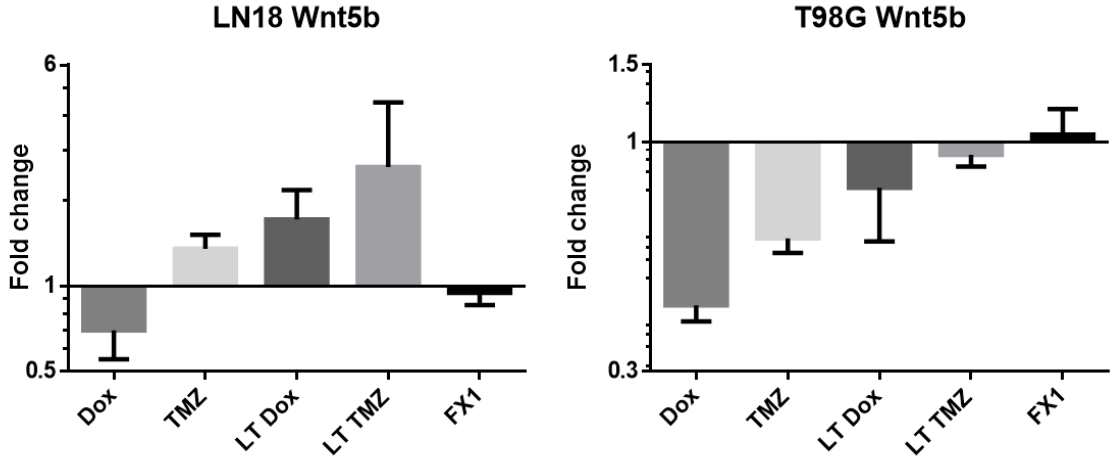

Figure 20 WNT5b gene expression in response to treatment. N=3 biological replicates with 3 technical replicates. Error bars represent the SEM. These results were found to be statistically insignificant.

The data were largely inconsistent between cell lines. Dox treatment resulted in a large downregulation of *WNT5b* in both glioma cell lines. *WNT5b* expression in response to TMZ, LT Dox, LT TMZ, FX1, and IWP-2 showed opposite results between the two glioma cell lines. This could be due to differences in pathway regulation between the two cell lines (Figure 16) however, as was shown in Figure 15, three separate products were present in the *WNT5b* qPCR products. This indicates that multiple products were amplified by the *WNT5b* primer. The identity of these products is unknown.

3.2. Discussion

The aim of this chapter was to validate and extend the results found in the RNA-seq data collected by Nicole Jones. This is the first question that needed to be answered in this project to ensure that research was led by results that were reproducible. To ensure reproducibility, the chosen genes were tested in two glioma cell lines, the first of which, LN18 was used for the initial RNA-seq work. The second cell line T98G was another commonly used glioma cell line and was used to determine that the results weren't cell-line dependent.

BCL6 has been shown to be upregulated significantly, and reproducibly in the past (McConnell et al., 2015) and has been suggested to be one of the mechanisms of treatment resistance in glioblastoma (Fabre et. al. 2017). *BCL6* is an anti-apoptotic protein which allows cells to continue through the cell cycle, even during DNA damaging events that would halt the cell cycle (Phan & Dalla-Favera, 2004).

RNA-seq data revealed significant fold changes in multiple *WNT* related genes in LN18 cells treated with FX1 suggesting an influence of *BCL6* on the *WNT* pathway. The *WNT* pathway has been implicated in Glioblastoma pathogenicity many times and with many different downstream effects recorded (Kim et al., 2015; Rheinbay et al., 2013; Sedgwick & D 'souza-Schorey, 2016; Wu et al., 2012; Yu et al., 2007). A link between these two proteins may be important in understanding chemo- and radio- resistance in Glioblastoma cells.

The expression of *BCL6* under chemotherapeutic treatment conditions, long and short term was upregulated relative to the carrier controls. This is consistent with the change in expression seen in previous studies when cells are treated with Dox (Fabre et. al. 2017) the authors observed that TMZ, Dox and IR all increased *BCL6* expression level. Both Dox and TMZ induce DNA damage, therefore upregulation of *BCL6* can allow a cell to better tolerate DNA damage to maintain the cell cycle in B-cell development (Katia Basso & Dalla-Favera, 2012).

When treated with FX1, *BCL6* was also upregulated. This is potentially due to an autoregulatory feedback loop as FX1 does not directly affect the production of the *BCL6*

transcript, but the activity of the protein itself (Katia Basso & Dalla-Favera, 2010; Cardenas et al., 2016; Mendez et al., 2008; X. Wang, Li, Naganuma, & Ye, 2002).

The long-term treatment of the two chemotherapeutics Dox and TMZ were intended to mimic clinically relevant treatment conditions. By delivering a low dose regularly over time, the result seen is more likely representative of the gene expression changes in a patient receiving treatment for glioblastoma (Beier et al., 2012). The increased expression of *BCL6* in these long-term chemotherapy-treated cells shows that these treatments increase and maintain increased expression of *BCL6* during treatment. This could have implications in chemotherapy resistance due to the anti-apoptotic action of *BCL6* (Fabre et. al. 2017).

The treatment with TMZ only resulted in a modest increase in *BCL6* expression, compared to the LT TMZ treated cells which had a much greater increase in expression. This shows that *BCL6* expression increases over time in response to multiple chemotherapeutic treatments. TMZ has been shown to be difficult to use in vitro as it is administered as a prodrug which then needs to be activated once inside the cell. This activation is much more efficient in an in vivo scenario and cannot be controlled in an in vitro system. This results in a variable response to the drug as the amount of TMZ that is converted to the active form can be variable. TMZ also has low solubility (Jian-jun, 2006) making it difficult to get higher treatment concentrations without either diluting the cell media with PBS further than acceptable or adding a concentration of DMSO higher than 0.1% which could affect viability. Due to these difficulties, TMZ is not a consistent or easy drug to work with in vitro.

The *DKK1* gene codes for the *DKK1* protein which inhibits the *WNT* pathway through binding LRP5 which is an essential coreceptor for *WNT* signalling (Pinzone et al., n.d.). When the glioma cell lines were treated with Dox, TMZ or LT Dox, there was an upregulation in *DKK1* expression. The effect of LT TMZ on the expression of *DKK1* was negligible suggesting that the initial effect of TMZ influences *DKK1* however, this does not continue over time and multiple treatments. The effect of Dox on *DKK1* is maintained under these conditions, with the expression remaining increased in the long term treated cells. This upregulation of *DKK1* in response to chemotherapeutic treatment is not consistent with the RNA-seq data (Figure 14). FX1 treatment on the glioma cell lines had the same effect on *DKK1*, causing

downregulation of expression from baseline. This opposite effect could be due to an influence of *BCL6* on *DKK1*. As shown in the *BCL6* data, chemotherapy increases *BCL6* expression, and increases *DKK1* expression. When *BCL6* is inhibited, *DKK1* expression decreases. This suggests *BCL6* influences *DKK1* expression.

WNT5a is a noncanonical signalling molecule in the *WNT* pathway. The noncanonical *WNT* pathways regulate many different functions including adhesion, migration, polarity, differentiation, and proliferation (Kikuchi, Yamamoto, Sato, & Matsumoto, 2012). When glioblastoma cells are treated with Dox, a downregulation in *WNT5a* was observed whereas after long term treatment, there was an upregulation. The difference indicates a change in regulation over time in response to Dox treatment. *WNT5a* is less involved in the initial response to Dox treatment but becomes more involved over time. An upregulation in *WNT5a* was seen under both short-term and LT TMZ treatment conditions. This is a consistent upregulation showing that *WNT5a* is involved in the cellular response to TMZ treatment. FX1 treatment also resulted in an upregulation in *WNT5a* expression. This could indicate that *BCL6* either has an inhibitory effect on *WNT5a* expression, or that *WNT5a* is involved in some sort of compensatory mechanism for the loss of *BCL6* function.

WNT5b is an important paralog of *WNT5a*, with an amino acid identity similarity of 87% (Kikuchi et al., 2012). The *WNT5b* results were inconsistent between the two cell lines. The melt curves for the qPCR analysis of this gene were messy and an agarose gel showed 3 different product bands. Multiple product amplification is unexpected. The clean melt curves and single product bands in the agarose gel for the PCR products of *BCL6, DKK1*, and *WNT5a* are a good example of what should have been expected from this primer assay however this was not the case for *WNT5b*. These products may be non-specific products, or if they may be different isoforms of the *WNT5b*. Due to the unknown identity of the products, the *WNT5b* results are not reliable.

These results validate the upregulation of *BCL6* in response to chemotherapeutic treatment as shown by Fabre et. al. They also validate the RNA-seq data showing the changes in expression of *WNT* genes. Under chemotherapeutic treatment conditions, *BCL6* is upregulated, as is *DKK1.* Conversely *BCL6* inhibition leads to the downregulation of DKK1, an

opposite response to chemotherapy treatment. This suggests that *BCL6* could influence the *WNT* signalling pathway.

4. Results II: Role of *BCL6* in chemotherapy induced canonical *WNT* signalling

4.1. Reporter assay: Canonical *WNT* signalling

The canonical *WNT* pathway is essential in many cellular functions including regulation of adult cell homeostasis, stem cell renewal, proliferation apoptosis, and differentiation. Aberrant canonical *WNT* signalling has been shown to have a role in carcinogenesis and may be a good target for cancer treatment (Sedgwick & D 'souza-Schorey, 2016; K. Yang et al., 2016). Little research has been conducted on the response of the *WNT* pathway to chemotherapeutic treatment. In this chapter canonical *WNT* activation in response to chemotherapeutic treatment, and *BCL6* inhibition is measured.

In order to obtain information on the induction of the canonical *WNT* pathway in response to different treatments a plasmid containing an mCherry fluorophore to indicate successful transfection, and 7-TCF binding sites followed by an eGFP reporter fluorophore to indicate *WNT* activation within cells was used (Fuerer & Nusse, 2010). TCFs are transcription factors which bind nuclear β-catenin in an active canonical *WNT* pathway therefore, when bound to the 7TCF binding sites on the 7TGC plasmid, activate the expression of eGFP indicating canonical *WNT* signalling.

4.1.1. Transfection Optimisation

Transfection of plasmid DNA into cell lines requires thorough optimisation before experimental use to minimise variables that could confound the outcome of the experiment, such as a decline in cell health. Many variables can contribute to overall cell health during plasmid transfections such as the cell type, and transfection reagents. Transfection reagents

are toxic to the cell and therefore the right balance of DNA and transfection reagent (ViaFect, Promega) must be used to achieve the highest viability of the transfected cell culture before experimentation can begin (Rose, 2003). Transfection of LN18 cells is difficult due to poor viability post-transfection (Jones, personal communication), therefore optimization of the transfection procedure was carried out prior to experimentation. As T98G cells are known to be readily transfectable, optimisation was forgone. The 7TGC plasmid, which contains an mCherry fluorophore for transfection identification was used for optimisation of the LN18 cell line. Cells were transfected with various ratios of plasmid DNA to ViaFect as shown in the methods section (Figure 6), and the resulting transfection was viewed under a fluorescence microscope (Figure 21). All cells were stained with Hoechst dye to visualise the nucleus. With the mCherry in conjunction with the nuclear stain, ImageJ could be used to quantify the number of cells in a microscopic field and determine how many of those cells had received and were expressing, the plasmid. It was determined that 2 µg of DNA to 4 µL of ViaFect per well was the optimal ratio of DNA to ViaFect as it had a relatively high transfection efficiency (27%) while the cells remained healthy (Figure 16). Although the 1:3 ViaFect ratio with 1.5 µg of DNA had a slightly higher transfection efficiency, it was decided that the 1:2 ViaFect ratio with 2 µg of DNA could minimise ViaFect use while maintaining a high transfection efficiency.

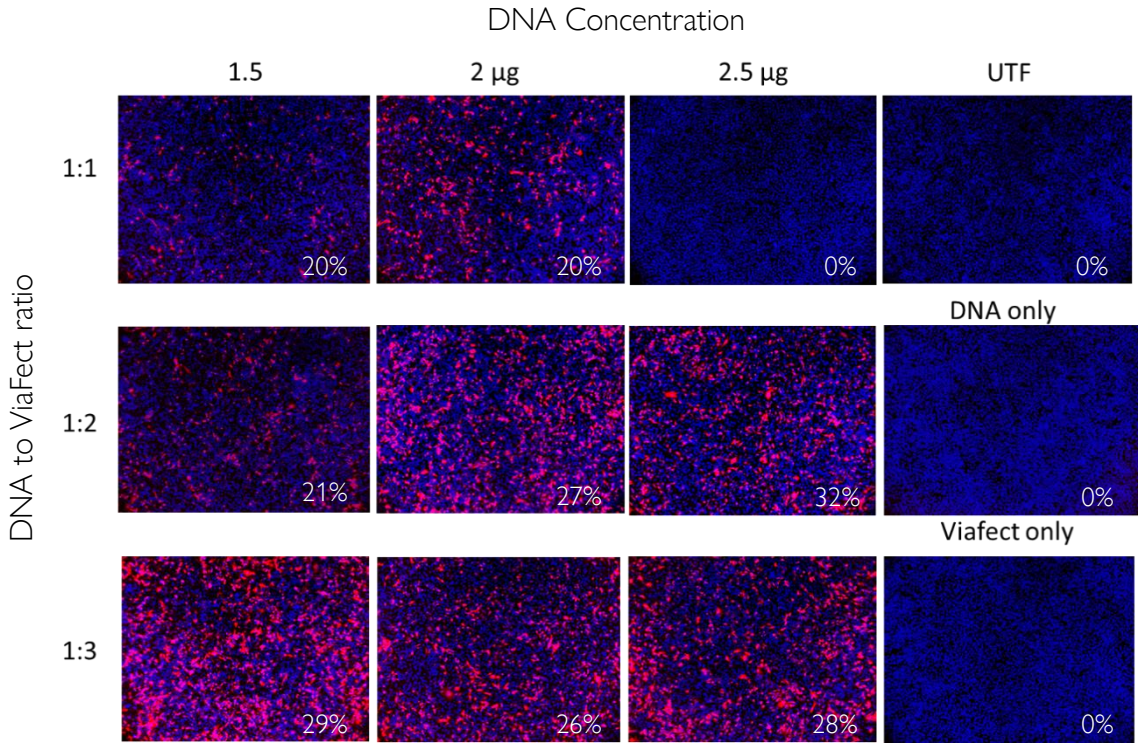

Figure 21 Optimization of ViaFect transfection of 7TGC plasmid into glioma cells. Transfection efficiencies are shown in white.

4.1.2. Stable cell line

Once optimal transfection conditions were found, the selection of a cell line that was stably transfected with 7TGC was attempted. A stably expressing cell line can eliminate the need to repeatedly transfect cells before each experiment, which can introduce unnecessary variation in experimental results, such as variation in plasmid expression and therefore the brightness of the fluorophore can alter detection of cells. A stably expressing cell line is usually made from a small number of cells that continue to express the transfected plasmid for more than two weeks post-transfection. This results in a relatively consistent expression level of the plasmid between cells within the culture. To create a stable expressing cell line, untransfected cells were treated with Unfortunately, after multiple attempts to create a stably expressing cell line, no cells expressed the fluorophores after the two-week selection period and it was decided to go ahead with transient transfections prior to each experiment.

Viability in response to IWP-2 dose

Inhibition of the PORCN protein has been shown to be an effective inhibitor of *WNT*, since PORCN1 is believed to be essential in the modification and release of *WNT* proteins from the endoplasmic reticulum (Proffitt & Virshup, 2012) . The PORCN1 inhibiting compound IWP-2 was chosen to be used as a positive control for suppression of the *WNT* pathway (Madan et al., 2016). An MTT dose-response assay was used to choose an appropriate working concentration for future experiments with IWP-2. IWP-2 is soluble in DMSO at 8 mM therefore the highest working concentration that could be used while keeping the DMSO concentration at or below 0.1% was 8 µM. From 8 µM nine two-fold dilutions of IWP-2 were made, and cell viability was measured after a three-day incubation with the drug.

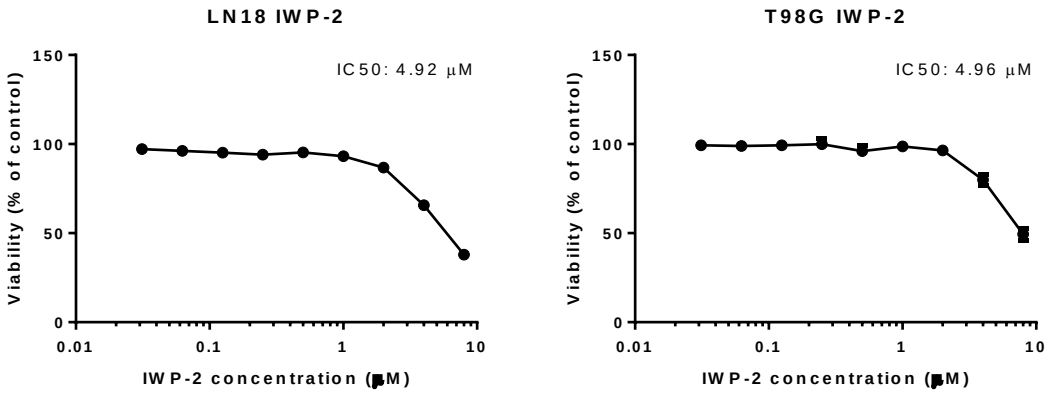

Figure 22 Dose response of IWP-2 in T98G and LN18 cells. N=3. Error bars represent the standard error of the mean (SEM).

IWP-2 was tested in both T98G cells and LN18 cells to find an appropriate working concentration. Viability started to decrease at concentrations of 2 µM and dropped below 50% at 8 µM (Figure 21). The IC_{50} in LN18 cells and T98G cells was calculated to be 4.92 µM and 4.96 µM respectively. A working concentration of 4 µM was chosen.

WNT activation measured by confocal microscopy

WNT activation was initially measured using confocal microscopy in LN18 cells. Cells were treated for 8 hours with 3 μM of Dox, 400 μM of TMZ, 25 μM of FX1, 0.1% DMSO, or were left untreated. Treatments groups were imaged in 10 different fields and red (transfected) to red and green (Transfected with active *WNT*) ratios were calculated and averaged among the 10 fields.

4.1.2.

Dox was found to be mildly autofluorescent in both the mCherry (559 nm laser with 575-675 nm filter set) and eGFP (473 nm laser with 485-545 nm filter set) channels, which made it difficult to distinguish transfection and *WNT* activation from autofluorescence (Motlagh, Parvin, Ghasemi, & Atyabi, 2016). Lasers had to be adjusted to remove autofluorescence from the images and analysis had to account for autofluorescence. To account for autofluorescence, non-transfected cells were treated with Dox and the lasers normalised using these cells so to keep them low enough that the autofluorescence could not be detected. *WNT* activation in \

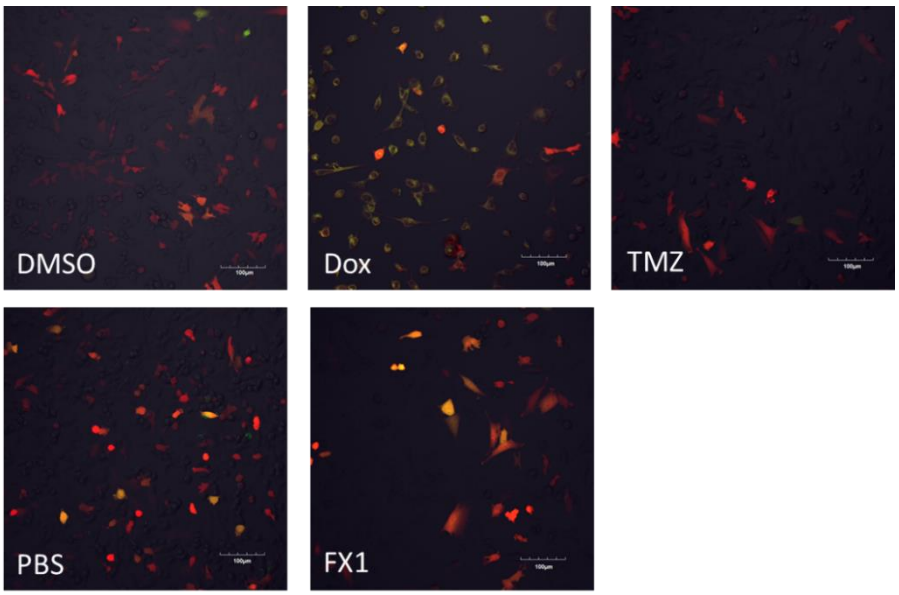

Figure 23 Representative confocal images of treatment groups in the reporter assay.

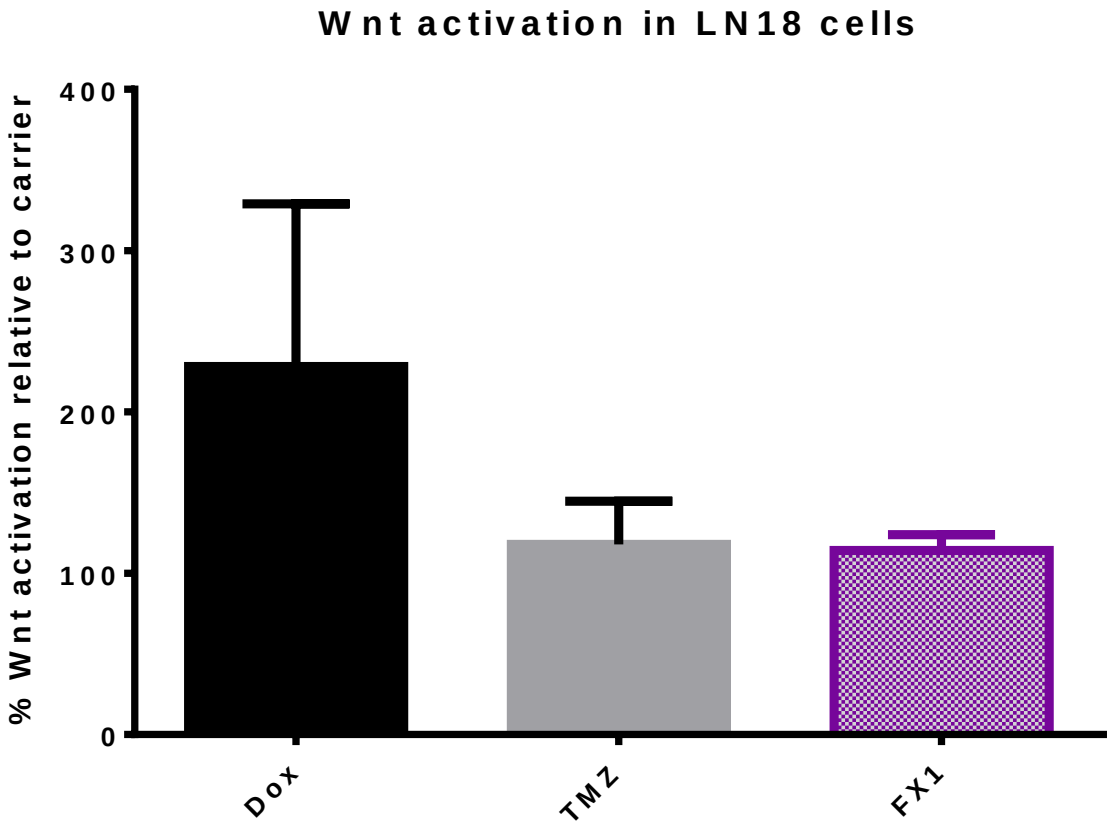

Figure 24 WNT activation in LN18 cells analysed by confocal microscopy. Dox and TMZ are normalised to a PBS control (shown in black and grey); FX1 was normalised to a DMSO control (shown in purple). N=4. Error bars represent the SEM.

Dox treated cells was increased 2.3-fold relative to a PBS control based on two replicate experiments (Figure 24). The method was found to be unreliable as much of the transfected cells had low levels of fluorescence resulting in little data from the Dox-treated samples and a high possibility of false negatives shown by the large variability in data. The method of removing bias introduced by the autofluorescence of the Dox was decided to be unreliable.

TMZ had a 1.2-fold increase in *WNT* activation relative to a PBS control, FX1 a 1.1-fold increase.

Due to the variability between replicates and the uncertainty with the method of removing the autofluorescence from the analysis, it was decided to measure *WNT* activation using a high-throughput method. Flow cytometry was used to quantify fluorescence and determine *WNT* activation in these treatment groups.

The effect of IWP-2 on *WNT* activity in glioblastoma cells

4.1.3.

IWP-2 was titrated from the highest concentration that could be used (8 μM) while maintaining acceptable concentrations of DMSO (0.1 %) in cultures, down to 1μM which showed little activity in the dose response assay shown in Figure 22.

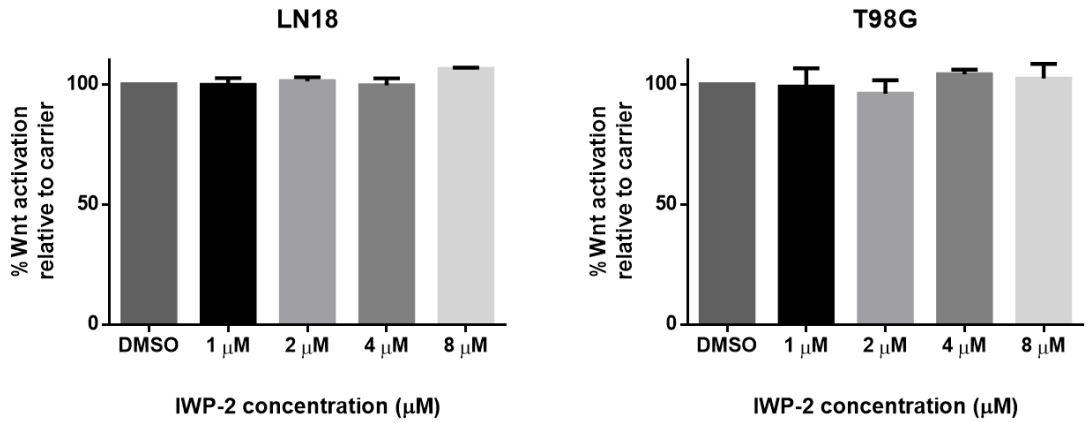

Figure 25 Titration on IWP-2 in 7TGC transfected cells. Measured by Flow cytometry. N=4. Error bars represent the SEM.

It was expected that eGFP expression would be reduced by IWP-2, however there was no significant difference was seen in the activation of *WNT* in any of the drug concentrations, in either T98G or LN18 cells. These results show that IWP-2 cannot be used as a positive control for *WNT* inhibition in these cell lines as it is not effective in this assay.

4.1.4. *WNT* activation measured by flow cytometry

Flow cytometry was used as an alternative method of analysing *WNT* activation. Flow cytometry is an effective, high throughput method for analysing fluorescent samples and more easily allows correction for autofluorescence than confocal microscopy. *WNT* activity in response to treatment could be assessed by comparing the amount of mCherry expressing cells that also express eGFP, which indicates active *WNT*, to the total number of mCherry expressing cells in different treatment groups (Figure 4).

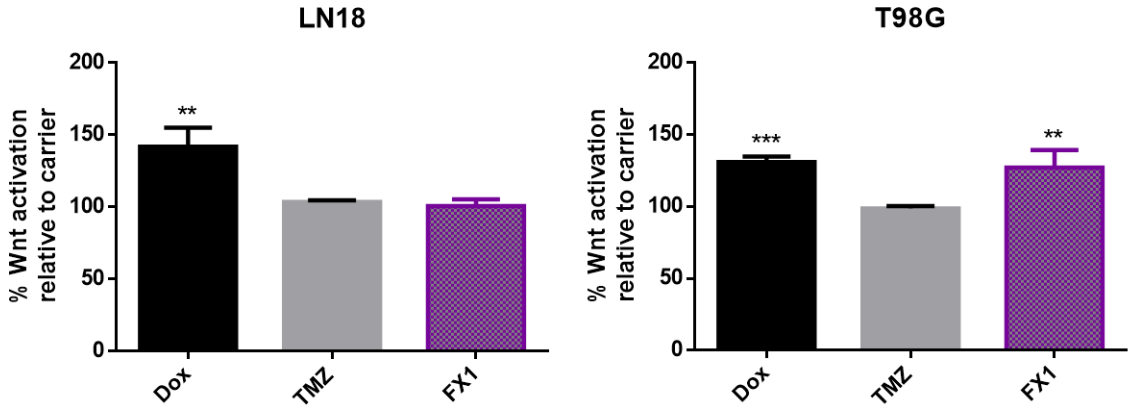

Figure 26 WNT activity in LN18 and T98G cells analysed by flow cytometry. N=3. Dox and TMZ are normalised to a PBS control. FX1 and IWP-2 (shown in purple) are normalised to a DMSO control. Error bars represent the SEM. Statistical significance was calculated using a one-way ANOVA.

WNT activation in Dox treated cells is increased by 42% and 31% in LN18 and T98G cells respectively. This increase in *WNT* pathway activation compared to the PBS control indicates that the *WNT* pathway is involved in the cellular response to Dox. There was no significant change in *WNT* activation in response to TMZ treatment with a 3% increase and 2% decrease in LN18 and T98G cells respectively.FX1 treatment resulted in no change in *WNT* activity compared to the DMSO control in LN18 cells, but a significant increase of 27% in *WNT* activity was observed in T98G cells.

4.1.1. Discussion

The aim of this chapter was to assess changes in intracellular canonical *WNT* activity in glioblastoma cell lines in response to treatment with chemotherapeutics and inhibition of *BCL6*.

The canonical *WNT* signalling pathway is β-catenin dependent and is essential in cell fate determination during development, and stem-cell renewal (Komiya & Habas, 2008). *WNT* signalling is also involved in cell-cell adhesion as β-catenin is an important cell surface adhesion molecule (Komiya & Habas, 2008). The loss of cell-cell adhesion is a key step in cancer cell invasion (Bienz, 2005; Heuberger & Birchmeier, 2010) and has been heavily linked to *WNT* signalling. The way glioblastoma invades along the vasculature into the normal brain tissue making its borders diffuse is why it near impossible to resect all cells during tumour removal without the loss of too much healthy brain tissue (Paw et al., 2015).

A reporter assay was used to measure the levels of intracellular canonical *WNT* in response to treatment. This would provide insight into the response of the canonical *WNT* pathway to treatment with chemotherapeutics. It would also provide a link, if any to the *BCL6* protein by testing for any changes in *WNT* activation levels upon inhibition of the *BCL6* protein.

This reporter assay used the 7TGC plasmid transfected into two glioblastoma cell lines. The 7TGC plasmid has constitutive expression of the fluorescent protein mCherry, which acts as a transfection marker. It also has 7 binding sites for TCF, which is a *WNT*-activated transcription factor, followed by an eGFP sequence. Upon activation of canonical *WNT*, the eGFP would be expressed, and the levels of activation in a cell population would be measurable. TCFs are transcription factors that bind DNA within the nucleus along with β-catenin upon activation of the canonical *WNT* pathway making them a great target to measure canonical *WNT* signalling (Fuerer & Nusse, 2010).

IWP-2, a small molecule inhibitor of the *WNT* pathway was tested using the 7TGC reporter assay. IWP-2 works through inhibiting the PORCN protein which is essential in the glycosylation of *WNT* proteins and their translocation out of the nucleus (Chen et al., n.d.; Proffitt & Virshup, 2012). No change in eGFP expression was seen in response to this

treatment. This unexpected result is likely due to the eGFP reporter of *WNT* activity. eGFP has a long-lasting expression (G. Zhang, Gurtu, & Kain, 1996) and although there may have been a decrease in *WNT* activity, there would not have been an instantly detectable decrease in eGFP from the basal level before treatment.

Initially it was attempted to measure *WNT* activation using the confocal microscope to image and analyse *WNT* activation. The confocal microscope had a suitable laser and filter set to excite and image both the mCherry and eGFP fluorophores and was accessible for use. While imaging the transfected, treated cells, it was observed that Dox has an autofluorescence in both channels used to excite the mCherry and eGFP. This phenomenon has been documented recently (Motlagh et al., 2016) and although it was attempted to correct for this, it was decided that flow cytometry would be a better, more high throughput method to collect this data. The correction for this using flow was much simpler than microscopy. While the entire population was shifted in basal fluorescence intensity, the transfected cells could easily be distinguished from the autofluorescence of the Dox.

Treatment with Dox showed a 1.3 to 1.4-fold increase in activation of the canonical *WNT* pathway in this assay. This is consistent with our RNA-seq data showing upregulation of canonical *WNT* transcripts in response to treatment with Dox, which indicates that the canonical *WNT* pathway is important in the cellular response to Dox. Dox acts by intercalating into the double helix of the DNA which in turn prevents the topoisomerase II-mediated double stranded break repair. This results in double stranded breaks in the DNA thereby activating the DNA damage response pathway. Doxorubicin also generates free radicals which damage DNA, proteins, and cell membranes (Thorn et al., 2011) . Past research has shown that there is a large amount of crosstalk between the *WNT* pathway and the DNA damage response pathway (Karimaian, Majidinia, Bannazadeh Baghi, & Yousefi, 2017). After DNA damage, the activation of the P53 tumour suppressor initiates DNA repair. P53 has other targets, one of which is the *WNT* pathway (Karimaian et al., 2017). P53 is involved in the ubiquitination of β-catenin (K.-H. Lee et al., n.d.). This ubiquitination and degradation of β-catenin reduces the activation of canonical *WNT*, so it seems that it would not be through this mechanism that *WNT* activation is increased. Several mechanisms have been suggested as to

how Dox treatment increases intracellular ROS levels, including mitochondrial NADH-dehydrogenase reducing Dox to produce an unstable semiquinone which then donates an electron to oxygen resulting in the formation of a superoxide radical (Davies & Doroshow, 1986). Another suggestion is that Dox treatment is linked to an increase in iron concentration in the mitochondria which makes the REDOX cycle ineffective resulting in an increase of ROS released (Ichikawa et al., 2014). *WNT* activation has separately been linked to an increase in ROS production through β-catenin however the mechanism for this has not been elucidated (Dai et al., 2009). More research into this area would be pertinent as although another study also showed that treatment with Dox resulted in the induction of canonical *WNT* signalling (Dai et al., 2009), no information on the mechanism of this increase in canonical *WNT* signalling has been found.

An increase in canonical *WNT* signalling in response to inhibition of *BCL6* by FX1 was observed in the T98G cells, but not the LN18 cells. The FX1 effect was not as strong as the Dox effect in *WNT* activation and was only present in T98G cells. *BCL6* has been shown to be a repressor of the *WNT* pathway (Katia Basso & Dalla-Favera, 2010) and therefore it would be logical that inhibition of *BCL6* would result in an upregulation of *WNT* signalling.

No difference in activation of canonical *WNT* signalling was observed in response to treatment with TMZ. This indicates that the response of the cell to the damage caused by TMZ does not involve the canonical *WNT* pathway. This result could however have been affected by the difficulties in using TMZ in vitro, TMZ is a prodrug, and cells in vitro have lowered ability to convert TMZ from the prodrug for to the active form in an in-vitro environment as opposed to an in-vivo one (J. Zhang et al., 2012).

The lack of difference of activation of canonical WNT signalling in conjunction with the WNT inhibitor IWP-1 showing no difference in levels of reporter, it is possible that the reporter assay was not working.

5. Results III: The effect of chemotherapy and *BCL6* inhibition on *WNT*-related cell functions.

The *WNT* pathways play a major role in many aspects of cell morphology and function (Komiya & Habas, 2008). This chapter aims to look the effect of *BCL6* inhibition and chemotherapeutic treatment on migration, the cell cycle, and clonogenicity and what this means in relation to *WNT* signalling.

5.1. Migration Assay

Cellular migration is essential for development and is largely controlled by the planar cell polarity *WNT* pathway. The canonical *WNT* pathway regulates cell polarity and cell-cell adhesion through β-catenin, which functions not only as an intracellular signalling molecule, but also as a cell-cell adhesion protein (Schambony & Wedlich, 2013; Sedgwick & D 'souza-Schorey, 2016). Dysregulation of these pathways results in increased migratory ability of these cells and is a potential driver of carcinogenesis and is responsible for the diffuse nature of glioblastoma (Claes et al., 2007). The non-canonical *WNT* pathways are important in cytoskeletal rearrangements and migration, cell fate and polarity. Both the canonical and noncanonical *WNT* pathways are involved in carcinogenesis (Gó Mez-Orte, Sá Enz-Narciso, Moreno, & Cabello, 2013).

Inhibition of the anti-apoptotic protein *BCL6* by FX1 increases activation of the canonical *WNT* pathway in T98G cells (Figure 26). In RNA-seq data from FX1 treated cells, both canonical and non-canonical transcripts underwent changes in expression. The influence chemotherapy and *BCL6* have on non-canonical pathways was explored using a migration assay to test the

ability of two migratory glioma cell lines to re-enter a wound in a cell monolayer under chemotherapeutic treatment and *BCL6* inhibition.

5.1.1. Cell Cycle Analysis

The migration assay was designed to analyse the speed of cell migration under different treatment conditions. If *BCL6* influences the *WNT* pathway, it is expected that migration may be affected by *BCL6*. To confirm that only migration, not replication, was being measured, the cells were starved for 24 hours prior to wounding the cell monolayer to ensure that starvation of FCS resulted in a block in the cell cycle and therefore block in replication. A minimal concentration of FCS (0.1%) was used to supplement the media post-wounding to allow for enough sustenance for the cells to carry out essential functions, but not enough for replication.

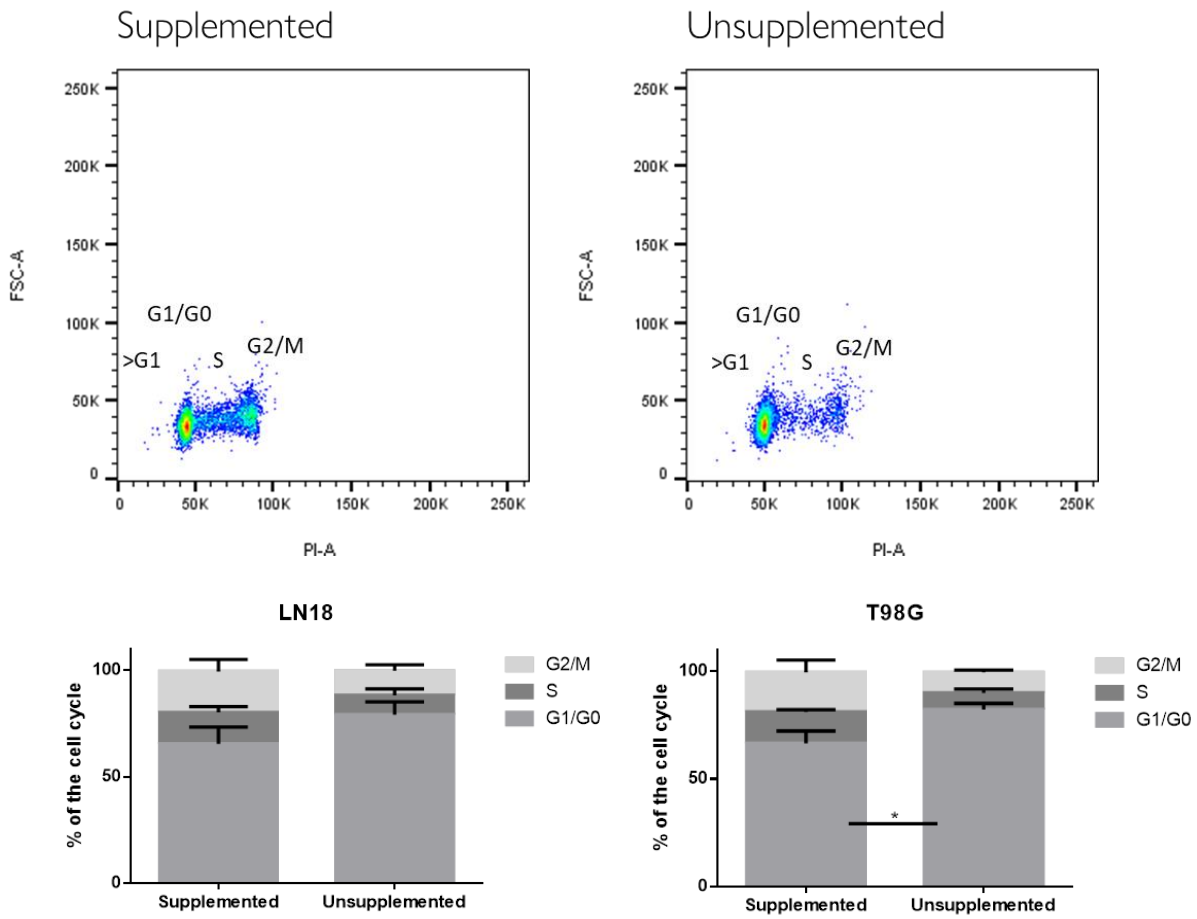

Figure 27 Cell cycle analysis of cells starved for 24 hours. A. Representative cell cycle plots showing a decrease in proportion of cells in G2/M via decrease in DNA content – PI fluorescence is directly proportionate to DNA content. B. Bar graphs of the average of cells in each proportion of the cells cycle across three replicates. N=3. Error bars represent the SEM.

As can be seen in Figure 27, a G1/G0 cell cycle block is present in both unsupplemented LN18 and T98G cells. In T98G cells there was an increase of 15% in the G1/G0 phase and decreases of 7% and 8% in the S phase and G2/M phase respectively. For LN18 cells there was an increase of 13% in G1/G0 phase and decreases of 6% and 9% in the S phase and G2/M phase respectively. There is a significant difference between the proportion of cells in G1/G0 in supplemented vs. unsupplemented in T98G cells. These results indicate that the 24-hour starvation period before the wound is made in the scratch assay successfully results in a halt in replication and therefore migration should be the only cause of movement into the wounded area of the monolayer.

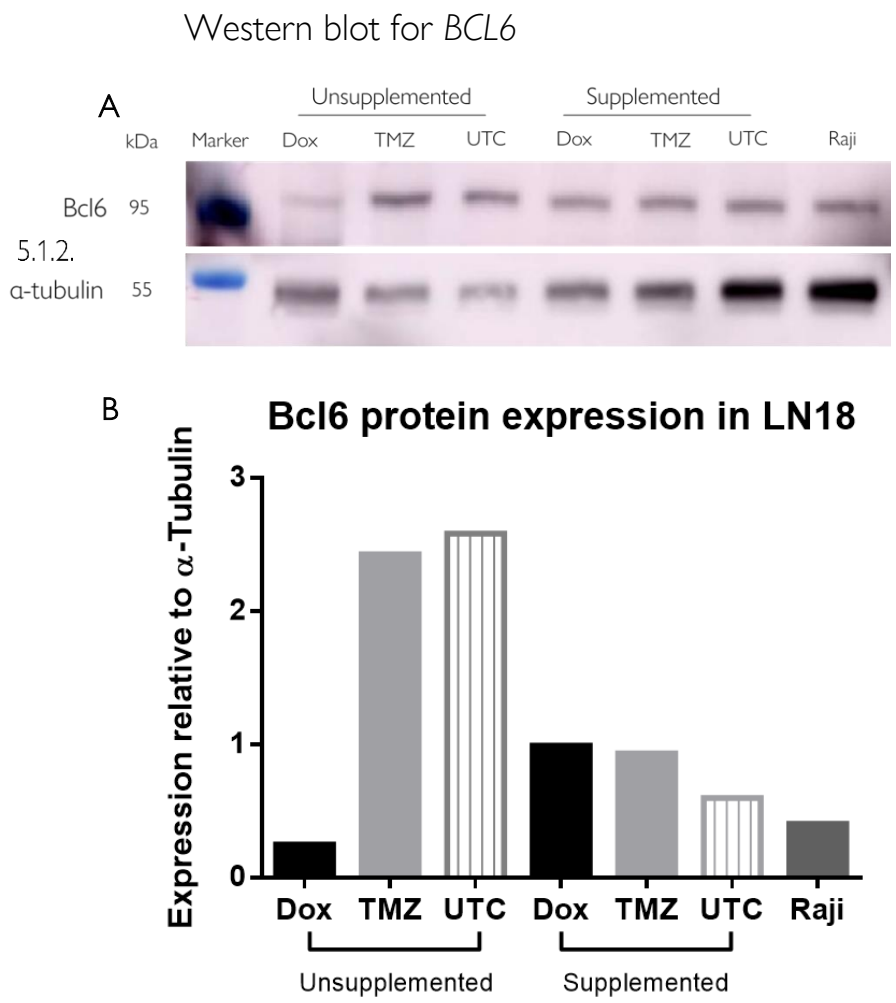

Figure 28 Western blot for BCL6 expression in LN18 cells. N=1. A. Protein blot for BCL6. B. Quantification of BCL6 relative to α-tubulin loading control.

It was important to confirm that under starvation conditions, cells still produced the *BCL6* protein. To test this, cells were incubated in RPMI and supplemented with either 5% FCS or unsupplemented. Cells were then lysed, and protein was extracted for western blot analysis. *BCL6* was expressed in cells cultured in both FCS supplemented and unsupplemented media (Figure 28A). The difference between treatment groups may have been due to uneven antibody staining as opposed to changes in *BCL6* protein expression and therefore more replicates of this western blot in LN18 cells, and a western blot in T98G cells run under the same conditions would be appropriate.

5.1.3. Migration assay

Migration is largely regulated by the *WNT* pathway. Migration plays a large role in the invasiveness of GBM and therefore has a role in recurrence due to cancer cells remaining in the brain post-resection (Y. Lee et al., 2016). A migration assay was performed to determine whether *BCL6* inhibition or treatment with chemotherapeutics plays a role in cell migration and therefore *WNT* signalling. The migratory ability of both LN18 cells and T98G cells when treated with chemotherapeutics, and when *BCL6* is inhibited was measured. Cells were treated with chemotherapeutic and either the *BCL6* inhibitor, FX1, or its carrier DMSO. Migration was measured over a 17-hour period and the difference in area gained by the cells was compared between treated and control wells.

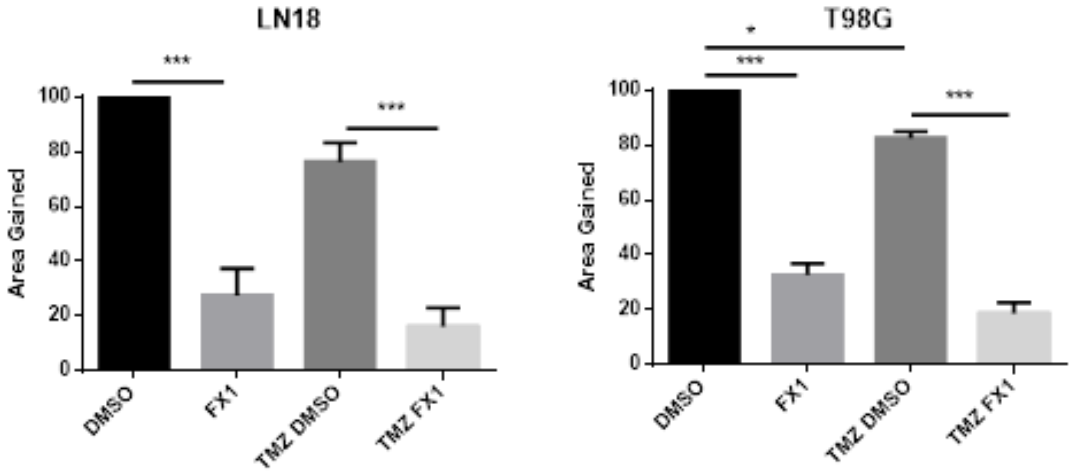

Figure 29 Migration in TMZ and FX1 treated LN18 and T98G cells.

*Migration is displayed as area gained over a 17-hour period. Cells were treated with 400 μM TMZ, and 60 μM FX1 or 0.24% DMSO. N=3. Error bars represent the SEM. * p-value less than 0.05 ** p-value less than 0.01 *** p-value less than 0.001*

In both cell lines, FX1 treatment resulted in a significant decrease of migration in comparison to the DMSO control (Figure 29). FX1 treated cells migrated only 27.6% the of the distance migrated by the control cells in LN18 cells, whereas T98G cells migrated 32.7%. TMZ treated cells migrated 76.4% and 82.7% in LN18 and T98G cells respectively. Cells treated with both

TMZ and FX1 migrated 16.2% of the DMSO control in LN18 cells, and 18.7% in T98G cells. The difference in migration between the TMZ only treated, and the TMZ and FX1 combined treatment was statistically different in both cells lines.

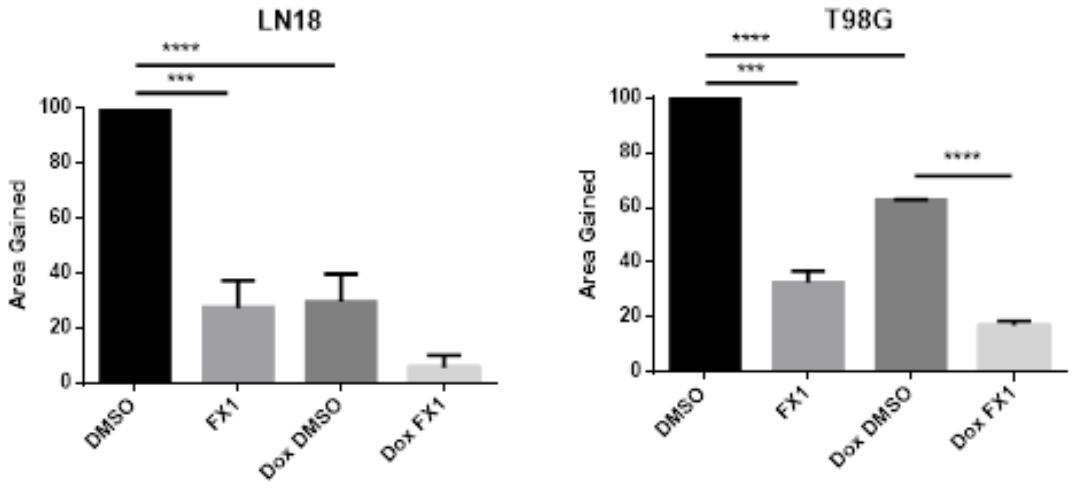

Figure 30 Migration in Dox and FX1 treated glioma cells. Migration is displayed as area gained over a 17-hour period. Cells were treated with 3 μM Dox and 60 μM FX1. N=3. Error bars represent the SEM.

Dox treated cells migrated 29.7% distance of the DMSO control cells in LN18 cells, and 62.9% as far in T98G cells. Under Dox and FX1 combined treatment conditions, cells migrated 5.9% and 17% as far as DMSO control cells. The difference in migration between Dox only and Dox and FX1 combination treated cells was statistically significant in T98G cells but not in LN18 cells. When the combined effect of two compounds is greater than their predicted additive effect, the compounds are said to be synergistic. Synergy can be beneficial as it minimizes the amount of a drug required to achieve the therapeutic effect (Tallarida, 2011) or to decipher whether two drugs are acting in the same or different pathways. Were the drugs to be synergistic, it could be assumed that they were working on different pathways. An additive effect can indicate that the drugs are working on the same pathway (R. Friedman, 2006; Pérez-Pérez, Candela, & Micol, 2009). FX1 and Dox both had a large effect on migration whereas TMZ has a smaller effect. The combination therapy of both Dox with FX1 and TMZ with FX1 resulted in a further decrease in migration.

	Migration relative to carrier				
	F	D + D	D + F	T + D	T + F
LN18	27.60%	29.70%	5.90%	76.40%	16.20%
T98G	32.70%	62.90%	17%	82.70%	18.70%

100 – area gained = effect of drug

A

	Effect of drug on migration				
	F	D + D	D + F	T + D	T + F
LN18	72.40%	70.30%	94.10%	23.60%	83.80%
T98G	67.30%	37.10%	83%	17.30%	81.30%

B

$$CI = \frac{E_A + E_B}{E_{AB}}$$

CI < 1 : Synergy
CI = 1 : additive effect
CI > 1 : Antagonism

C

	CI: D + F	CI: T + F
LN18	1.52	1.15
T98G	1.26	1.04

Figure 31 Combination index calculation. A. Conversion of area gained to effect of drug. B. CI = combination index. E_A = Effect of Drug A. E_B = Effect of drug B. E_{AB} = Effect of combination of A and B. C. Combination index for Dox + FX1 and TMZ + FX1 in LN18 and T98G cells.

A calculation was applied to the results of the migration assay to assess whether the combination of Dox or TMZ and FX1 was synergistic, additive, or antagonistic (Foucquier & Guedj, 2015). The area gained is the inverse of the effect the drug had on migration, so first the inverse of the area gained was calculated. Next, the combination index was calculated from these values. The value calculated by the combination index indicates the type of effect the drug combination has. The combination index for the drug combinations of Dox and TMZ with FX1 in both glioma cell lines showed a CI higher than 1 and therefore a 'less than additive', or an 'antagonistic' effect between the two drugs.

5.1.4. Migration assay in long term chemotherapy treated cells

The long-term, low dose chemotherapy treatment of LN18 and T98G cells had a large effect on cell health and made the cells difficult to work with. When treated with Dox, after 2 treatments proliferation was significantly reduced and the cells became difficult to maintain. Due to the fragile nature of the long term Dox treated cells, only one replicate was successfully carried out for this migration assay.

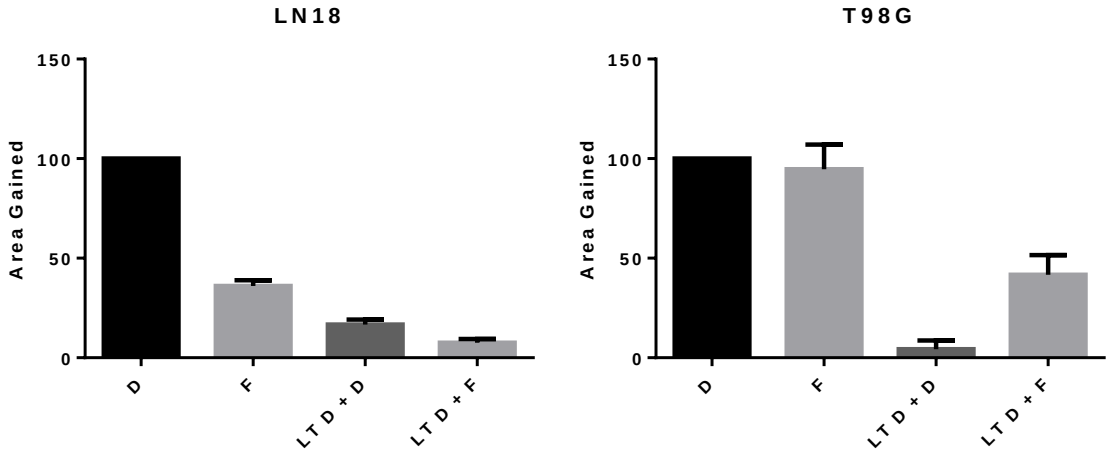

Figure 32 Migration in long term, low dose Dox treated glioma cells. Cells were treated with 15 nM Dox every two days for 14 days. These cells were treated with 25 µM FX1. N=1. Key: DMSO (D) FX1 (F) Long term treated Dox (LT D). Error bars represent the SEM.

In LN18 cells, FX1 treatment resulted in cells migrating 36% relative to the DMSO control (Figure 32). The Long term Dox treatment resulted in a large reduction of cell migration compared to DMSO with only 16.7% of the relative area covered by the LT treated cells. The combination treatment of LT Dox and FX1 resulted in a migration of 7.5% relative to the DMSO control. FX1 treatment reduced cell migration by an unexpectedly small margin in T98G cells. Cells migrated 94.6% of the area gained by the DMSO control. As these cells were only treated in the short term, it would be accurate to compare these cells and their migration to the cells in the migration assay shown in Figure 29 where FX1 inhibited migration in T98G cells by a large margin relative to the DMSO only treated cells. The long term treated Dox cells showed near complete inhibition of migration with only 4.3% of the migration relative to the DMSO control. The combination treatment resulted in migration of 42% of the DMSO control.

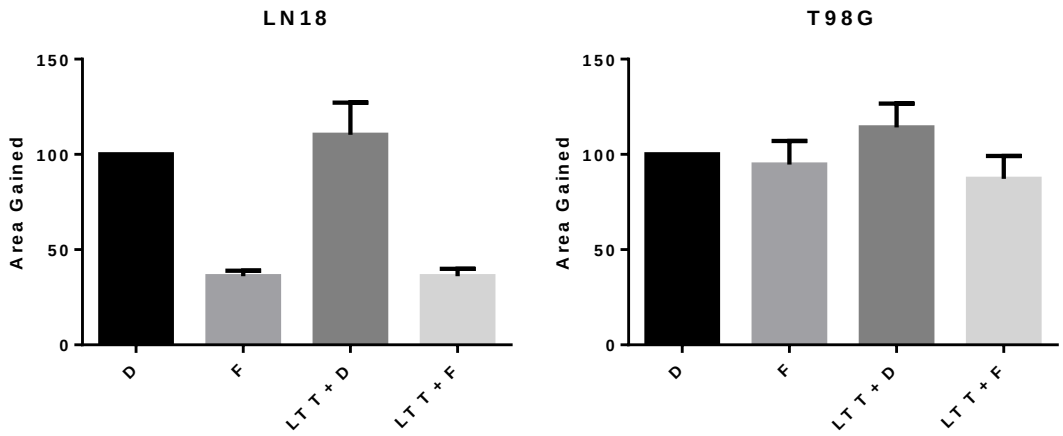

Figure 33 Migration in long term, low dose TMZ treated glioma cells. Cells were treated with 10 nM TMZ every two days for 14 days. These cells were treated with 25 μM FX1. Key: DMSO (D) FX1 (F) Long term treated TMZ (LT T). N=1. Error bars represent the SEM. These results were not statistically significant.

Long-term treatment of TMZ resulted in an increase in migration relative to the DMSO control, with an area gained of 110.3% and 114% relative to the DMSO control in LN18 and T98G cells respectively (Figure 33). This is the opposite of the effect observed in the short term treated cells which was unexpected. Long term treatment with TMZ is the current treatment used clinically for glioblastoma and an increase in migration in response to this could increase the likelihood of re-occurrence of a tumour post-resection. The combination treatment of LT TMZ and FX1 resulted in a large decrease in migration, with 36.1% area gained relative to the DMSO control in LN18 cells. T98G cells showed a modest decrease with FX1 treated cells migrating 87.1% of the migration of cells treated with DMSO (Figure 33).

	Migration relative to carrier				
	F	LT D + D	LT D + F	LT T + D	LT T + F
LN18	36.00%	16.70%	7.50%	110.30%	36.10%
T98G	94.60%	4.30%	42%	114.00%	87.10%

100 – area gained = effect of drug

A

	Effect of drug on migration				
	F	LT D + D	LT D + F	LT T + D	LT T + F
LN18	64.00%	83.30%	92.50%	-10.30%	63.90%
T98G	5.40%	95.70%	58.30%	-14.00%	12.90%

B

$$CI = \frac{E_A + E_B}{E_{AB}}$$

CI < 1 : Synergy
CI = 1 : additive effect
CI > 1 : Antagonism

C

	CI: LT D + F	CI: LT T + F
LN18	1.592	0.841
T98G	1.734	-0.667

Figure 34 Combination index calculation in LT treated cells. A. Conversion of area gained to effect of drug. B. CI = combination index. E_A = Effect of Drug A. E_B = Effect of drug B. E_{AB} = Effect of combination of A and B. C. Combination index for LT Dox + FX1 and LT TMZ + FX1 in LN18 and T98G cells.

Calculations to test for synergy between the long-term treatment of Dox and TMZ in conjunction with FX1 treatment were carried out as described in section 5.1.3 and Figure 34. The CI showed that there was a less than additive effect or an 'antagonistic' effect on migration under combination treatment with FX1 and LT Dox treatment. A synergistic effect was seen in cells under combination treatment conditions with FX1 and LT TMZ. This effect however is questionable due to the increased migration seen in LT TMZ treated cells.

5.2. Cell cycle

There is evidence of a complex interaction between canonical *WNT* signalling and the cell cycle. Mitogenic *WNT* signalling promotes G1 phase of the cell cycle and canonical *WNT* pathway has a direct effect on gene regulation in spindle formation and cytoskeletal changes in mitosis (Davidson, 2010). *BCL6* targets many genes involved in the cell cycle and the DNA damage response (Cerchietti, Figueroa, Shaknovich, & Melnick, 2006). Cell cycle analysis was used to assess if treatment with chemotherapeutics or FX1 had an influence on the cell cycle.

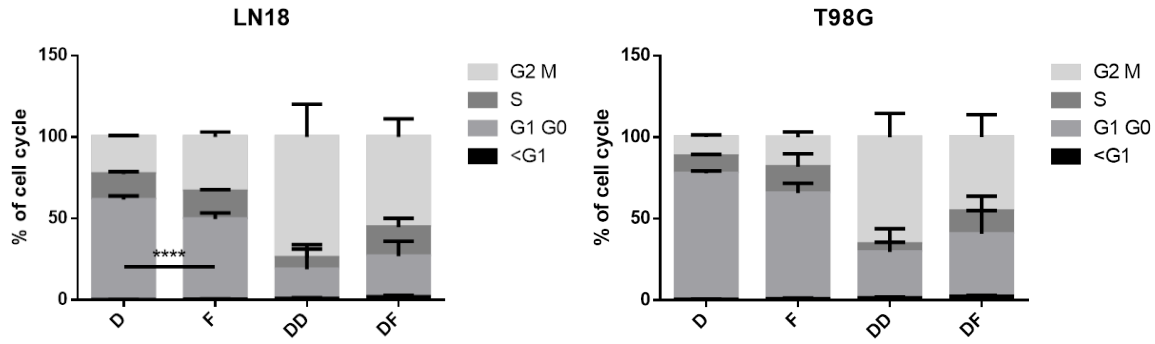

Figure 35 The effect of 300 nM of Doxorubicin and 60 μM of FX1 on the proportion of cells in each phase of the cell cycle. N=3. Error bars represent the SEM. Key: DMSO (D), FX1 (F), Dox and DMSO (DD), Dox and FX1 (DF).

Inhibition of *BCL6* results in a small accumulation of cells in the G2/M phase of the cell cycle. This indicates that *BCL6* influences cell cycle regulation. The effect is larger in LN18 cells with an 11% increase in cells in G2/M, than in T98G cells, which shows a 7% increase in cells in G2/M.

In Dox treated cells, there is a large accumulation of cells in the G2/M phase with a difference of 52% between Dox treated and DMSO control in LN18 cells. In T98G cells, this difference is 54%.

The combination of Dox and FX1 treatments showed a rescue effect of cell cycle inhibition as the proportion of cells in the G2/M phase of the cell cycle is decreased compared to the Dox treated cells. There is a decrease of 19% in LN18 cells and 20% in T98G cells.

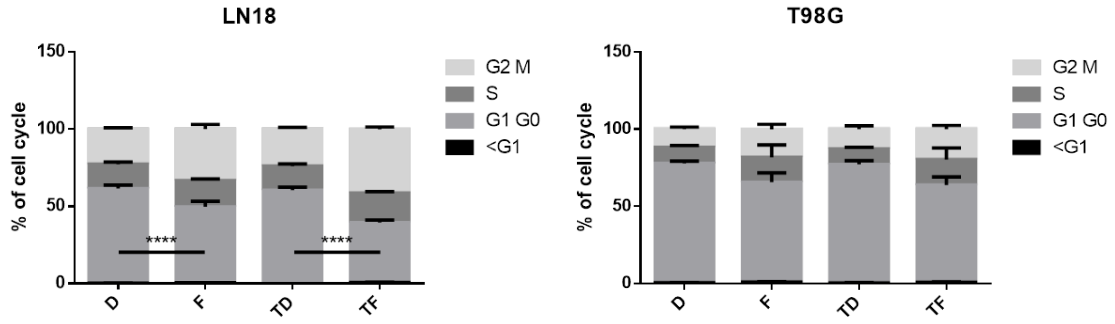

Figure 36 The effect of 400 μM Temozolomide and 60 μM of FX1 on the proportion of cells in each phase of the cell cycle. Key: DMSO (D), FX1 (F), Dox and DMSO (DD), Dox and FX1 (DF). N=3. Error bars represent the SEM.

Treatment with TMZ had very little effect on the cell cycle in either cell line. Proportions were negligibly different from the DMSO control with a 1% difference in both cell lines. The combination treatment of TMZ and FX1 had an increase in the proportion of cells in the G2/M phase of the cell cycle of 17% in LN18 and 7% in T98G cells. The difference between the cells treated with FX1 only and the combination of TMZ and FX1 had a negligible difference in the proportion of cells in the G2/M phase in T98G cells with a difference of 1%. In LN18 cells the difference was higher than in T98G cells, with 8% more cells in the G2/M phase in TMZ and FX1 combined treated cells than in FX1 treatment alone.

5.3. Clonogenic assay

The clonogenicity of a cell measures the effectiveness of a treatment in analysing the long-term viability of a cell. The ability of a cell to continue to grow and divide post-treatment is an important factor in tumour relapse after resection. Glioblastoma is usually removed from the brain via surgical resection and the area is treated with both TMZ and radiation to impede the cancer's ability to regrow (Stupp et al., 2005).

Clonogenic assays were carried out to analyse the long-term viability and the ability of cells to re-attach and form colonies after treatment with chemotherapeutics. Cells were also treated with FX1 to test whether the inhibition of *BCL6* may increase the effectiveness of the chemotherapeutic, resulting in a decreased ability to form colonies. Cells were treated with 25 μM FX1, and 60 μM FX1. As described in section 0, the original dose of FX1, which has been historically used within our lab group was found to be less effective in the batch used for this project than the previous batch. A concentration of 60 μM was found to have a similar effect to a 25 μM dose from the previous batch, therefore this experiment was carried out using both doses of FX1. During the course of this experiment, it was discovered that Dox is an incredibly effective chemotherapeutic and when cells were treated with a 3 μM, the standard dose for other experiments, the plating efficiency was 0%. It was therefore decided to reduce the dose to get a result for Dox treated cells. The dose was reduced to 300 nM, a 10-fold decrease in concentration.

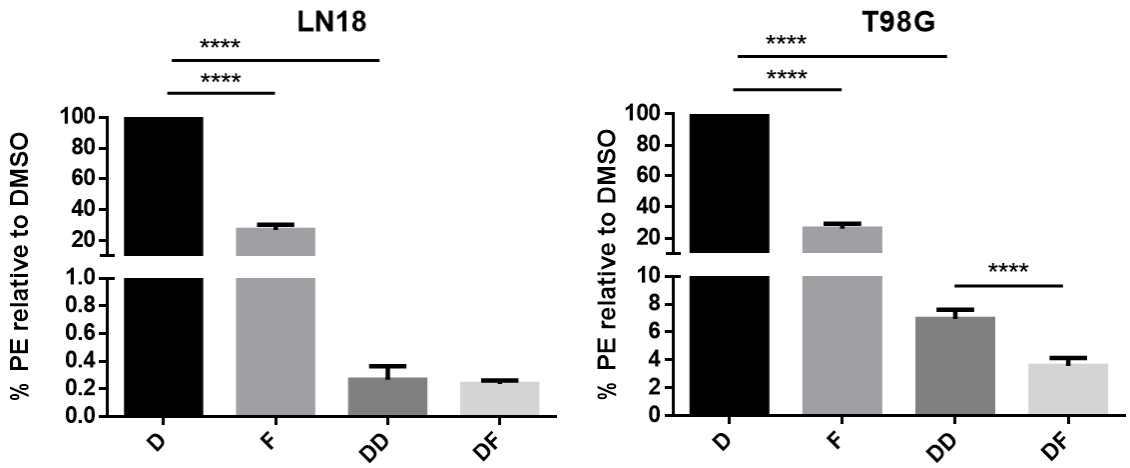

Figure 37 The plating efficiency of LN18 and T98G cells after treatment with 300 nM Doxorubicin and 60 μM FX1.

Key: DMSO (D), FX1 (F), Dox and DMSO (DD), Dox and FX1 (DF). N=3. Error bars represent the SEM. Statistical analysis was carried out using a one-way ANOVA.

Inhibition of *BCL6* results in a significant decrease in clonogenicity for both LN18 and T98G cells with 26.1% and 26.8% clonogenicity respectively. Treatment with Dox resulted in a significant decrease in clonogenicity in both cell lines. The combination treatment of Dox and FX1 resulted in a further decrease in the clonogenicity of both cell lines.

In LN18 cells, Dox treatment alone resulted in a clonogenicity of 0.27% of the PE relative to the DMSO control. There was no difference seen between the Dox alone and Dox with FX1 treatments.

In T98G cells, Dox treatment resulted in a relative PE of 7%. In the combination treatment group of Dox and FX1, a relative PE of 3.6% was observed. This is a significant decrease from Dox treatment alone.

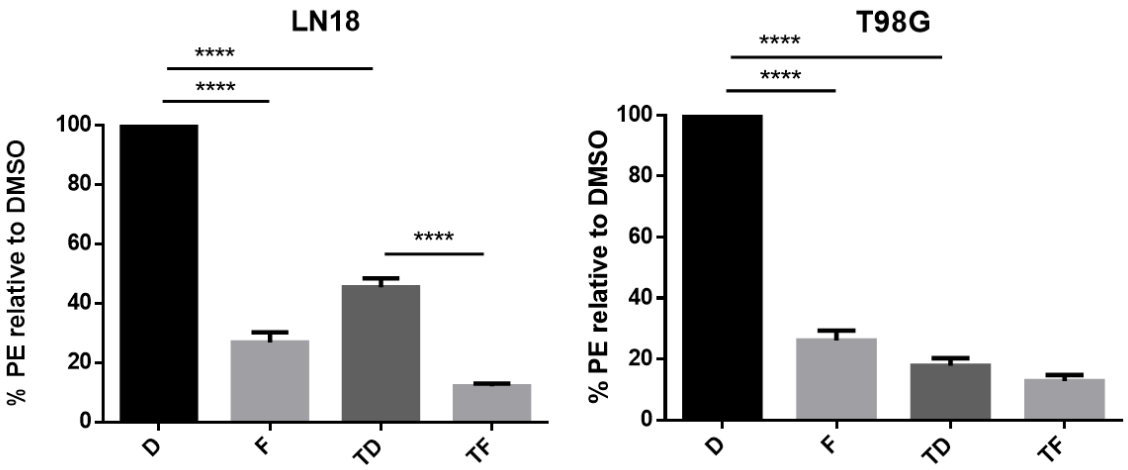

Figure 38 The plating efficiency of LN18 and T98G cells after treatment with 400 μM Temozolomide and 60 μM FX1. Key: DMSO (D), FX1 (F), TMZ and DMSO (TD), TMZ and FX1 (TF). N=3. Error bars represent the SEM. Statistical analysis carried out using a one-way ANOVA.

TMZ treatment significantly decreased clonogenicity in both cell lines, with a PE relative to control of 45.4% in LN18 cells and 17.8% in T98G cells. Combination treatment of TMZ and FX1 further reduced clonogenicity in both cells lines, but to a larger degree in LN18 cells. A significant decrease was seen with the combination treatment reducing the clonogenicity to 12.2% of the control. The combination treatment further reduced clonogenicity of T98G cells to 12.8% of the control however this difference between TMZ alone and TMZ and FX1 combination treatment was not statistically significant.

	Clonogenicity relative to carrier				
	F	LT D + D	LT D + F	LT T + D	LT T + F
LN18	26.80%	0.27%	0.24%	45.40%	12.00%
T98G	26.10%	6.95%	4%	17.80%	12.80%

100 – clonogenicity = effect of drug

A

	Effect of drug on clonogenicity				
	F	LT D + D	LT D + F	LT T + D	LT T + F
LN18	73.20%	99.73%	99.76%	54.60%	88.00%
T98G	73.90%	93.05%	96.00%	82.20%	87.20%

B

$$CI = \frac{E_A + E_B}{E_{AB}}$$

CI < 1 : Synergy
CI = 1 : additive effect
CI > 1 : Antagonism

C

	CI: LT D + F	CI: LT T + F
LN18	1.733	1.452
T98G	1.739	1.79

Figure 39 Combination index of clonogenicity. A. Conversion of clonogenicity to effect of drug. B. CI = combination index. E_A = Effect of Drug A. E_B = Effect of drug B. E_{AB} = Effect of combination of A and B. C. Combination index for Dox + FX1 and TMZ + FX1 in LN18 and T98G cells.

The combination index calculated using the method described in Figure 39 was applied to the clonogenicity data. The CI for treatment with Dox or TMZ and FX1 showed a value greater than 1, therefore a 'less than additive' or 'antagonistic' effect.

5.4. Discussion

The influence of *BCL6* and chemotherapy on the physiological aspects governed by the non-canonical *WNT* pathway was explored in this chapter. These pathways regulate cell polarity, cytoskeletal rearrangements, cell migration, and cell fate during development (Gó Mez-Orte et al., 2013). Dysregulation of these pathways can be a driver of carcinogenesis (Suwala, Hanaford, Kahlert, & Maciaczyk, 2016; Wu et al., 2012). Analysis of migration, clonogenicity, and the cell cycle in response to chemotherapeutic treatment and inhibition of *BCL6* was carried out. Migration is largely governed by the non-canonical *WNT* pathway and is critical in cancer cell invasion into surrounding tissues (Gó Mez-Orte et al., 2013; Y. Lee et al., 2016). Clonogenicity is a measure of the long-term survival and replicative ability of cells post treatment. This is important in re-occurrence of a tumour after resection, TMZ treatment and irradiation. It has been observed that *WNT* inhibition reduces clonogenicity in glioblastoma (Kahlert et al., 2015).

Migration is an important factor in the recurrence of GBM as it is responsible for the cellular invasion of the neighbouring healthy brain tissue and therefore the diffuse borders of GBM. These diffuse borders make complete resection of cancerous tissue impossible without removing healthy brain tissue and hindering function of the organ itself. Migration was measured to assess the influence of DNA damaging chemotherapy and *BCL6* inhibition. Replication was blocked by incubation in unsupplemented RPMI to make sure that only migration was measured (Figure 27). Migration in response to short term treatment with chemotherapeutic agents was reduced significantly in both TMZ and Dox treated cells, however to a larger extent in response to Dox treatment. Dox has been shown to induce p53 activation, which induces cytoskeletal rearrangements and inhibits proliferation and migration (Brum et al., 2013). Migration in response to *BCL6* inhibition by FX1 was significantly reduced showing that *BCL6* does have an influence on migration, and by extension, the *WNT* pathway. The combination of TMZ and FX1; and Dox and FX1 resulted in a reduction in migration, but this effect was less than additive. A less than additive effect, or an 'antagonistic' effect can indicate that the compounds are working within the same pathway or that there is

some sort of responsive regulation happening to correct for the inhibition of migration caused by these compounds (Yin et al., 2014). Long term Dox treatment resulted in a large decrease in migration, effectively halting migration altogether. The addition of FX1 to the LT Dox treatment also resulted in a halt in migration. The LT TMZ treatment resulted in an increase in migration relative to the DMSO control. This effect has been seen in previous literature (Stepanenko et al., 2016) but it does bring into question the effect of clinical long term TMZ treatment in patients on GBM migration (William, Walther, Schneider, Linnebacher, & Classen, 2018). The addition of FX1 to the LT treated TMZ cells resulted in a decrease in migration relative to control, however due to the increase in migration seen in the LT TMZ treated cells alone, the model to calculate synergy did not apply.

The migration data shows that *BCL6* plays a role in migration and is potentially involved in regulating the *WNT* pathway. Dox treatment was also shown to have a substantial effect on migration, with Dox treatment under more clinical, long term treated conditions results in a complete halt in migration. TMZ has a small effect on migration and therefore likely the *WNT* pathway. There is potentially an autoregulatory pathway correcting for the inhibition caused by this combination treatment (Yin et al., 2014).

The cell cycle is tightly regulated to maintain cellular and genetic integrity throughout replication. There are checkpoints at each phase of the cell cycle to survey progress, and ensure there are no problems before the cell can progress to the next stage of the cycle (Baserga, 1981). Physical division of the replicated daughter cells relies on restructuring of the cytoskeleton to split the cell in two, and to form the spindle in mitosis. Alterations of the cytoskeleton are regulated by *WNT* signalling (Akiyama & Kawasaki, 2006; Dai et al., 2009; Sedgwick & D 'souza-Schorey, 2016). *WNT* is involved in many aspects of the cell cycle through direct and indirect mechanisms (Bryja, Červenka, & Čajánek, 2017). The β-catenin dependent arm of the *WNT* pathway has been shown to oscillate in time with the cell cycle, and controls the transcription of C-myc and cyclin D (Davidson & Niehrs, 2010). The CDK14/cyclinY complex promotes *WNT* signalling by phosphorylating LRP6 (D. Liu et al., n.d.). A few of the mechanisms of interplay between the cell cycle and the *WNT* pathway have been mentioned

above, but this interaction is much more complex than our current understanding. The proportion of cells in each phase of the cell cycle can be measured by flow cytometry. When stained with PI, a fluorescent, intercalating dye, DNA content in each cell can be measured by fluorescence. The more DNA, such as during S-phase the greater the fluorescence emitted by the cell (Pozarowski & Darzynkiewicz, 2004). Using this methodology, cells treated with DNA damaging chemotherapeutics and FX1 were analysed, and proportions of cells in each phase of the cell cycle were assessed. Dox treatment resulted in a large G2/M accumulation. FX1 treatment caused a small accumulation of cells in the G2/M phase suggesting possible regulation of the cell cycle by *BCL6* (Phan, Saito, Basso, Niu, & Dalla-Favera, 2005). Dox treatment leads to p53 activation, G2 arrest and increase in apoptosis (Ling, el-Naggar, Priebe, & Perez-Soler, 1996; Lüpertz, Wätjen, Kahl, & Chovolou, 2010). Combination treatment with Dox and FX1 had a slight rescue effect on the cell cycle returning the S-phase of the cell cycle proportionally closer to the control, and the G2/M block was much smaller. This suggests that *BCL6* plays a role in the Dox effect on the cell cycle and when inhibited, that effect is minimized. *BCL6* has been shown to suppress p53 expression which could allow cell re-entry into the cell cycle therefore accounting for the minimization of the Dox effect (Phan & Dalla-Favera, 2004). TMZ treatment alone has no effect on the cell cycle, however when treated in combination with FX1, a larger effect was seen than with either TMZ or FX1 alone. This suggests some sort of interaction between thet pathways being targeted by these compounds. These results suggest that *BCL6* plays a role in the regulation of the cell cycle and inhibition of this protein increases the effectiveness of TMZ on the cell cycle.

Clonogenicity is a measure of long term survival post treatment (Franken, Rodermond, Stap, Haveman, & van Bree, 2006). The ability of a GBM cell to recolonise after treatment is essential for recurrence after resection and chemotherapeutic and radiation treatments. Recurrence is a huge problem in GBM as patients may get more time after undergoing treatment, unfortunately the tumour always grows back and GBM is always fatal (Kahlert et al., 2015; Stupp et al., 2005). Inhibition of the *WNT* pathway has been shown to decrease clonogenicity in GBM cells (Kahlert et al., 2015). Cells were treated with FX1, and chemotherapeutics Dox

or TMZ either alone or in combination with FX1 for 24 hours, then clonogenicity was measured. FX1 treatment caused a large decrease in clonogenicity showing that *BCL6* plays a role in the ability of these cells to colonise, possibly through modulation of the *WNT* pathway. Dox treatment alone resulted in a huge decrease in clonogenicity. This is likely due to the G2/M accumulation in the cell cycle data above. Dox halts replication and forces cells to apoptose from the multitudes of double stranded DNA breaks caused by the intercalation and inhibition of topoisomerase II (F. Yang, Teves, Kemp, & Henikoff, 2014). Combination treatment with Dox and FX1 caused a further decrease in clonogenicity relative to Dox treatment alone. As *BCL6* has been shown to be upregulated in response to Dox treatment (Figure 17)(Fabre et. al. 2017), it is likely that the anti-apoptotic effects of this protein are important in maintaining cellular function after Dox treatment. Treating GBM cells with the *BCL6* inhibitor, FX1, in conjunction with Dox significantly reduces cellular survival. Treatment with TMZ alone resulted in a significant decrease in clonogenicity. This is expected as TMZ damages DNA resulting in apoptosis (J. Zhang et al., 2012). The double stranded breaks in the DNA inhibit replication and therefore reduce clonogenicity (Agarwala & Kirkwood, 2000). The combination treatment of TMZ and FX1 further reduces clonogenicity indicating that *BCL6* plays a role in the cells ability to retain clonogenicity under TMZ treatment conditions. The combination is antagonistic so there may be an autoregulatory feedback loop compensating for the loss of *BCL6* function (Yin et al., 2014).

Both Dox and TMZ combinations with FX1 resulted in an antagonistic loss of clonogenicity. This indicates that there is some sort of network compensation for the loss of *BCL6* activity when treated with DNA damaging agents.

6. Final Discussion and Conclusion

The aim of this study was to assess the impact of *BCL6* on the *WNT* pathway in treatment-resistance in GBM.

This influence was identified in RNA-seq data from cells treated with the *BCL6* inhibitor, FX1. Expression changes in important *WNT* genes were observed which suggested a possible connection between the *WNT* pathway and the action of *BCL6*. Three different angles were taken to explore this possibility. The first was a genetic approach. The changes in expression of *WNT5a* seen in the RNA-seq data were confirmed by qRT-PCR. Once these were confirmed, a cellular approach was taken. Observing changes in *WNT* expression through a *WNT* reporter assay showed that treatment with Dox increased activation of the *WNT* pathway by a large margin, as did the inhibition of *BCL6*. Dox treatment upregulates the expression of *BCL6* and activates the *WNT* pathway. This result further validated the hypothesis that a connection between *BCL6* and *WNT* exists. The third approach was to look at the physiological effect of *BCL6* inhibition on the cell which, subsequently, decreased activity of the *WNT*-related physiological processes. Taken together, these results showed that *BCL6* influences many facets of the *WNT* pathway: via gene expression changes, in the activation of the β-catenin dependent pathway, and in cellular physiological mechanisms governed by the *WNT* pathway.

There are off-target effects of FX1 (Cardenas et al., 2016). Cardenas et al. showed that FX1, used at concentrations above 10 μM, inhibited some kinases. As a concentration 2.5 times higher than this was used, it is likely that there were off-target effects of this drug in this study. The commercially available compound 79-6, another *BCL6* inhibitor, was trialled, which has inhibitory effects on *BCL6* (Cardenas et al., 2016). A dose-response was carried out on this compound (Appendix section 9.1) but no inhibition of GBM cell growth was seen in either cell line tested. This indicates that a higher concentration might be necessary to elicit an effect from this compound. However, due to its solubility of 180 mM in DMSO, to retain non-toxic levels of DMSO in growth medium (Singh et al., 2017), the highest concentration that could

be tested was 180 μM. This concentration was too low to have an effect. The compound was tested in the reporter assay but showed no effect on *WNT* activation at 180 μM. There was also no effect on gene expression. `Comparing FX1 results to another *BCL6* inhibitor would have been optimal to confirm that the results seen were due to the inhibition of *BCL6* and not any off-target effects, but the 79-6 compound was ineffective. Other approaches to silence *BCL6* have been attempted in the MMc lab group however GBM cells lacking *BCL6* appear to be inviable. Zinc finger nuclease inactivation of the *BCL6* locus was used but cells were inviable.

At the outset of this project, it was known that DNA damaging therapy induced *BCL6* expression. This study demonstrated that the same therapies also altered *WNT* gene expression, and this *WNT* gene expression was affected by the inhibition of *BCL6*. This study showed that there is an influence of *BCL6* on the *WNT* pathway. Determining whether this influence is direct or indirect will widen the range of potential therapeutic targets.

This connection found between DNA damaging chemotherapeutic treatment, *BCL6*, and the *WNT* pathway, could help elucidate the mechanisms behind GBM treatment resistance. This could ultimately contribute towards finding more effective treatment regimens for this devastating disease.

7. Future Directions

To further this study, the following experiments could be carried out:

- First, to determine the identity of the *WNT5b* qPCR products, each band could be cut from the gel, the DNA purified and the products sequenced. Designing a new primer to measure levels of *WNT5b* transcript and comparing the results to the *WNT5b* results in section 3.1.6 would give a more clear picture of the effect of these compounds on the expression of the *WNT5b* transcript.

- Carrying out more replicates of the western blot performed in section 5.1.2 would give a better idea of the changes in expression of the *BCL6* protein in response to incubation in unsupplemented medium.

- Using CFSE staining the replicative ability of cells grown in unsupplemented medium vs. supplemented medium would give a more solid background for the method of inhibiting replication for a successful migration assay.

- Another *WNT*-related cellular physiological aspect that could be measured would be the morphology of the cytoskeleton of cells under the treatment conditions used in this study. After treatment, cells can be stained with phalloidin, which stabilises the cytoskeleton while also staining it with AF488. This could then be viewed under a microscope and difference in cytoskeletal morphology could be measured and compared between treatment groups.

- The bioavailability of TMZ *in vitro* is much lower than *in vivo*. A way to enhance the conversion of TMZ from prodrug to active form would make *in vitro* results more reliable. TMZ spontaneously converts to active form at physiological pH. The RPMI medium used is initially at physiological pH, however as the cells excrete waste products into the medium, the pH quickly changes (ThermoFisher Scienfitic). The addition of a buffer to maintain physiological pH for longer may increase the conversion of TMZ to active form making the TMZ effect more consistent in *in vitro* studies.

- The experiments used to measure IWP-2 activity were not successful. The *WNT* reporter assay was unsuccessful likely due the eGFP reporter. The eGFP reporter protein remains fluorescent for much longer than the GFP molecule. The decrease in *WNT* signalling post treatment was not visible as the eGFP remained fluorescent after the production stimulus for the reporter was removed. A way to measure the effect of IWP-2 would be to carry out qRT-PCR using primers for genes activated by the *WNT* pathway such as Cyclin D or c-myc (Davidson et al., 2009).

- The inhibition of *WNT* genes at different levels of the *WNT* pathways and in different arms of the pathways such as *DKK1* or *WNT5a* and measuring levels of *BCL6* could give an idea of where in the *WNT* pathway *BCL6* is having an effect.

- Repeating the experiments carried out in this thesis using another *BCL6* inhibitor to confirm the results would be optimal. 79-6 was trialled however it was not successful. Other options for inhibition of *BCL6* could include over-expression of mutant *BCL6* protein, or gene editing via CRISPR or similar.

- The final experiment I would like to suggest is to investigate the increase in migration under long term TMZ treatment. This increase in migration if it were to occur *in vivo* may have an influence on patient survival. I would first suggest testing this *in vivo* in an

animal model by transplanting fluorescent GBM cells into the brain of a mouse. After allowing time for a tumour to form, treat the mouse with TMZ in a manner as similar to clinical conditions as possible. Migration into the healthy brain tissue in TMZ treated vs. untreated brains could be measured by examining brain sections using microscopy. If this effect was to be seen *in vivo* also, I would then suggest an RNA-seq experiment comparing untreated, short term TMZ treated, and long term TMZ treated cells. Using the changes in gene expression observed in these results, the mechanism behind this increase in migration could be elucidated and work could begin to prevent this effect.

8. References

Agarwala, S. S., & Kirkwood, J. M. (2000). Temozolomide, a novel alkylating agent with activity in the central nervous system, may improve the treatment of advanced metastatic melanoma. *The Oncologist*, *5*(2), 144–151. https://doi.org/10.1634/THEONCOLOGIST.5-2-144

Akiyama, T., & Kawasaki, Y. (2006). *WNT* signalling and the actin cytoskeleton. *Oncogene*, *25*(57), 7538–7544. https://doi.org/10.1038/sj.onc.1210063

Alcantara Llaguno, S. R., & Parada, L. F. (2016). Cell of origin of glioma: biological and clinical implications, *115*. https://doi.org/10.1038/bjc.2016.354

Anastas, J. N., & Moon, R. T. (2013). *WNT* signalling pathways as therapeutic targets in cancer. *Nature Reviews Cancer*, *13*(1), 11–26. https://doi.org/10.1038/nrc3419

Bahmanyar, S., Kaplan, D. D., DeLuca, J. G., Giddings, T. H., O'Toole, E. T., Winey, M., … Barth, A. I. M. (2008). Beta-Catenin is a Nek2 substrate involved in centrosome separation. *Genes & Development*, *22*(1), 91–105. https://doi.org/10.1101/gad.1596308

Bao, S., Wu, Q., McLendon, R. E., Hao, Y., Shi, Q., Hjelmeland, A. B., … Rich, J. N. (2006). Glioma stem cells promote radioresistance by preferential activation of the DNA damage response. *Nature*, *444*(7120), 756–760. https://doi.org/10.1038/nature05236

Baserga, R. (1981). The Cell Cycle. *New England Journal of Medicine*, *304*(8), 453–459. https://doi.org/10.1056/NEJM198102193040803

Basso, K. (2009). Toward a systems biology approach to investigate cellular networks in normal and malignant B cells. *Leukemia*, *23*(7), 1219–1225. https://doi.org/10.1038/leu.2009.4

Basso, K., & Dalla-Favera, R. (2010). *BCL6*: Master Regulator of the Germinal Center Reaction and Key Oncogene in B Cell Lymphomagenesis. *Advances in Immunology*, *105*, 193–210. https://doi.org/10.1016/S0065-2776(10)05007-8

Basso, K., & Dalla-Favera, R. (2012). Roles of *BCL6* in normal and transformed germinal center B cells. *Immunological Reviews*, *247*(1), 172–183.

Beier, D., Schriefer, B., Brawanski, K., Hau, P., Weis, J., Schulz, J. B., & Beier, C. P. (2012). Efficacy of clinically relevant temozolomide dosing schemes in glioblastoma cancer stem cell lines. *Journal of Neuro-Oncology*, *109*(1), 45–52. https://doi.org/10.1007/s11060-012-0878-4

Biasoli, D., Sobrinho, M. F., da Fonseca, A. C. C., de Matos, D. G., Romão, L., de Moraes Maciel, R., … Lima, F. R. S. (2014). Glioblastoma cells inhibit astrocytic p53-expression favoring cancer malignancy. *Oncogenesis*, *3*(10), e123–e123. https://doi.org/10.1038/oncsis.2014.36

Bienz, M. (2005). β-Catenin: A Pivot between Cell Adhesion and *WNT* Signalling. *Current Biology*, *15*(2), R64–R67. https://doi.org/10.1016/J.CUB.2004.12.058

Bowman, A., & Nusse, R. (2011). Location, location, location: FoxM1 mediates beta-catenin nuclear translocation and promotes glioma tumorigenesis. *Cancer Cell*, *20*(4), 415–416. https://doi.org/10.1016/j.ccr.2011.10.003

Brennan, C. W., Verhaak, R. G. W., Mckenna, A., Campos, B., Noushmehr, H., Salama, S. R., … Network, T. R. (2013). The Somatic Genomic Landscape of Glioblastoma. *Cell*, *155*(155), 462–477. https://doi.org/10.1016/j.cell.2013.09.034

Brum, G., Carbone, T., Still, E., Correia, V., Szulak, K., Calianese, D., … Wan, Y. (2013). N-acetylcysteine potentiates doxorubicin-induced ATM and p53 activation in ovarian cancer cells. *International Journal of Oncology*. https://doi.org/10.3892/ijo.2012.1680

Bryja, V., Červenka, I., & Čajánek, L. (2017). The connections of *WNT* pathway components with cell cycle and centrosome: side effects or a hidden logic? *Critical Reviews in Biochemistry and Molecular Biology*, *52*(6), 614–637. https://doi.org/10.1080/10409238.2017.1350135

Cardenas, M. G., Oswald, E., Yu, W., Xue, F., MacKerell, A. D., & Melnick, A. M. (2017). The expanding role of the *BCL6* oncoprotein as a cancer therapeutic target. *Clinical Cancer*

Research, *23*(4), 885–893.

Cardenas, M. G., Yu, W., Beguelin, W., Teater, M. R., Geng, H., Goldstein, R. L., … Cohen, J. (2016). Rationally designed *BCL6* inhibitors target activated B cell diffuse large B cell lymphoma. *The Journal of Clinical Investigation*, *126*(9), 3351–3362.

Castro, S. V., de Carvalho, A. A., da Silva, C. M. G., Faustino, L. R., Campello, C. C., Lucci, C. M., … Rodrigues, A. P. R. (2011). Freezing solution containing dimethylsulfoxide and fetal calf serum maintains survival and ultrastructure of goat preantral follicles after cryopreservation and in vitro culture of ovarian tissue. *Cell and Tissue Research*, *346*(2), 283–292. https://doi.org/10.1007/s00441-011-1257-8

Cerchietti, L., Figueroa, M. E., Shaknovich, R., & Melnick, A. (2006). *BCL6* Regulates Diffuse Large B-Cell Lymphoma Cell Cycle and Apoptosis Checkpoints through Direct Repression of the p300 Histone Acetyl-Transferase. *Blood*, *108*(11). Retrieved from http://www.bloodjournal.org/content/108/11/1413?sso-checked=true

Chai, R., Kuo, B., Wang, T., Liaw, E. J., Xia, A., Jan, T. A., … Cheng, A. G. (2012). *WNT* signaling induces proliferation of sensory precursors in the postnatal mouse cochlea. *Proceedings of the National Academy of Sciences of the United States of America*, *109*(21), 8167–8172. https://doi.org/10.1073/pnas.1202774109

Chen, B., Dodge, M. E., Tang, W., Lu, J., Ma, Z., Fan, C.-W., … Lum, L. (n.d.). Small molecule-mediated disruption of *WNT*-dependent signaling in tissue regeneration and cancer. https://doi.org/10.1038/nchembio.137

Claes, A., Idema, A. J., & Wesseling, P. (2007). Diffuse glioma growth: a guerilla war. *Acta Neuropathologica*, *114*(5), 443–458. https://doi.org/10.1007/s00401-007-0293-7

Combs, S. E., Rieken, S., Wick, W., Abdollahi, A., von Deimling, A., Debus, J., & Hartmann, C. (2011). Prognostic significance of IDH-1 and MGMT in patients with glioblastoma: one step forward, and one step back? *Radiation Oncology (London, England)*, *6*, 115. https://doi.org/10.1186/1748-717X-6-115

Dai, C., Stolz, D. B., Kiss, L. P., Monga, S. P., Holzman, L. B., & Liu, Y. (2009). *WNT*/beta-

catenin signaling promotes podocyte dysfunction and albuminuria. *Journal of the American Society of Nephrology : JASN*, *20*(9), 1997–2008. https://doi.org/10.1681/ASN.2009010019

Davidson, G. (2010). The cell cycle and *WNT*. *Cell Cycle*, *9*(9), 1667–1668.

Davidson, G., & Niehrs, C. (2010). Emerging links between CDK cell cycle regulators and *WNT* signaling. *Trends in Cell Biology*, *20*(8), 453–460. https://doi.org/10.1016/j.tcb.2010.05.002

Davidson, G., Shen, J., Huang, Y.-L., Su, Y., Karaulanov, E., Bartscherer, K., … Niehrs, C. (2009). Cell cycle control of *WNT* receptor activation. *Developmental Cell*, *17*(6), 788–799. https://doi.org/10.1016/j.devcel.2009.11.006

Davies, K. J., & Doroshow, J. H. (1986). Redox cycling of anthracyclines by cardiac mitochondria. I. Anthracycline radical formation by NADH dehydrogenase. *The Journal of Biological Chemistry*, *261*(7), 3060–3067. Retrieved from http://www.ncbi.nlm.nih.gov/pubmed/3456345

De, A. (2011). *WNT*/Ca2+ signaling pathway: a brief overview. *Acta Biochimica et Biophysica Sinica*, *43*(10), 745–756. https://doi.org/10.1093/abbs/gmr079

Duy, C., Yu, J. J., Nahar, R., Swaminathan, S., Kweon, S.-M., Polo, J. M., … Müschen, M. (2010). *BCL6* is critical for the development of a diverse primary B cell repertoire. *The Journal of Experimental Medicine*, *207*(6), 1209–1221. https://doi.org/10.1084/jem.20091299

Egli, R. J., Sckell, A., Fraitzl, C. R., Felix, R., Ganz, R., Hofstetter, W., & Leunig, M. (2003). Cryopreservation with dimethyl sulfoxide sustains partially the biological function of osteochondral tissue. *Bone*, *33*(3), 352–361. Retrieved from http://www.ncbi.nlm.nih.gov/pubmed/13678777

Foltz, G., Yoon, J.-G., Lee, H., Ma, L., Tian, Q., Hood, L., & Madan, A. (2010). Epigenetic Regulation of *WNT* Pathway Antagonists in Human Glioblastoma Multiforme. *Genes & Cancer*, *1*(1), 81–90. https://doi.org/10.1177/1947601909356103

Foucquier, J., & Guedj, M. (2015). Analysis of drug combinations: current methodological

landscape. *Pharmacology Research & Perspectives*, *3*(3), e00149. https://doi.org/10.1002/prp2.149

Franken, N. A. P., Rodermond, H. M., Stap, J., Haveman, J., & van Bree, C. (2006). Clonogenic assay of cells in vitro. *Nature Protocols*, *1*(5), 2315–2319. https://doi.org/10.1038/nprot.2006.339

Friedman, H. S., Kerby, T., & Calvert, H. (2000). Temozolomide and Treatment of Malignant Glioma. *Clinical Cancer Research*, *6*, 2585–2597. Retrieved from http://clincancerres.aacrjournals.org/content/6/7/2585.full-text.pdf

Friedman, R. (2006). The mechanistic implications of additive versus synthetic double mutant phenotypes. Retrieved from http://web.mit.edu/7.72/restricted/readings/SyntheticPhenotypes.pdf

Fuerer, C., & Nusse, R. (2010). Lentiviral Vectors to Probe and Manipulate the *WNT* Signaling Pathway. *PLoS ONE*, *5*(2), e9370. https://doi.org/10.1371/journal.pone.0009370

García-Martín, E., Majewska, A. K., Guizzetti, M., Jäkel, S., & Dimou, L. (2017). Glial Cells and Their Function in the Adult Brain: A Journey through the History of Their Ablation. https://doi.org/10.3389/fncel.2017.00024

Gó Mez-Orte, E., Sá Enz-Narciso, B., Moreno, S., & Cabello, J. (2013). Multiple functions of the noncanonical *WNT* pathway. *Trends in Genetics*, *29*, 545–553. https://doi.org/10.1016/j.tig.2013.06.003

Grzeschik, K.-H., Bornholdt, D., Oeffner, F., König, A., del Carmen Boente, M., Enders, H., … Happle, R. (2007). Deficiency of PORCN, a regulator of *WNT* signaling, is associated with focal dermal hypoplasia. *Nature Genetics*, *39*(7), 833–835. https://doi.org/10.1038/ng2052

Hao, H.-X., Xie, Y., Zhang, Y., Charlat, O., Oster, E., Avello, M., … Cong, F. (2012). ZNRF3 promotes *WNT* receptor turnover in an R-spondin-sensitive manner. *Nature*, *485*(7397), 195–200. https://doi.org/10.1038/nature11019

Hatzi, K., & Melnick, A. (2014). Breaking bad in the germinal center: how deregulation of

BCL6 contributes to lymphomagenesis. *Trends in Molecular Medicine*, *20*, 343–352. https://doi.org/10.1016/j.molmed.2014.03.001

Heuberger, J., & Birchmeier, W. (2010). Interplay of cadherin-mediated cell adhesion and canonical *WNT* signaling. *Cold Spring Harbor Perspectives in Biology*, *2*(2), a002915. https://doi.org/10.1101/cshperspect.a002915

Hou, L. C., Veeravagu, A., Hsu, A. R., & Tse, V. C. K. (2006). Recurrent glioblastoma multiforme: a review of natural history and management options. *Neurosurgical Focus*, *20*(4), E5. Retrieved from http://www.ncbi.nlm.nih.gov/pubmed/16709036

Ichikawa, Y., Ghanefar, M., Bayeva, M., Wu, R., Khechaduri, A., Prasad, S. V. N., … Ardehali, H. (2014). Cardiotoxicity of doxorubicin is mediated through mitochondrial iron accumulation. *Journal of Clinical Investigation*, *124*(2), 617–630. https://doi.org/10.1172/JCI72931

Jackson, S. P., & Bartek, J. (2009). The DNA-damage response in human biology and disease. *Nature*, *461*(7267), 1071–1078. https://doi.org/10.1038/nature08467

Jian-jun, T. X. (2006). Determining the solubility and o/w partiton coefficient of temozolomide by HPLC. *En.cnki.com.cn*. Retrieved from http://en.cnki.com.cn/Article_en/CJFDTOTAL-SDPK200606016.htm

Jones, T. R., Bigner, S. H., Schold, S. C., Eng, L. F., & Bigner, D. D. (1981). Anaplastic human gliomas grown in athymic mice. Morphology and glial fibrillary acidic protein expression. *The American Journal of Pathology*, *105*(3), 316–327. Retrieved from http://www.ncbi.nlm.nih.gov/pubmed/6274201

Kahlert, U. D., Suwala, A. K., Koch, K., Natsumeda, M., Orr, B. A., Hayashi, M., … Eberhart, C. G. (2015). Pharmacologic *WNT* Inhibition Reduces Proliferation, Survival, and Clonogenicity of Glioblastoma Cells. *J Neuropathol Exp Neurol*, *74*(9), 889–900. https://doi.org/10.1097/NEN.0000000000000227

Karimaian, A., Majidinia, M., Bannazadeh Baghi, H., & Yousefi, B. (2017). The crosstalk between *WNT*/β-catenin signaling pathway with DNA damage response and oxidative

stress: Implications in cancer therapy. *DNA Repair*, *51*, 14–19. https://doi.org/10.1016/j.dnarep.2017.01.003

Kikuchi, A., Yamamoto, H., Sato, A., & Matsumoto, S. (2012). *WNT5a*: its signalling, functions and implication in diseases. *Acta Physiologica*, *204*(1), 17–33. https://doi.org/10.1111/j.1748-1716.2011.02294.x

Kim, Y., Hong, M., Do, I. G., Ha, S. Y., Lee, D., & Suh, Y. L. (2015). *WNT5a*, Ryk and Ror2 expression in glioblastoma subgroups. *Pathol Res Pract*, *211*(12), 963–972. https://doi.org/10.1016/j.prp.2015.10.001

Komiya, Y., & Habas, R. (2008). *WNT* signal transduction pathways. *Organogenesis*, *4*(2), 68–75. Retrieved from http://www.ncbi.nlm.nih.gov/pubmed/19279717

Lathia, J. D., Mack, S. C., Mulkearns-Hubert, E. E., Valentim, C. L. L., & Rich, J. N. (n.d.). Cancer stem cells in glioblastoma. https://doi.org/10.1101/gad.261982

Lee, K.-H., Li, M., Michalowski, A. M., Zhang, X., Liao, H., Chen, L., … Huang, J. (n.d.). A genomewide study identifies the *WNT* signaling pathway as a major target of p53 in murine embryonic stem cells. https://doi.org/10.1073/pnas.0909734107

Lee, Y., Lee, J. K., Ahn, S. H., Lee, J., & Nam, D. H. (2016). *WNT* signaling in glioblastoma and therapeutic opportunities. *Lab Invest*, *96*(2), 137–150. https://doi.org/10.1038/labinvest.2015.140

Lefranc, F., Sadeghi, N., Camby, I., Metens, T., Dewitte, O., & Kiss, R. (2006). Present and potential future issues in glioblastoma treatment. *Expert Review of Anticancer Therapy*, *6*(5), 719–732. https://doi.org/10.1586/14737140.6.5.719

Lesniak, M. S., Upadhyay, U., Goodwin, R., Tyler, B., & Brem, H. (2005). Local delivery of doxorubicin for the treatment of malignant brain tumors in rats. *Anticancer Research*, *25*(6B), 3825–3831. Retrieved from http://www.ncbi.nlm.nih.gov/pubmed/16312042

Liebelt, B. D., Shingu, T., Zhou, X., Ren, J., Shin, S. A., & Hu, J. (2016). Glioma Stem Cells: Signaling, Microenvironment, and Therapy. *Stem Cells International*, *2016*, 1–10. https://doi.org/10.1155/2016/7849890

Ling, Y. H., el-Naggar, A. K., Priebe, W., & Perez-Soler, R. (1996). Cell cycle-dependent cytotoxicity, G2/M phase arrest, and disruption of p34cdc2/cyclin B1 activity induced by doxorubicin in synchronized P388 cells. *Molecular Pharmacology*, *49*(5), 832–841. Retrieved from http://www.ncbi.nlm.nih.gov/pubmed/8622633

Lipinski, C. (2008). Drug Solubility in Water and Dimethylsulfoxide (pp. 255–282). https://doi.org/10.1002/9783527621286.ch10

Liu, D., Guest, S., & Finley, R. L. (n.d.). Why cyclin Y? A highly conserved cyclin with essential functions. *Fly*, *4*(4), 278–282. Retrieved from http://www.ncbi.nlm.nih.gov/pubmed/20699655

Liu, Y., Yan, W., Zhang, W., Chen, L., You, G., Bao, Z., … Jiang, T. (2012). MiR-218 reverses high invasiveness of glioblastoma cells by targeting the oncogenic transcription factor LEF1. *Oncol Rep*, *28*(3), 1013–1021. https://doi.org/10.3892/or.2012.1902

Logan, C. Y., & Nusse, R. (2004). The *WNT* Signaling Pathway in Development and Disease. *Annu. Rev. Cell Dev. Biol*, *20*, 781–810. https://doi.org/10.1146/annurev.cellbio.20.010403.113126

Lüpertz, R., Wätjen, W., Kahl, R., & Chovolou, Y. (2010). Dose- and time-dependent effects of doxorubicin on cytotoxicity, cell cycle and apoptotic cell death in human colon cancer cells. *Toxicology*, *271*(3), 115–121. https://doi.org/10.1016/j.tox.2010.03.012

Macdonald, B. T., Tamai, K., & He, X. (2010). *WNT*/β-Catenin Signaling: Components, Mechanisms, and Diseases. *Developmental Cell*, *17*, 9–26. https://doi.org/10.1016/j.devcel.2009.06.016

Madan, B., Ke, Z., Harmston, N., Ho, S. Y., Frois, A. O., Alam, J., … Virshup, D. M. (2016). *WNT* addiction of genetically defined cancers reversed by PORCN inhibition. *Oncogene*, *35*(17), 2197–2207. https://doi.org/10.1038/onc.2015.280

Mao, J., Wang, J., Liu, B., Pan, W., Farr, G. H., Flynn, C., … Wu, D. (2001). Low-density lipoprotein receptor-related protein-5 binds to Axin and regulates the canonical *WNT* signaling pathway. *Molecular Cell*, *7*(4), 801–809. https://doi.org/10.1016/S1097-

2765(01)00224-6

Maréchal, A., & Zou, L. (2013). DNA damage sensing by the ATM and ATR kinases. *Cold Spring Harbor Perspectives in Biology*, *5*(9). https://doi.org/10.1101/cshperspect.a012716

Mazur, P., Leibo, S. P., & Chu, E. H. Y. (1972). A two-factor hypothesis of freezing injury: Evidence from Chinese hamster tissue-culture cells. *Experimental Cell Research*, *71*(2), 345–355. https://doi.org/10.1016/0014-4827(72)90303-5

McConnell, M., Fabre, M.-S., Jones, N., Rowe, M., Hung, N., Melnick, A., & Slatter, T. (2015). CBIO-24 Glioblastoma multiforme cells are addicted to the oncogenic survival factor *BCL6*. *Neuro-Oncology*, *17*(suppl_5), v60–v60.

Mendez, L. M., Polo, J. M., Yu, J. J., Krupski, M., Ding, B. B., Melnick, A., & Ye, B. H. (2008). CtBP Is an Essential Corepressor for *BCL6* Autoregulation. *Molecular and Cellular Biology*, *28*(7), 2175–2186. https://doi.org/10.1128/MCB.01400-07

Miles, R. R., Crockett, D. K., Lim, M. S., & Elenitoba-Johnson, K. S. J. (2005). Analysis of *BCL6*-interacting proteins by tandem mass spectrometry. *Molecular & Cellular Proteomics : MCP*, *4*(12), 1898–1909. https://doi.org/10.1074/mcp.M500112-MCP200

Miller, T. E., Liau, B. B., Wallace, L. C., Morton, A. R., Xie, Q., Dixit, D., … Rich, J. N. (2017). Transcription elongation factors represent in vivo cancer dependencies in glioblastoma. *Nature*, *547*(7663), 355–359. https://doi.org/10.1038/nature23000

Motlagh, N. S. H., Parvin, P., Ghasemi, F., & Atyabi, F. (2016). Fluorescence properties of several chemotherapy drugs: doxorubicin, paclitaxel and bleomycin. *Biomedical Optics Express*, *7*(6), 2400–2406. https://doi.org/10.1364/BOE.7.002400

Munthe, S., Petterson, S. A., Dahlrot, R. H., Poulsen, F. R., Hansen, S., & Kristensen, B. W. (2016). Glioma Cells in the Tumor Periphery Have a Stem Cell Phenotype. *PloS One*, *11*(5), e0155106. https://doi.org/10.1371/journal.pone.0155106

Niida, A., Hiroko, T., Kasai, M., Furukawa, Y., Nakamura, Y., Suzuki, Y., … Akiyama, T. (2004). *DKK1*, a negative regulator of *WNT* signaling, is a target of the β-catenin/TCF pathway. *Oncogene*, *23*(52), 8520–8526. https://doi.org/10.1038/sj.onc.1207892

Olmeda, D., Castel, S., Vilaró, S., & Cano, A. (2003). Beta-catenin regulation during the cell cycle: implications in G2/M and apoptosis. *Molecular Biology of the Cell*, *14*(7), 2844–2860. https://doi.org/10.1091/mbc.E03-01-0865

Osuka, S., & Meir, E. G. Van. (2017). Overcoming therapeutic resistance in glioblastoma: the way forward. *The Journal of Clinical Investigation*, *127*(2), 415–426. https://doi.org/10.1172/JCI89587

Paw, I., Carpenter, R. C., Watabe, K., Debinski, W., & Lo, H.-W. (2015). Mechanisms regulating glioma invasion. *Cancer Letters*, *362*(1), 1–7. https://doi.org/10.1016/j.canlet.2015.03.015

Pérez-Pérez, J. M., Candela, H., & Micol, J. L. (2009). Understanding synergy in genetic interactions. *Trends in Genetics*, *25*(8), 368–376. https://doi.org/10.1016/j.tig.2009.06.004

Phan, R. T., & Dalla-Favera, R. (2004). The *BCL6* proto-oncogene suppresses p53 expression in germinal-centre B cells. *Nature*, *432*(7017), 635.

Phan, R. T., Saito, M., Basso, K., Niu, H., & Dalla-Favera, R. (2005). *BCL6* interacts with the transcription factor Miz-1 to suppress the cyclin-dependent kinase inhibitor p21 and cell cycle arrest in germinal center B cells. *Nature Immunology*, *6*(10), 1054.

Pinzone, J. J., Hall, B. M., Thudi, N. K., Vonau, M., Qiang, Y.-W., Rosol, T. J., & Shaughnessy, J. D. (n.d.). The role of Dickkopf-1 in bone development, homeostasis, and disease. https://doi.org/10.1182/blood-2008-03

Pozarowski, P., & Darzynkiewicz, Z. (2004). Analysis of Cell Cycle by Flow Cytometry. In *Checkpoint Controls and Cancer* (pp. 301–312). New Jersey: Humana Press. https://doi.org/10.1385/1-59259-811-0:301

Proffitt, K. D., & Virshup, D. M. (2012). Precise Regulation of Porcupine Activity Is Required for Physiological *WNT* Signaling * □ S. *The Journal of Bilogical Chemistry*. https://doi.org/10.1074/jbc.M112.381970

Pulvirenti, T., Van Der Heijden, M., Droms, L. A., Huse, J. T., Tabar, V., & Hall, A. (2011). Dishevelled 2 signaling promotes self-renewal and tumorigenicity in human gliomas.

Cancer Res, *71*(23), 7280–7290. https://doi.org/10.1158/0008-5472.CAN-11-1531

Ramirez, Y. P., Weatherbee, J. L., Wheelhouse, R. T., & Ross, A. H. (2013). Glioblastoma multiforme therapy and mechanisms of resistance. *Pharmaceuticals*, *6*(12), 1475–1506.

Ray, A., Blevins, C., Wani, G., & Wani, A. A. (2016). ATR- and ATM-Mediated DNA Damage Response Is Dependent on Excision Repair Assembly during G1 but Not in S Phase of Cell Cycle. *PLOS ONE*, *11*(7), e0159344. https://doi.org/10.1371/journal.pone.0159344

Reya, T., & Clevers, H. (2005). *WNT* signalling in stem cells and cancer. *Nature*, *434*(7035), 843–850. https://doi.org/10.1038/nature03319

Rheinbay, E., Suvà, M. L., Gillespie, S. M., Wakimoto, H., Patel, A. P., Shahid, M., … Bernstein, B. E. (2013). An Aberrant Transcription Factor Network Essential for *WNT* Signaling and Stem Cell Maintenance in Glioblastoma. https://doi.org/10.1016/j.celrep.2013.04.021

Rose, J. K. (2003). Optimization of Transfection. In *Current Protocols in Cell Biology* (Vol. 19, p. 20.7.1-20.7.4). Hoboken, NJ, USA: John Wiley & Sons, Inc. https://doi.org/10.1002/0471143030.cb2007s19

Rousselle, C., Clair, P., Lefauconnier, J. M., Kaczorek, M., Scherrmann, J. M., & Temsamani, J. (2000). New advances in the transport of doxorubicin through the blood-brain barrier by a peptide vector-mediated strategy. *Molecular Pharmacology*, *57*(4), 679–686. Retrieved from http://www.ncbi.nlm.nih.gov/pubmed/10727512

Sardi, I., Fantappiè, O., la Marca, G., Giovannini, M. G., Iorio, A. L., da Ros, M., … Mazzanti, R. (2014). Delivery of doxorubicin across the blood–brain barrier by ondansetron pretreatment: a study in vitro and in vivo. *Cancer Letters*, *353*(2), 242–247. https://doi.org/10.1016/J.CANLET.2014.07.018

Sardi, I., la Marca, G., Cardellicchio, S., Giunti, L., Malvagia, S., Genitori, L., … Giovannini, M. G. (2013). Pharmacological modulation of blood-brain barrier increases permeability of doxorubicin into the rat brain. *American Journal of Cancer Research*, *3*(4), 424–432. Retrieved from http://www.ncbi.nlm.nih.gov/pubmed/23977451

Schambony, A., & Wedlich, D. (2013). *WNT* Signaling and Cell Migration. Retrieved from

https://www.ncbi.nlm.nih.gov/books/NBK6303/?report=reader

Schubert, M., & Holland, L. Z. (2013). The *WNT* Gene Family and the Evolutionary Conservation of *WNT* Expression. Retrieved from https://www.ncbi.nlm.nih.gov/books/NBK6212/?report=reader

Sedgwick, A. E., & D 'souza-Schorey, C. (2016). *WNT* Signaling in Cell Motility and Invasion: Drawing Parallels between Development and Cancer. https://doi.org/10.3390/cancers8090080

Singh, M., Mckenzie, K., & Ma, X. (2017). Effect of dimethyl sulfoxide on in vitro proliferation of skin fibroblast cells. *Journal of Biotech Research*, *8*, 1944–328578. Retrieved from http://www.btsjournals.com/assets/2017v8p78-82.pdf

Sottoriva, A., Spiteri, I., Piccirillo, S. G. M., Touloumis, A., Collins, V. P., Marioni, J. C., … Tavare, S. (2013). Intratumor heterogeneity in human glioblastoma reflects cancer evolutionary dynamics. *Proceedings of the National Academy of Sciences*, *110*(10), 4009–4014. https://doi.org/10.1073/pnas.1219747110

Stepanenko, A. A., Andreieva, S. V, Korets, K. V, Mykytenko, D. O., Baklaushev, V. P., Huleyuk, N. L., … Dmitrenko, V. V. (2016). Temozolomide promotes genomic and phenotypic changes in glioblastoma cells. *Cancer Cell International*, *16*, 36. https://doi.org/10.1186/s12935-016-0311-8

Stupp, R., Mason, W. P., Van Den Bent, M. J., Weller, M., Fisher, B., Taphoorn, M. J. B., … Bogdahn, U. (2005). Radiotherapy plus concomitant and adjuvant temozolomide for glioblastoma. *New England Journal of Medicine*, *352*(10), 987–996.

Suwala, A. K., Hanaford, A., Kahlert, U. D., & Maciaczyk, J. (2016). Clipping the Wings of Glioblastoma: Modulation of *WNT* as a Novel Therapeutic Strategy. *J Neuropathol Exp Neurol*, *75*(5), 388–396. https://doi.org/10.1093/jnen/nlw013

Tallarida, R. J. (2011). Quantitative methods for assessing drug synergism. *Genes & Cancer*, *2*(11), 1003–1008. https://doi.org/10.1177/1947601912440575

TCGA. (2008). Comprehensive genomic characterization defines human glioblastoma genes

and core pathways, *455*(23), 1061–1069. https://doi.org/10.1038/nature07385

ThermoFisher Scienfitic. (n.d.). RPMI 1640 Medium - Thermo Fisher Scientific. Retrieved May 11, 2018, from https://www.thermofisher.com/order/catalog/product/11875093

Thorn, C. F., Oshiro, C., Marsh, S., Hernandez-Boussard, T., McLeod, H., Klein, T. E., & Altman, R. B. (2011). Doxorubicin pathways: pharmacodynamics and adverse effects. *Pharmacogenetics and Genomics*, *21*(7), 440.

Toyama, H., Okada, S., Hatano, M., Takahashi, Y., Takeda, N., Ichii, H., … Tokuhisa, T. (2002). Memory B cells without somatic hypermutation are generated from *BCL6*-deficient B cells. *Immunity*, *17*(3), 329–339.

Verhaak, R. G. W., Hoadley, K. A., Purdom, E., Wang, V., Qi, Y., Wilkerson, M. D., … Cancer Genome Atlas Research Network, T. C. G. A. R. (2010). Integrated genomic analysis identifies clinically relevant subtypes of glioblastoma characterized by abnormalities in PDGFRA, IDH1, EGFR, and NF1. *Cancer Cell*, *17*(1), 98–110. https://doi.org/10.1016/j.ccr.2009.12.020

Vladar, E. K., Antic, D., & Axelrod, J. D. (2009). Planar cell polarity signaling: the developing cell's compass. *Cold Spring Harbor Perspectives in Biology*, *1*(3), a002964. https://doi.org/10.1101/cshperspect.a002964

von Bartheld, C. S., Bahney, J., & Herculano-Houzel, S. (2016). The search for true numbers of neurons and glial cells in the human brain: A review of 150 years of cell counting. *Journal of Comparative Neurology*, *524*(18), 3865–3895. https://doi.org/10.1002/cne.24040

Wang, J., Ma, Y., & Cooper, M. K. (2013). Cancer stem cells in glioma: challenges and opportunities. *Translational Cancer Research*, *2*(5), 429–441. https://doi.org/10.3978/j.issn.2218-676X.2013.08.01

Wang, X., Li, Z., Naganuma, A., & Ye, B. H. (2002). Negative autoregulation of BCL-6 is bypassed by genetic alterations in diffuse large B cell lymphomas. *Proceedings of the National Academy of Sciences of the United States of America*, *99*(23), 15018–15023.

https://doi.org/10.1073/pnas.232581199

Wen, P. Y., & Kesari, S. (2008). Malignant Gliomas in Adults. *New England Journal of Medicine*, *359*(5), 492–507. https://doi.org/10.1056/NEJMra0708126

William, D., Walther, M., Schneider, B., Linnebacher, M., & Classen, C. F. (2018). Temozolomide-induced increase of tumorigenicity can be diminished by targeting of mitochondria in in vitro models of patient individual glioblastoma. *PLOS ONE*, *13*(1), e0191511. https://doi.org/10.1371/journal.pone.0191511

Wu, J., Fang, J., Yang, Z., Chen, F., Liu, J., & Wang, Y. (2012). *WNT* inhibitory factor-1 regulates glioblastoma cell cycle and proliferation. *J Clin Neurosci*, *19*(10), 1428–1432. https://doi.org/10.1016/j.jocn.2011.12.023

Xu, L., Chen, Y., Dutra-Clarke, M., Mayakonda, A., Hazawa, M., Savinoff, S. E., … Watkins, A. (2017). *BCL6* promotes glioma and serves as a therapeutic target. *Proceedings of the National Academy of Sciences*, *114*(15), 3981–3986.

Yang, F., Teves, S. S., Kemp, C. J., & Henikoff, S. (2014). Doxorubicin, DNA torsion, and chromatin dynamics. https://doi.org/10.1016/j.bbcan.2013.12.002

Yang, K., Wang, X., Zhang, H., Wang, Z., Nan, G., Li, Y., … He, T.-C. (2016). The evolving roles of canonical *WNT* signaling in stem cells and tumorigenesis: implications in targeted cancer therapies. *Laboratory Investigation*, *96*(2), 116–136. https://doi.org/10.1038/labinvest.2015.144

Yin, N., Ma, W., Pei, J., Ouyang, Q., Tang, C., & Lai, L. (2014). Synergistic and Antagonistic Drug Combinations Depend on Network Topology. *PLoS ONE*, *9*(4), e93960. https://doi.org/10.1371/journal.pone.0093960

Yu, J. M., Jun, E. S., Jung, J. S., Suh, S. Y., Han, J. Y., Kim, J. Y., … Jung, J. S. (2007). Role of *WNT5a* in the proliferation of human glioblastoma cells. *Cancer Lett*, *257*(2), 172–181. https://doi.org/10.1016/j.canlet.2007.07.011

Zhang, G., Gurtu, V., & Kain, S. R. (1996). An Enhanced Green Fluorescent Protein Allows Sensitive Detection of Gene Transfer in Mammalian Cells. *Biochemical and Biophysical*

Research Communications, *227*(3), 707–711. https://doi.org/10.1006/bbrc.1996.1573

Zhang, J., FG Stevens, M., & D Bradshaw, T. (2012). Temozolomide: mechanisms of action, repair and resistance. *Current Molecular Pharmacology*, *5*(1), 102–114.

Zhang, K., Zhang, J., Han, L., Pu, P., & Kang, C. (2012). *WNT*/beta-Catenin Signaling in Glioma. *Journal of Neuroimmune Pharmacology*, *7*(4), 740–749. https://doi.org/10.1007/s11481-012-9359-y

Zong, H., Verhaak, R. G., & Canoll, P. (2012). The cellular origin for malignant glioma and prospects for clinical advancements. https://doi.org/10.1586/erm.12.30

Zou, D., Wang, W., Lei, D., Yin, Y., Ren, P., Chen, J., … Wang, Y. (2017). Penetration of blood–brain barrier and antitumor activity and nerve repair in glioma by doxorubicin-loaded monosialoganglioside micelles system. *International Journal of Nanomedicine*, *Volume 12*, 4879–4889. https://doi.org/10.2147/IJN.S138257

9. Appendices

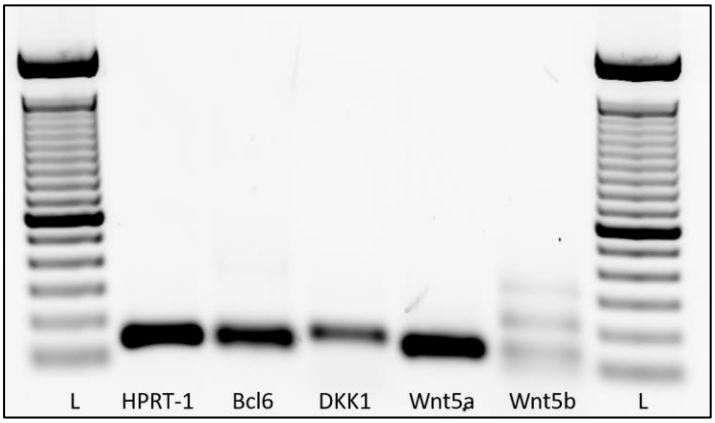

Figure 40 Agarose gel containing qPCR products.

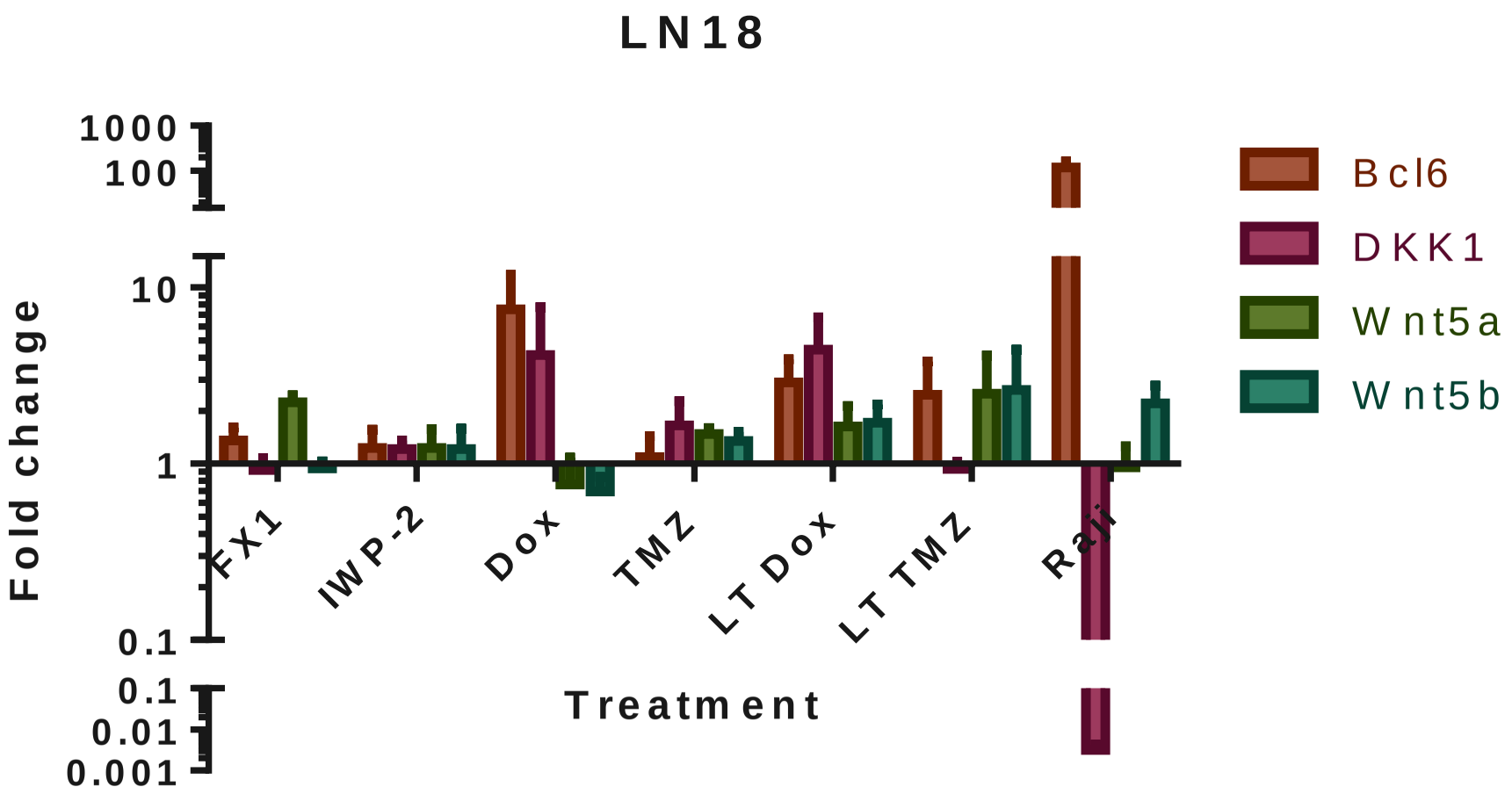

Figure 41 qPCR data from LN18 cells. N=3.

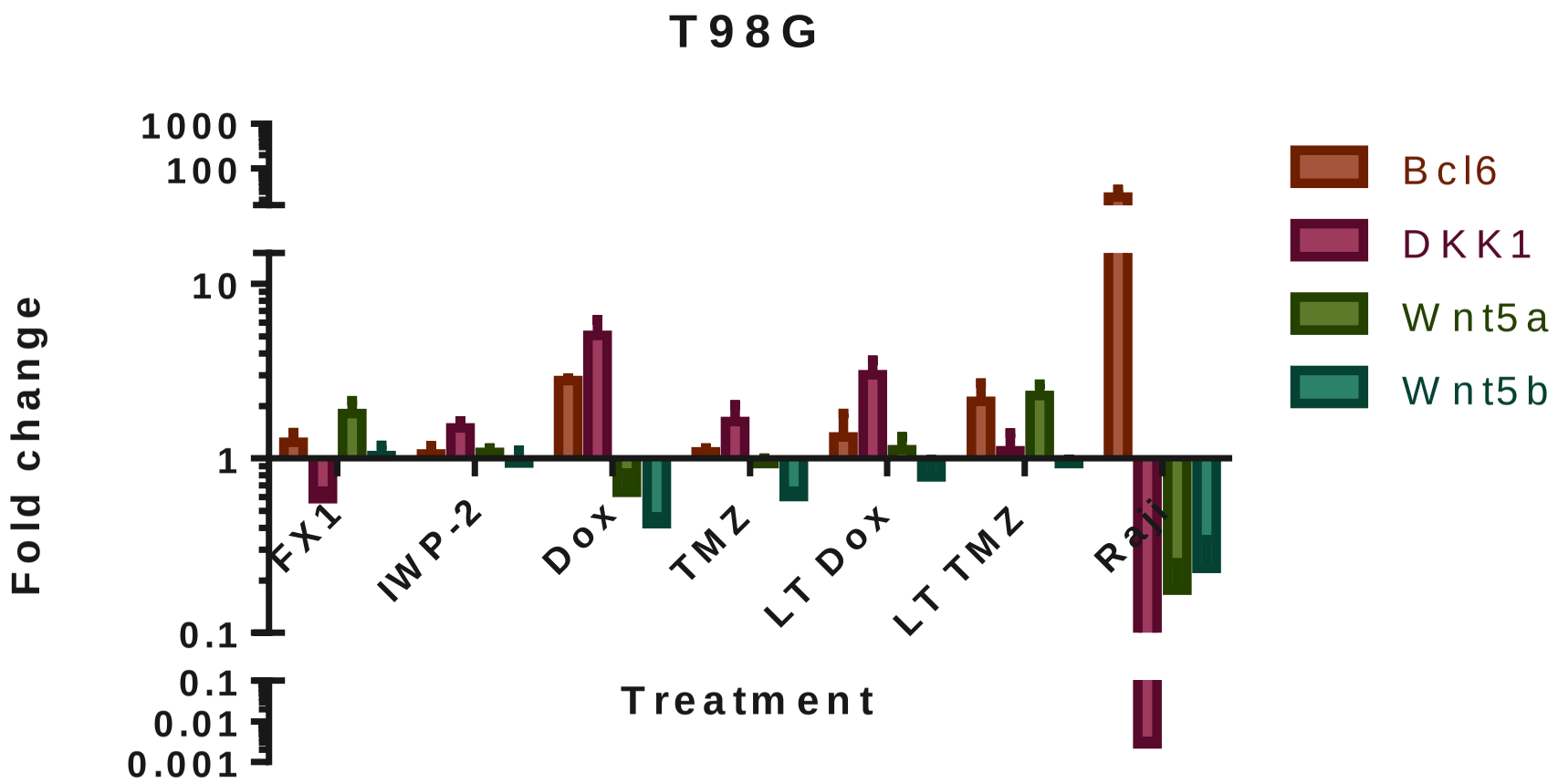

Figure 42 qPCR data from T98G treated cells. N=3

9.1. Dose response for working concentration of 79-6

To determine whether endogenous *BCL6* regulated the *WNT* signalling pathway, cells expressing the *WNT* reporter were treated with *BCL6* inhibitors, either … FX1 or a commercially available inhibitor, 79-6 (company reference …)

79-6 was analysed to choose a working concentration for future experiments by MTT dose-response assay. The MTT assay was carried out in the same two glioma cells lines, LN18 and T98G. Due to 79-6 having a maximum solubility of 180 mM in DMSO, the highest working concentration that could be used was 180 μM .

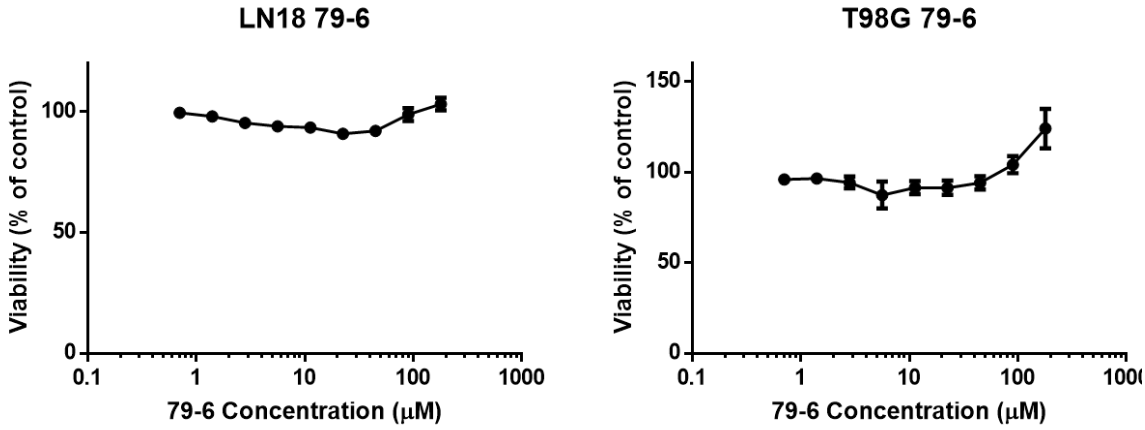

Figure 43 Dose response of 79-6 in two glioma cells lines. N=3 biological replicates with 3 technical replicates. Error bars represent the SEM.

Due to the unusual dose-response curves obtained from this assay, an IC_{50} value could not be calculated in either the T98G or LN18 cell line. These curves show that 79-6 is non-toxic to the cell lines tested. This was different to the effect of FX1, which has an IC_{50} of 35 μM (Cardenas et al., 2016).

The oncogenic transcription factor BCL6 drives survival of glioblastoma and is up-regulated in response to DNA damage.

Marie-Sophie Fabre* [1,2], Nicole M. Jones* [1,2] Tania L. Slatter[3], Matthew R. Rowe[1,2], Rosemary Gordon[1], M. Leticia Castro[1], Ahmad Taha[4], Janice A. Royds[3], Noelyn Hung[3], Ari M. Melnick[5], and Melanie J. McConnell[1,2]

1. Centre for Biodiscovery and School of Biological Sciences, Victoria University of Wellington, New Zealand
2. Malaghan Institute of Medical Research, Wellington, New Zealand
3. Department of Pathology, Dunedin School of Medicine, University of Otago, New Zealand
4. Neurosugery, Southern District Health Board, Dunedin, New Zealand
5. Weill Cornell Medical College, New York, NY USA

* These authors made an equal contribution

Key words: BCL6; glioblastoma; DNA damage; transcription factor; cell death

Corresponding Author: Melanie J. McConnell, PhD. Centre for Biodiscovery and School of Biological Sciences, Victoria University of Wellington. PO Box 600, Wellington 6140, New Zealand.

Phone +64 4 463 5233 x8136; fax +64 4 463 5331. Melanie.mcconnell@vuw.ac.nz

Abstract

The prognosis for people with the high-grade brain tumor glioblastoma is very poor, due largely to poor cell death in response to therapy. The transcription factor BCL6 was identified as a transcription factor mediating survival in glioblastoma. Expression was observed in glioblastoma tumour specimens and cell lines. Treatment with ionizing radiation, temozolomide or doxorubicin induced endogenous BCL6 expression, which was shown to be able to bind DNA and was transcriptionally active. BCL6 expression and activity were reduced by siRNA, peptide inhibitor, small molecule inhibitor or dominant negative BCL6 mutant in a panel of glioblastoma cell lines. This caused a small increase in apoptosis, but a profound loss in proliferative ability. Both transcriptional and pro-survival activity were blocked by inhibitors of protein-protein interaction in the BTB/POZ domain of BCL6, but co-repressor expression was not required for BCL6 activity in glioblastoma. Instead it appears that BCL6 induced by therapy could activate transcription. Together these data demonstrate that BCL6 is an active transcription factor in glioblastoma, that it drives survival of cells, and that levels of BCL6 increased after DNA damage, potentially increasing the survival rate of therapy-treated cells. This makes BCL6 an excellent therapeutic target in glioblastoma. By increasing sensitivity to standard DNA damaging therapy, BCL6 inhibitors have real potential to improve the outcome for people with this terrible disease, who currently have no effective options for therapy.

1. Introduction

The prognosis for people diagnosed with the WHO grade IV brain tumor glioblastoma is very poor, due largely to the lack of response to therapy. The gold-standard therapy for glioblastoma is surgery to debulk the tumor, followed by fractionated radiation and temozolomide chemotherapy [1]. This aims to induce significant DNA damage to the remaining, non-resected tumor - both single and double-stranded DNA breaks from radiation-induced radical species, and alkylation of purine residues by temozolomide. The expected cellular response to this DNA damage should be apoptosis. In glioblastoma, this does not occur – there is little or no apoptosis in response to therapy [2], so damaged cells continue to proliferate, exacerbating the mutagenic and genome instability effects of DNA damaging therapy. New approaches in glioblastoma such as targeted therapy and immunotherapy continue to be developed, but these are expensive, experimental, and have had very limited success [3]. If the block to cell death could be identified, glioblastoma could be sensitized to DNA damage induced by standard therapies, which would have an immediate impact on patient outcome.

Cell death blockade in response to DNA damage is observed during B-cell maturation, driven by the transcription factor BCL6. BCL6 dimers bind DNA using six zinc fingers at the C-terminus, and recruit co-repressors and chromatin remodeling machinery via the BTB domain to target gene loci. BCL6 is normally expressed in germinal center B-cells during class switch recombination and somatic hyper-mutation, where it represses expression of cell cycle checkpoint and apoptosis genes. This prevents the usual cellular response to double-stranded breaks, allowing cells to successfully break and rearrange immune genes to generate unique immune receptors. Due to this anti-apoptotic activity BCL6 is a strong oncogene, with ectopic expression in B-cells a key driver event in lymphoma [4, 5].

Increasingly BCL6 has been found expressed in solid malignancies, including squamous cell carcinoma [6] colorectal [7] gallbladder [8], and breast cancer [9]. In most cases, BCL6 expression is associated with poor prognosis and worse outcome, although not always – BCL6 can suppress tumorigenesis in medulloblastoma [10] and is associated with a better prognosis in a subset of gastric lymphoma [11]. A recent publication showed that the BCL6 locus was translocated and expressed in a subset of glioblastoma with IDH1 expression [12] and

very recently, BCL6 expression was observed in glioblastoma where it correlated with increased expression of the Axl kinase [13].

Apoptotic and cell death defects are critical in survival of glioblastoma and resistance to treatment, and these defects could be driven by BCL6. Apoptosis induced by chemotherapeutic agents was prevented by BCL6 over-expression in lymphoma cell lines, in part through enhancement of the antioxidant defense systems [14]. BCL6 is central to a receptor tyrosine kinase inhibitor (TKI) drug-resistance pathway, and BCL6 inhibition eradicated drug-resistant leukemia-initiating cells [15]. In GBM, BCL6 expression can be found associated with defects in apoptosis – for example, BCL6 and the BCL6 target gene EP300 [16] are among anti-apoptosis genes in a signature of survival in primary glioblastoma [17].

Here, we confirmed that glioblastoma express BCL6, and further demonstrated that DNA damaging therapy up-regulated BCL6 expression *in vitro* and in intra-cranial tumor model *in vivo*. BCL6 was transcriptionally active, and inhibition of BCL6 activity in a panel of glioblastoma cells showed that it was essential for proliferation and survival of glioblastoma.

2. Material and methods

2.1 Tumour immunohistochemistry: Sixty-two glioblastomas were obtained from neurosurgical units in Dunedin, New Zealand. The study had National ethics approval (MEC/08/02/016/AM01) and all patients provided written informed consent. Tumors had mutations in *TP53* identified by sequencing DNA extracted from frozen material. Tissue sections from paraffin-embedded material were subjected to heat-mediated antigen retrieval. BCL6 staining used the PG-B6p primary antibody (Dako, Glostrup, Denmark). MGMT staining used the MT3.1 primary antibody (Abcam, Cambridge, UK). Positive cells were identified using EDL (Dako) and DAB. Positive cells were counted in at least 10-high-powered fields (x400 magnification) using the Aperio Scancope CS digital pathology system (Aperio, Vista, CA, USA) and the percentage of positive cells per total cells measured. MGMT positive tumours had >30% positive tumor cells.

2.2 Cell lines: Human GBM lines LN18, U87-MG and T98G were obtained from ATCC and used within 20 passages. NZG-1003 and NZ-G0906 primary GBM cell lines were previously derived from primary tumors in our laboratory [18, 19]. Raji cells were a gift from Ian Morison, University of Otago, New Zealand. All cells were maintained at 37°C/5% CO_2 and cultured in RPMI-1640 with 10% FBS without antibiotics. Regular PCR testing (e-Myco, Intron BioTechnology, Korea) showed cultures were mycoplasma free.

2.3 Intra-cranial tumors: Male C57/Bl6 mice, 8 weeks old, weighing 25-30 g, were injected intra-cranially with 25,000 viable GL261 cells as previously described, then exposed to 10Gy of whole-brain ionizing radiation, with 7Gy delivered to the brain [20] at the onset of symptoms (at least two consecutive days of weight loss). They were culled by CO_2 inhalation either 24 or 48 hours after treatment and cardiac perfusion of saline performed before collection of brain tissue. Untreated tumor bearing mice were used as controls. All procedures were approved by the Victoria University of Wellington Animal Ethics committee, approval 2012R7M. Brain were then frozen and kept at -80C until sectioning.

2.4 Drugs: Doxorubicin (Merck, Billercia, USA) was dissolved at 10mM in PBS. Cells were treated with 1-3 μM and harvested at 1-3 days. TMZ was dissolved in PBS at 0.33 mg/mL, and cells treated with 10 μM TMZ every 2 days for 7 treatments. Cells were harvested 2 days after the last treatment. Cells received ionizing radiation from a cesium-137 source (Gammacell 3000 Elan, Theratronics, Ottowa, CA). After irradiation, cells were incubated for 24 hours before harvest. The peptide mimetic inhibitor RI-BPI[21] was dissolved in sterile pre-gassed water pH6.2, at 50°C and used at 2 μM. The small molecule inhibitor FX1[22] was dissolved in DMSO at 25 mM.

2.5 Antibodies: Mouse monoclonal anti Bcl-6 D8, anti-mouse IgG-HRP and anti-rabbit IgG-HRP were from Santa Cruz Biotechnology, (Santa Cruz, CA); mouse monoclonal anti-α-Tubulin Clone B-5-1-2 from Sigma-Aldrich (Auckland, NZ), goat anti-mouse Alexa 488 from Invitrogen (ThermoFisher Scientific, Auckland, NZ); FITC anti-active Caspase3 and annexinV-APC (BD Pharmingen, Auckland, NZ); mouse monoclonal anti-BCOR, mouse monoclonal anti-NCOR2 (SMRT), and mouse monoclonal anti-β-actin were from Sigma-Aldrich (Auckland, NZ); goat polyclonal anti-BCOR and rabbit polyclonal anti-NCOR were from Abcam (Cambridge,

UK); mouse monoclonal anti-SMRT from GeneTex (Irvine, CA); mouse monoclonal anti-RNA polymerase II from EMD-Millipore (Auckland, NZ)

2.6 Western Blotting: Soluble protein was extracted into lysis buffer (140 mM NaCl, 50 mM Tris pH 7.5–8, 1% triton, protease inhibitor (Complete EDTA free, Roche, Auckland NZ)) and quantified using the DC assay (Bio-Rad, Auckland NZ). Forty microgram of protein was electrophoresed through 10% SDS PAGE and transferred to PVDF membrane (Bio-Rad, Auckland, NZ). After blocking in 3% skim milk at room temperature, upper part of the membrane was incubated with 1:500 (3% skim milk) of anti-BCl6 monoclonal antibody D8 and lower part with 1:2,000 (3% skim milk) of anti-tubulin. Goat anti-mouse IgG HRP secondary antibody was used at 1:10,000 (3% skim milk). Detection by enhanced chemiluminescence (Ultrasignal ECL kit, Pierce) was imaged with Gel Logic 4000 PRO Imaging System (Carestream, Rochester, NY USA). Raji lysate was a positive control for BCL6 expression. Corepressor blots were done as above, but whole cell lysate electrophoresed through 6% acrylamide gels, and blocked in 5% BSA. All co-repressor primary antibodies were used at 1:1000 dilution. ECL detection used Western Lightning Pro (Perkin Elmer, Waltham MA), imaged on the Amersham Imager 600 (GE Healthcare Life Sciences, Auckland, NZ).

2.7 Immunofluorescence: Cells grown on sterile glass coverslips were fixed 15 minutes in 4% paraformaldehyde, then permeabilized 15 minutes on ice in 0.1% Triton X-100 in PBS. Samples were blocked in 3% BSA in PBS 1 hour then anti-BCL6 antibody (1:50) was added and incubated 4°C overnight. Coverslips were washed in PBS then incubated 1:500 anti-mouse Alexa 488 secondary antibody, 3% BSA in PBS, room temperature 1 hour. After washing, samples were mounted by inversion onto mounting medium on glass slides. Images were acquired using a BX51 compound microscope (Olympus, Auckland NZ). For analysis of tumors, slides were thawed at room temperature for 10 minutes then rehydrated in PBS for 10 minutes. Non-specific binding was prevented by blocking antigenic sites for 30 minutes in PBS containing 1% FBS. A mouse monoclonal anti- BCL-6 antibody (Dako PG B6p at 1/20 or D8, at 1/50) was diluted in incubation buffer (PBS containing 1%FBS and 3% triton X-100) and applied overnight at 4C. Slides were then washed 3x 15 minutes in PBS. A goat anti mouse IgG labelled with AF488 (A-11029, 1/250 dilution) was used as a secondary antibody and incubated for 1 hour at room temperature. After 3 washes in PBS, slides were mounted using

ProLong™ Gold Antifade Mount (ThermoFisher Scientific, Auckland, NZ).

2.8 Transfection: pcDNA3-hBCL6ΔZNF, pcDNA3-GFP BCL6$_4$-tkLUC, and pGL3 control plasmids were purified using PureLink® HiPure Plasmid Filter Maxiprep Kit (Invitrogen, Auckland NZ). All cells were transfected using Viafect (Promega, Auckland NZ) at 70% confluence following manufacturers instructions, and cells were harvested at 24-48 hrs. siRNA against BCL6 and control (Santa Cruz Biotechnology, Santa Cruz, CA, USA) were used according to the manufacturers siRNA gene silencing protocol. For hypoxic transfection, cells were pre-incubated in 0.5% oxygen for 24 hours, then transfected and replaced into 0.5% oxygen for an additional 24 hours.

2.9 Clonogenic assay: Transfected cells were flow sorted according to GFP status (Influx, BD Biosciences) then 400, 200 and 100 GFP positive or negative cells were seeded into 10 cm dishes and incubated for 2 weeks. Colonies were washed twice with PBS followed by fixation with neutral buffered formalin, 6% v/v for 30 minutes followed by overnight staining with 0.5% methylene blue, on a rocking platform. Plates were washed in cold tap water until the water ran clear, drained and allowed to dry. Plates were scanned (GE ImageScanner III) and colonies >50 cells were counted using Fiji (ImageJ2) software. Plating efficiency and surviving fractions were calculated as follows: Plating efficiency (PE) = number of colonies counted / number of colonies plated. Surviving fraction (SF) = PE sample / PE control.

2.10 Cell death and apoptosis: Cells were washed in PBS+1% BSA with 50 ng/mL PI, and PI positive cells were identified by standard flow cytometry techniques using the LSRII flow cytometer with FACSDiva 6.2 acquisition software (BD Biosciences, Auckland, NZ). Data were analysed using FlowJo software (FlowJo, Ashland, OR, USA). Annexin V positive cells were detected using either AnxV-FITC or AnxV-APC (ThermoFisher Scientific, Auckland NZ). For Caspase3 activation, cells were trypsinised, washed in PBS then fixed and permeabilised using the FoxP3 Fixation/Permeabilisation Concentrate and Diluent Reagent (e-Biosciences, San Diego, CA). Fixed-permeabilised cells were stained overnight with FITC anti-Active Caspase3 apoptosis kit (BD Pharmingen, Auckland NZ) then washed and analysed.

2.11 Luciferase reporter assay: Luciferase activity was assessed with the Promega Luciferase Assay System (Madison, WI). Cells were washed in PBS and then lysed and scraped in cell culture lysis reagent (25 mM Tris-phosphate, 2 mM Dithiothreitol, 2 mM 1,2-diaminocyclohexane-N,N,N',N,-tetraacetic acid, 10% (v/v) glycerol, 1% (v/v) Triton X-100). Lysate was added to a 96 well solid white flat bottom plate (Corning, NY). Luciferase assay reagent (LAR) was prepared according to the manufacturer's instructions. LAR was injected into the plate and read by the Tecan Infinite M1000 Pro Plate Reader (Männedorf, Switzerland). Light values were normalized to cell counts (luciferase value/number of cells) taken before lysis of the cells and then relative change (double transfection or treated value/single transfected untreated value) value in light compared to untreated single-transfected control was calculated.

2.12 Quantitative Reverse Transcriptase PCR(q-RT-PCR): RNA was extracted using the Zymo Quick RNA MiniPrep kit (Zymo Research, Irvine, CA) according to the manufacturer's instructions. RNA was quantified with the Qubit RNA high sensitivity assay (Life Technologies, Auckland, NZ) according to the manufacturer's instructions. Reverse transcription was performed using the iScript cDNA synthesis kit (BioRad, Auckland, NZ) according to the manufacturer's instructions, with 250 ng of RNA in each reaction. qPCR was performed with KAPA SYBR® FAST Universal One-Step qRT-PCR Kit (KAPA Biosystems, Wilmington, MA) and Qiagen Quantitect Primer assays (Qiagen, Hilden, Germany) for BCL6, BCOR, HPRT, NCOR1, and NCOR2 (SMRT) with 4 µl cDNA per reaction. DCt was calculated relative to HPRT.

2.13 Nuclear Extract preparation and Electrophoretic Mobility Shift Assay (EMSA): Nuclear extracts were prepared from cells by hypotonic lysis [23] (Buffer A:10 mM HEPES-KOH (pH 7.9); 1.5 mM $MgCl_2$;10 mM KCl; 0.5 mM Dithiothreitol). Buffer B: 20 mM HEPES-KOH (pH 7.9), 420 mM NaCl, 1.5 mM $MgCl_2$ 0.2 mM EDTA, 0.5 mM Dithiothreitol) and were prepared fresh for each EMSA performed. For EMSA, sequence-specific 3'-biotin labeled oligonucleotides with the native binding site for BCL6[24] were purchase from Integrated DNA Technologies (Singapore): 5'-GAAAATTCCTAGAAAGCATA-3'. EMSA procedure was done using the Lightshift Chemiluminescent EMSA Kit (Thermo Scientific, Auckland, NZ) according to the manufacturer's recommendation. In brief, 4 µg of nuclear extract was incubated with 20 fmol of biotin-labeled probe, 50 ng/µl poly dI.dC (in 10mM Tris and 1 mM EDTA, pH 7.5), 2.5% glycerol, 5 mM $MgCl_2$, 0.05% NP-40 and 2 µl of 10x

2.11 Luciferase reporter assay: Luciferase activity was assessed with the Promega Luciferase Assay System (Madison, WI). Cells were washed in PBS and then lysed and scraped in cell culture lysis reagent (25 mM Tris-phosphate, 2 mM Dithiothreitol, 2 mM 1,2-diaminocyclohexane-N,N,N',N,-tetraacetic acid, 10% (v/v) glycerol, 1% (v/v) Triton X-100). Lysate was added to a 96 well solid white flat bottom plate (Corning, NY). Luciferase assay reagent (LAR) was prepared according to the manufacturer's instructions. LAR was injected into the plate and read by the Tecan Infinite M1000 Pro Plate Reader (Männedorf, Switzerland). Light values were normalized to cell counts (luciferase value/number of cells) taken before lysis of the cells and then relative change (double transfection or treated value/single transfected untreated value) value in light compared to untreated single-transfected control was calculated.

2.12 Quantitative Reverse Transcriptase PCR(q-RT-PCR): RNA was extracted using the Zymo Quick RNA MiniPrep kit (Zymo Research, Irvine, CA) according to the manufacturer's instructions. RNA was quantified with the Qubit RNA high sensitivity assay (Life Technologies, Auckland, NZ) according to the manufacturer's instructions. Reverse transcription was performed using the iScript cDNA synthesis kit (BioRad, Auckland, NZ) according to the manufacturer's instructions, with 250 ng of RNA in each reaction. qPCR was performed with KAPA SYBR® FAST Universal One-Step qRT-PCR Kit (KAPA Biosystems, Wilmington, MA) and Qiagen Quantitect Primer assays (Qiagen, Hilden, Germany) for BCL6, BCOR, HPRT, NCOR1, and NCOR2 (SMRT) with 4 µl cDNA per reaction. DCt was calculated relative to HPRT.

2.13 Nuclear Extract preparation and Electrophoretic Mobility Shift Assay (EMSA): Nuclear extracts were prepared from cells by hypotonic lysis [23] (Buffer A:10 mM HEPES-KOH (pH 7.9); 1.5 mM $MgCl_2$;10 mM KCl; 0.5 mM Dithiothreitol). Buffer B: 20 mM HEPES-KOH (pH 7.9), 420 mM NaCl, 1.5 mM $MgCl_2$ 0.2 mM EDTA, 0.5 mM Dithiothreitol) and were prepared fresh for each EMSA performed. For EMSA, sequence-specific 3'-biotin labeled oligonucleotides with the native binding site for BCL6[24] were purchase from Integrated DNA Technologies (Singapore): 5'-GAAAATTCCTAGAAAGCATA-3'. EMSA procedure was done using the Lightshift Chemiluminescent EMSA Kit (Thermo Scientific, Auckland, NZ) according to the manufacturer's recommendation. In brief, 4 µg of nuclear extract was incubated with 20 fmol of biotin-labeled probe, 50 ng/µl poly dI.dC (in 10mM Tris and 1 mM EDTA, pH 7.5), 2.5% glycerol, 5 mM $MgCl_2$, 0.05% NP-40 and 2 µl of 10x

Binding Buffer in a total volume of 20 µl for 20 min at room temperature. For the competition assay, 4 pmol of identical unlabeled competitor DNA was added to this reaction. For the supershift assay, 2 µg of antibody was added. After incubation, probes were loaded onto a 6% native polyacrylamide gel, electrophoresed at 100V until the bromophenol blue dye had migrated approximately two-thirds to three-quarters down the gel and further blotted crosslinked on a positively charged nylon membrane (Sigma Aldrich, Auckland, NZ). Lastly, biotin-labeled DNA protein complexes were detected by chemiluminescence on Amersham Imager 600 (GE Healthcare Life Sciences, Auckland, NZ), using the Lightshift Chemiluminescent EMSA Kit reagents (Thermo Fisher, Auckland, NZ).

2.13 Chromatin Immunoprecipitation: Cells were fixed in 1% formaldehyde for 10 min at room temperature. The crosslinking reaction was stopped by addition of 125 mM glycine and cells were washed twice in cold PBS and scraped and pelleted in cold PBS. Nuclear preparation was performed by addition of Swelling Buffer (50 mM Hepes-KOH (pH 7.5), 140 mM NaCl, 10% glycerol, 1 mM EDTA (pH 8.0), 0.5% IGEPAL, 0.25% Triton X-100), nuclei were pelleted and washed with Washing Buffer (10 mM Tris-Cl (pH 8.0), 200 mM NaCl, 1 mM EDTA (pH 8.0), 0.5 mM EGTA (pH 8.0)). Isolated nuclei were resuspended in Shearing Buffer (50 mM Tris-Cl (pH 8.1), 0.1% SDS, 10 mM EDTA (pH 8.0)) and sonicated to generate fragments of DNA <400 bp. Sonicated nuclei were incubated with either BCL6 (N3), RNA polymerase II or β-actin antibodies pre-bound to Protein G Dynabeads (Invitrogen, Auckland, NZ) in RIPA buffer (50 mM NaCl, 1% IGEPAL, 0.5% Na-DOC, 0.1% SDs, 50 mM Tris-Cl (pH 8.0), 5 mM EDTA (pH 8.0) overnight at 4°C. Immunocomplexes were recovered by magnet and washed twice with RIPA buffer, followed by increasing stringency ChIP wash buffers (150 mM NaCl, 250 mM NaCl, 250 mM LiCl). Immunocomplexes were eluted by adding elution buffer (1% SDS, 100mM $NaHCO_3$) and cross-linking was reverted by addition of 300 mM NaCl and incubation at 65°C overnight. DNA was purified with the QIAQuick PCR Purification Kit (Qiagen, Hilden, Germany) according to the manufacturer's instructions. The ChIP product was used as template for RT-PCR reactions using SYBR Green (KAPA Biosystems, Wilmington, MA) and primers for BCL6 Exon 1, BCL6 Intron 9, and *TARS*. Enrichment of DNA bound to BCL6 was calculated relative to the signal obtained from the β-actin antibody, using the 2^{-DCt} method.

	Forward	Reverse

BCL6 Exon 1	5'-GCAGTGGTAAAGTCCGAAGC	5'-AGCAACAGCAATAATCACCTG
BCL6 Intron 9	5'-AACCTGCAAAACATGGTTATTT	5'-AATTTGCCCAAACAGCAAGT
TARS	5'-TATCTACGGTGTCCGGGAAG	5'-CCTACTCTCCGCTGACCTTG

3. Results

BCL6 expression was analysed in glioma using publically available microarray data (Oncomine, Rhodes et al 2007). BCL6 transcript was higher in glioblastoma than in normal brain in several independent studies (Fig 1A), and the level of transcript increased with grade (data not shown). BCL6 protein expression was examined by immunohistochemistry in >60 GBM tumor specimens (Fig 1B). Tumor sections examined had an average of 10% BCL6 positive cells, although the number ranged from 0-45% (Fig 1C). In many sections the BCL6+ cells appeared to be perivascular, so the variation in BCL6+ cells between tumors may represent a coincidental difference in the vascularity of sections sampled. Next, the p53 and MGMT status of each tumor was determined and correlated to BCL6 expression (Fig 1C). The proportion of each tumor that was BCL6 positive was similar regardless of whether the tumor had wild-type or mutant p53. Intriguingly, MGMT expressing tumors had a higher proportion of BCL6-positive cells.

Next, BCL6 expression in a panel of glioblastoma cell lines was examined by immunofluorescence microscopy (Fig 1D and data not shown). BCL6 protein level varied - the LN18 cell line had substantial nuclear expression in most cells, while the primary tumour-derived line NZG-0906 had strong expression in a proportion of cells, and NZG-1003 had very low, but detectable nuclear expression in the majority of cells. Other glioblastoma lines, including U87-MG and T98G, also expressed nuclear BCL6 protein (data not shown).

To assess the effect of DNA damaging therapy on BCL6, the cell line panel were treated with temozolomide, ionizing radiation and doxorubicin, then BCL6 protein level and sub-cellular localization assessed by both western blot and immunofluorescence. Consistent with Fig 1D, LN18 cells had a low but generally detectable basal level of BCL6 expression (Fig 2A). Cells were treated with multiple doses of a physiologically achievable

concentration of temozolomide (10 μM) over 2 weeks. This led to significant BCL6 induction in all cells tested - LN18 (Fig 2A), T98G (Fig 2B), NZG-1003 and NZG-0906 (data not shown). Similarly, cells were exposed to 5 daily fractions of 2 Gy ionizing radiation, or one dose of 10 Gy. Both of these induced BCL6 expression in all lines tested – LN18, T98G, NZG-0906, and NZG-1003 (Fig 2 and data not shown). The effect of doxorubicin was also determined, because although does not cross the blood-brain barrier *in vivo* it has demonstrable efficacy against glioblastoma *in vitro* [19]. All cell lines tested up-regulated BCL6 with doxorubicin exposure, similar to temozolomide and ionising radiation. At very low dose, down to 15 nM, doxorubicin had little direct impact on viability of glioblastoma cell lines, but led to significant induction of BCL6 over 24 hours. The doxorubicin effect on BCL6 level increased with dose and was sustained up to 72 hours. Immunofluorescence of dox-treated cells confirmed that induced BCL6 was predominantly nuclear, (Fig 2C), suggesting that it should be transcriptionally active.

The effect of therapy on BCL6 expression was assessed *in vivo* using a murine intracranial model. Consistent with all the human cell lines, BCL6 protein was up-regulated by doxorubicin, radiation and temozolomide treatment *in vitro* (data not shown). GL261 cells were implanted intra-cranially into C57/BL6 mice, and once significant tumor burden was demonstrated by the onset of weight loss, 7 Gy of whole brain irradiation was delivered [20] then tissue collected 24 or 48 hours after irradiation. BCL6 protein was analysed by immunofluorescence in the brain tumor, and compared to normal brain in the opposite hemisphere (Fig 2D). Localisation of tumor was determined by DAPI-staining of nuclei, which showed the densely packed irregular nuclei typical of this model [19]. There was a low level of basal BCL6 expression in the tumors, which was higher 24h post-irradiation, and very prominent by 48 hours. No BCL6 was observed in the normal brain tissue, either before or after irradiation.

The transcriptional activity of BCL6 in glioblastoma was determined using a BCL6-luciferase reporter construct ($BCL6_4$-tk-LUC) [25]. In order to determine the effect of BCL6 on transcription in glioblastoma, each reporter construct was co-transfected into either LN18 or U87-MG cells with over-expressed wild-type BCL6. Western blotting showed that BCL6 was strongly over-expressed upon transfection (Fig 3A). There was consistently a slight negative effect on cell viability from over-expression of BCL6 (data not shown), so in

order to control for this effect every transfection was imaged and relative cell number determined before cell lysis. Luciferase activity was measured in cell lysate, and normalized back to cell number. The level of luciferase was then compared to cells transfected with the respective reporter construct alone. These data clearly showed that over-expressed BCL6 specifically repressed transcription from the BCL6 reporter, indicating that the BCL6 repression pathway was intact and functional in the glioblastoma cell lines.

Given that doxorubicin and ionizing radiation both induced BCL6 protein, LN18 cells were transfected with either the BCL6 or control reporter plasmid, then treated with either doxorubicin or ionizing radiation to determine whether induced BCL6 had transcriptional repressor activity, similar to over-expressed BCL6. Three different doses of doxorubicin - 50, 100 and 200 nM – were used for 48 hours prior to imaging, cell quantitation and lysis. Luciferase activity from the control plasmid decreased by 50% in response to doxorubicin, suggesting a general negative effect of doxorubicin, either on transcription, expression or activity of the luciferase enzyme. In contrast, luciferase activity from the BCL6 reporter increased, doubling relative to the untreated control (Fig 3C). When compared to the effect of dox on the control plasmid, the activation was even greater. This apparent activation of transcription was unexpected, given the transcriptional repression activity of BCL6 observed upon over-expression. In confirmation, an even larger increase was observed in cells treated with 10Gy of ionizing radiation – there was little or no effect of radiation on the control reporter, but activity from the BCL6 reporter increased by more than 300% (Fig 3D). These data strongly suggested that therapy-induced BCL6 acted as an activator of transcription, rather than a repressor. Similar data were obtained from the U87-MG cell line (data not shown).

Transcriptional repression by BCL6 generally requires the co-repressor proteins BCOR, NCOR1 and SMRT (NCOR2), so co-repressor expression was examined by quantitative RT-PCR (Fig 4A) and Western blot (Fig 4B). Each co-repressor was expressed in untreated LN18 and U87-MG cells, and transcription of each was not altered by treatment with either doxorubicin or ionising radiation. Interestingly, doxorubicin treatment reproducibly dropped the protein level of each co-repressor in LN18 cells, as well as that of alpha tubulin, used as a loading control. Dox also modestly reduced co-repressor levels in U87-MG cells, but had little to no effect on beta-actin expression. Ionising radiation treatment did not affect co-repressor levels in either cell

line. The loss of co-repressor protein was consistent with the lack of transcriptional repression by induced BCL6 in doxorubicin-treated cells.

We wanted to determine whether dox-induced BCL6 had the same DNA binding ability as over-expressed BCL6. An electrophoretic mobility shift assay was performed, using the BCL6 consensus binding site TTCCTAGAA. LN18 cells were transfected with wild-type BCL6 or GFP, then nuclear extracts isolated after 48 hours and incubated with biotin-labeled DNA probe, before electrophoresis of the probe-protein complex and detection with streptavidin-HRP. Three specific DNA-bound complexes containing over-expressed BCL6 were identified by competition with unlabeled probe (a, b and c, Fig 5A). Supershift analysis with specific antibodies demonstrated that endogenous co-repressors BCOR, NCOR1 and SMRT were in complex with BCL6, consistent with robust repression by over-expressed BCL6 observed in the luciferase assay. Cells were then incubated with doxorubicin concentration used in the reporter assay, before nuclear extracts were collected for analysis. However, no binding to the BCL6 consensus binding site could be observed, either with endogenous or with doxorubicin-induced BCL6 (Fig 5B).

To determine whether endogenous BCL6 could bind DNA at all, chromatin immunoprecipitation was carried out in LN18 cells. Initially, the ability of endogenous BCL6 to bind to a positive control sequence was examined. Interaction was observed between BCL6 and exon 1 of the BCL6 gene, and not to the negative control region of BCL6 intron 9 (Fig 5C). The strength of the interaction varied somewhat but was consistently detected above background. BCL6 was also found on a region of the TARS gene, another known BCL6 interacting genomic region[26], confirming that endogenous BCL6 could bind DNA in an appropriate context, although not always at a high level. Doxorubicin treatment did not significantly change BCL6 binding at either the *BCL6* or *TARS* loci, as assessed at 8 and 48 hours post-treatment. This suggested that DNA binding by BCL6 did not require the presence of the co-repressors, consistent with the lack of direct transcriptional repression.

In other cell types, BCL6 activity is dependent on co-repressor interaction with the lateral groove of the BTB domain. Given the lack of repression, and of co-repressor expression in glioblastoma after doxorubicin

treatment, we used two inhibitors that specifically block protein interactions at the BTB domain – the peptide mimetic RI-BPI and the small molecule FX1 – and compared them to a general loss of BCL6 activity, by siRNA and a dominant negative BCL6 mutant.

The effect of BCL6 reduction by siRNA was determined in three different lines – LN18, NZG-1003, and T98G, and the effect on apoptosis quantified by analysis of active caspase-3 (Figure 6A). Consistent with poor apoptosis in glioblastoma, the total number of cells with active caspase-3 was low. However, apoptotic cells increased from control siRNA to BCL6-siRNA treated cells, 2-fold for NZG-1003 and T98G, and 7-fold in LN18. The efficacy of siRNA knockdown was measured by flow cytometry for intracellular BCL6 protein. Knock-down of BCL6 was not highly efficient but within the apoptotic population, BCL6 expression decreased (Fig 6A, right panel), consistent with a protective effect of BCL6 expression in glioblastoma.

As a comparison, BCL6 was inhibited using the peptide mimetic inhibitor RI-BPI, which specifically blocks BCL6 co-repressor interaction by binding in the lateral groove of the BTB domain, a major protein interaction domain [27]. Both NZG-1003 and LN18 cell lines were treated with 2 μM RI-BPI for 24 hours, then apoptosis quantified by annexin-V positivity. Consistent with the caspase-3 data, an annexin-V positive apoptotic phenotype emerged with BCL6 inhibition (Figure 6B). Again, only a small population of cells were involved. In LN18 cells, anxV+/PI- cells increased 10-fold, from 0.2% to 2.1%, while the anxv+/PI+ increased from 0.02% to 0.9%. This led to a 10-fold increase in the total anxV+ apoptotic cells, from 0.2% to 3%. In NZG-1003, total anxV+ cells increased by 50% with BCL6 inhibition, from 12.4 to 17.9%. There was a 2.5-fold increase in anxV+/PI negative cells, from 1.9% to 4.8%, as well as increased anxV+/PI+ population. Again, the cell numbers were low but the data were reproducible across 3-5 independent experiments.

The effect of total BCL6 reduction was equivalent to specifically blocking protein-protein interaction at the BTB pocket, suggesting that the BTB pocket is a key mediator of BCL6 activity. This was not sufficient to induce widespread apoptosis. However, the induction of apoptosis *per se* is not critical for effective therapy - as long as cells die, the actual mechanism is arguably unimportant.

To look at "all death" after short-term loss of BCL6 activity, we simply used propidium iodide uptake. Three cell lines were transfected with DN-BCL6-GFP, a BCL6 construct with intact BTB dimerisation domain, but a deletion in the zinc finger domain. This dimerizes with and inhibits endogenous BCL6 binding DNA, hence blocking transcription activity of the endogenous protein. GFP expression allowed identification and purification of transfected cells. GFP + cells were gated and the effect of DN-BCL6-GFP on viability determined as the proportion of PI+ GFP+ cells (Figure 7A), compared to the effect of GFP alone. GFP expression had a negligible effect in LN18 cells, but was detrimental to NZG-0906 and NZG-1003, with 9-16% of GFP+ cells PI+ after 24hrs. In LN18 and NZG-0906, DN-BCL6-GFP expression doubled the proportion of PI+ cells, from 2-4% and from 16-31% respectively. In NZG-1003, DN-BCL6-GFP caused a 4-fold increase in non-viable cells, from 9-36%. In hypoxic conditions, hypoxia alone increased PI+ cells, but inhibition of BCL6 by DN-BCL6-GFP still increased the number of non-viable cells 2.5 times, from 4% to 10% (Fig 7A, right panel).

The proportion of non-viable cells after BCL6 inhibition was reproducible but small. To determine the long-term consequence of BCL6 inhibition, transfected DN-BCL6-GFP+ cells were sorted from the non-transfected GFP- cells, and the clonogenic potential of each sub-population compared (Figure 7B), again with GFP+ cells as a control. Relative plating efficiency, or the number of colonies formed from a specific number of sorted GFP+ cells was determined by comparison to colonies from the same number of sorted GFP- cells, was determined for DN-BCL6-GFP and GFP alone. GFP alone had a detrimental effect on LN18 cells, with a 30% reduction in plating efficiency. However, DN-BCL6-GFP doubled the effect, with a 60% reduction. In T98G there was no effect of GFP expression on long-term survival, and greater than 50% reduction in plating efficiency with DN-BCL6-GFP, demonstrating clearly that loss of BCL6 activity was sufficient to reduce viability. Similar results were seen with the other cell lines NZG1003 and NZG0906 (data not shown).

To compare loss of overall activity, to a specific interruption of the BTB protein interaction domain, clonogenicity was determined using the small molecule BCL6 inhibitor FX1[22], which also binds the lateral groove. The IC50 for FX1 on LN18, NZG-1003 and NZG-0906 was determined, and shown to be 25-40 uM, similar to lymphoma cell lines (data not shown and [22]). LN18 cells were treated with either 25 or 40 uM for 24 hours, then the relative plating efficiency compared between treated and untreated cells. At 40 uM, BCL6

inhibition decreased clonogenicity completely, so that no colonies were formed (data not shown). At 25 uM there was a 50-70% reduction in colony formation across all cell lines (Fig 7C).

4. Discussion

In this study, we assessed the potential role of the BCL6 protein in glioblastoma survival and therapy resistance. We directly demonstrated a key role for BCL6 in survival of glioblastoma cells *in vitro*. Differential expression analysis showed that BCL6 transcript level is higher in GBM than in normal brain. These findings are consistent with the recent literature, with reported BCL6 overexpression in many cancer cells compared to normal tissue, including gall bladder, breast, and colorectal cancer [6, 7, 9]. We also demonstrated endogenous BCL6 in glioblastoma tumor specimens. The localization of BCL6 in glioblastoma was particularly interesting - in many cases, it appeared to localize to perivascular regions of glioblastoma. If this is confirmed upon further analysis it might suggest BCL6 is expressed in cancer stem cells that inhabit the perivascular niche [28]. Co-staining BCL6 with GBM cancer stem cell markers such as CD133, integrin a6, notch or IL8 receptors [29, 30] would support this, and this is currently under investigation.

A previous publications to link glioma and BCL6 [12] saw a correlation between BCL6 and p53, predominantly in IDH1+ glioblastoma, a subset of secondary tumors arising from lower grade glioma. Our collection was predominantly primary glioblastoma, but did include some secondary disease. We did not see any correlation between p53 status and BCL6 expression. However, an interesting correlation was observed between BCL6 and MGMT expression, with higher BCL6 expression observed in MGMT positive tumours. Recent data show MGMT expression is commonly expressed by macrophages, and some tumours classified as MGMT+ actually reflect high levels of MGMT+ macrophage infiltration [31]. The observed association between MGMT and BCL6 could therefore simply mean that BCL6 is higher in tumours with greater macrophage infiltration. The relevance of this is not yet clear - BCL6 expression in glioblastoma cells *in vitro* is clearly not in macrophages, and more investigation is required.

Consistent with literature in other cell types[32], genotoxic stress induced by the standard glioblastoma therapy temozolomide and ionizing radiation, as well as doxorubicin, induced more BCL6 expression in glioblastoma, which was nuclear-localized. The induced protein could bind DNA, as observed by chromatin immunoprecipitation, and activate expression from a reporter gene. The exact identity of the DNA sequence recognized by BCL6 in glioblastoma, and how BCL6 interacts with the transcriptional machinery in the glioblastoma cell, is not yet clear. A single copy of a known consensus binding site was not enough to bind endogenous BCL6, but 4 sites multimerised in front of a reporter could direct BCL6-mediated activity, and BCL6 could bind genomic DNA, as determined by chromatin immunoprecipitation. Clearly, the DNA sequence context is important, and more work will be required to determine the requirements for BCL6 binding in glioblastoma, and the identity of the BCL6 target genes.

More curious is the apparent transcriptional activation activity of BCL6 in glioblastoma, a protein generally thought of as a transcriptional repressor. It is not unheard of for a transcription factor to switch from repression to activation – PLZF, a BTB/ZF protein closely related to BCL6 can be converted from a repressor to an activator in different cell contexts, by deacetylation followed by phosphorylation [33]. Whether a similar mechanism has occurred for BCL6 is glioblastoma is now under investigation. Interestingly, a recent publication also supports the hypothesis that BCL6 has become an activator in glioma – while not explicitly describing the mechanism, nor proving it was a direct effect, an association was seen between BCL6 and increased expression of the Axl tyrosine kinase [13].

We tested the hypothesis that BCL6 drives apoptosis resistance in glioblastoma, and that loss of BCL6 would allow apoptosis to occur. Our data are the first direct measure of the effect of BCL6 inhibition on apoptosis in glioblastoma. The apoptotic effect of BCL6 loss was consistent but not strong, either with siRNA or with inhibitors. While BCL6 may have a small role in preventing apoptosis, supported by the previously observed correlation between apoptosis and BCL6 expression[12], we concluded that BCL6 activity is not largely responsible for poor apoptosis in glioblastoma. Instead, we took an agnostic approach to cell death, measuring just loss of viability and long term proliferative potential. This clearly demonstrated that BCL6 is very important in glioblastoma cell survival - BCL6 inhibition using the small molecule FX1 at 40 uM stopped all

long-term proliferation, which decreased significantly at 25 uM. The importance of this is supported by the recent finding that BCL6 inhibition stopped proliferation [13], although contrary to Xu et al. we can see no evidence of senescence in any of our BCL6-inhibited cells.

In order to confirm the importance of BCL6 for glioblastoma, and to begin to understand the mechanism of action, we made multiple attempts to knock out the BCL6 locus using nuclease-mediated genome editing. These were all unsuccessful – while the BCL6 locus could be edited in other cell types, and other loci edited in glioblastoma cells, any glioblastoma cell that had nuclease editing of the BCL6 locus died within 48 hours and could not be selected (data not shown). These data strengthened our hypothesis that BCL6 is essential for survival of glioblastoma cells *in vitro*.

Evidence for a role of BCL6 in survival of people with glioblastoma is important for translation of BCL6 inhibition to the clinic. We could not find proof that BCL6 was associated with a worse outcome in our cohort of tumor samples, perhaps because the clinical data were incomplete. However, analysis of copy number and survival using the Rembrandt database [34] provided a hint of support. Three GBM patients had loss of 3q27, including the BCL6 locus, and increased survival (data not shown). While three is not a significant sample, this supports our hypothesis that BCL6 plays an important role in survival of glioblastoma *in vivo*. Further, a recent publication has suggested that expression of BCL6 protein was associated with worse survival in a cohort of glioblastoma patients [13].

These data strongly suggest BCL6 is a genuine target for therapy in glioblastoma. People diagnosed with glioblastoma have few options for treatment, and those options are not effective. BCL6 inhibition has been shown to be highly effective in animal models of lymphoma and leukemia, and inhibitors are currently in clinical development. BCL6 inhibition in glioblastoma is highly feasible – several inhibitors, both peptide and small molecule, have been developed for BCL6 in lymphoma and leukemia [4, 27], and some have been identified that pass through the blood brain barrier and accumulate in the brain (unpublished data). In glioblastoma, BCL6 inhibition presents a highly tumor-specific target and has real potential to improve the outcome for people with this disease.

Acknowledgements. We would like to thank Maria Celina Capistrano and Mathew Storey for their technical assistance. Financial support came from the Cancer Society of New Zealand CSNZ13/25; Genesis Oncology Trust 1155-RPG and 1457-RPG, and Victoria University of Wellington, to MJM. Cancer Society of New Zealand, Wellington Division, CT Collins PhD scholarship to NMJ. The funding bodies had no role in study design, analysis or interpretation of data, writing of the report or the decision to submit the manuscript for publication.

References

1. Stupp, R., et al., *Effects of radiotherapy with concomitant and adjuvant temozolomide versus radiotherapy alone on survival in glioblastoma in a randomised phase III study: 5-year analysis of the EORTC-NCIC trial.* Lancet Oncol, 2009. **10**(5): p. 459-66.
2. Stegh, A.H., et al., *What drives intense apoptosis resistance and propensity for necrosis in glioblastoma? A role for Bcl2L12 as a multifunctional cell death regulator.* Cell Cycle, 2008. **7**(18): p. 2833-9.
3. Xu, Y.Y., et al., *Development of targeted therapies in treatment of glioblastoma.* Cancer Biol Med, 2015. **12**(3): p. 223-37.
4. Parekh, S., G. Prive, and A. Melnick, *Therapeutic targeting of the BCL6 oncogene for diffuse large B-cell lymphomas.* Leuk Lymphoma, 2008. **49**(5): p. 874-82.
5. Cerchietti, L.C., et al., *A small-molecule inhibitor of BCL6 kills DLBCL cells in vitro and in vivo.* Cancer Cell, 2010. **17**(4): p. 400-11.
6. Ribeiro, I.P., et al., *Genetic gains and losses in oral squamous cell carcinoma: impact on clinical management.* Cell Oncol (Dordr), 2014. **37**(1): p. 29-39.
7. Sena, P., et al., *Morphological and quantitative analysis of BCL6 expression in human colorectal carcinogenesis.* Oncol Rep, 2014. **31**(1): p. 103-10.
8. Liang, P.I., et al., *BCL6 overexpression is associated with decreased p19 ARF expression and confers an independent prognosticator in gallbladder carcinoma.* Tumour Biol, 2014. **35**(2): p. 1417-26.
9. Walker, S.R., et al., *The transcriptional modulator BCL6 as a molecular target for breast cancer therapy.* Oncogene, 2015. **34**(9): p. 1073-82.
10. Tiberi, L., et al., *A BCL6/BCOR/SIRT1 complex triggers neurogenesis and suppresses medulloblastoma by repressing Sonic Hedgehog signaling.* Cancer Cell, 2014. **26**(6): p. 797-812.
11. Chen, Y.W., et al., *High BCL6 expression predicts better prognosis, independent of BCL6 translocation status, translocation partner, or BCL6-deregulating mutations, in gastric lymphoma.* Blood, 2006. **108**(7): p. 2373-83.
12. Ruggieri, S., et al., *Translocation of the proto-oncogene Bcl-6 in human glioblastoma multiforme.* Cancer Lett, 2014. **353**(1): p. 41-51.
13. Xu, L., et al., *BCL6 promotes glioma and serves as a therapeutic target.* Proc Natl Acad Sci U S A, 2017. **114**(15): p. 3981-3986.
14. Kurosu, T., et al., *BCL6 overexpression prevents increase in reactive oxygen species and inhibits apoptosis induced by chemotherapeutic reagents in B-cell lymphoma cells.* Oncogene, 2003. **22**(29): p. 4459-68.
15. Duy, C., et al., *BCL6 enables Ph+ acute lymphoblastic leukaemia cells to survive BCR-ABL1 kinase inhibition.* Nature, 2011. **473**(7347): p. 384-8.
16. Cerchietti, L.C., et al., *BCL6 repression of EP300 in human diffuse large B cell lymphoma cells provides a basis for rational combinatorial therapy.* J Clin Invest, 2010. **120**(12): p. 4569-82.

17. Patel, V.N., et al., *Network signatures of survival in glioblastoma multiforme.* PLoS Comput Biol, 2013. **9**(9): p. e1003237.
18. Authier, A., et al., *Enhanced immunosuppression by therapy-exposed glioblastoma multiforme tumor cells.* Int J Cancer, 2015. **136**(11): p. 2566-78.
19. Broadley, K.W., et al., *Side population is not necessary or sufficient for a cancer stem cell phenotype in glioblastoma multiforme.* Stem Cells, 2011. **29**(3): p. 452-61.
20. Grasso, C., et al., *Pharmacological doses of daily ascorbate protect tumors from radiation damage after a single dose of radiation in an intracranial mouse glioma model.* Front Oncol, 2014. **4**: p. 356.
21. Cerchietti, L.C., et al., *A peptomimetic inhibitor of BCL6 with potent antilymphoma effects in vitro and in vivo.* Blood, 2009. **113**(15): p. 3397-405.
22. Cardenas, M.G., et al., *Rationally designed BCL6 inhibitors target activated B cell diffuse large B cell lymphoma.* J Clin Invest, 2016. **126**(9): p. 3351-62.
23. Andrews, N.C. and D.V. Faller, *A rapid micropreparation technique for extraction of DNA-binding proteins from limiting numbers of mammalian cells.* Nucleic Acids Res, 1991. **19**(9): p. 2499.
24. Wegner, W., G. Burckhardt, and M. Henjakovic, *Transcriptional regulation of human organic anion transporter 1 by B-cell CLL/lymphoma 6.* Am J Physiol Renal Physiol, 2014. **307**(11): p. F1283-91.
25. Chang, C.C., et al., *BCL-6, a POZ/zinc-finger protein, is a sequence-specific transcriptional repressor.* Proc Natl Acad Sci U S A, 1996. **93**(14): p. 6947-52.
26. Polo, J.M., et al., *Transcriptional signature with differential expression of BCL6 target genes accurately identifies BCL6-dependent diffuse large B cell lymphomas.* Proc Natl Acad Sci U S A, 2007. **104**(9): p. 3207-12.
27. Polo, J.M., et al., *Specific peptide interference reveals BCL6 transcriptional and oncogenic mechanisms in B-cell lymphoma cells.* Nat Med, 2004. **10**(12): p. 1329-35.
28. Pietras, A., et al., *Osteopontin-CD44 signaling in the glioma perivascular niche enhances cancer stem cell phenotypes and promotes aggressive tumor growth.* Cell Stem Cell, 2014. **14**(3): p. 357-69.
29. Infanger, D.W., et al., *Glioblastoma stem cells are regulated by interleukin-8 signaling in a tumoral perivascular niche.* Cancer Res, 2013. **73**(23): p. 7079-89.
30. Lathia, J.D., et al., *Cancer stem cells in glioblastoma.* Genes Dev, 2015. **29**(12): p. 1203-17.
31. Hsu, C.Y., et al., *Exclusion of histiocytes/endothelial cells and using endothelial cells as internal reference are crucial for interpretation of MGMT immunohistochemistry in glioblastoma.* Am J Surg Pathol, 2013. **37**(2): p. 264-71.
32. Phan, R.T., et al., *Genotoxic stress regulates expression of the proto-oncogene Bcl6 in germinal center B cells.* Nat Immunol, 2007. **8**(10): p. 1132-9.
33. Xu, D., et al., *Promyelocytic leukemia zinc finger protein regulates interferon-mediated innate immunity.* Immunity, 2009. **30**(6): p. 802-16.
34. Madhavan, S., et al., *Rembrandt: helping personalized medicine become a reality through integrative translational research.* Mol Cancer Res, 2009. **7**(2): p. 157-67.

Figure Legends:

Figure 1. BCL6 is expressed in glioblastoma tumours and cell lines. A. Plots of BCL6 mRNA expression in normal brain tissue (1) compared to GBM tissue (2) in three independent representative studies (Sun, Lee and, Murat Brain respectively) from Oncomine (https://www.oncomine.org/resource/login.html). B. Representative IHC staining of 3/62 human GBM tumours, highlighting heterogeneous BCL6 protein expression (brown staining). C. BCL6 expression level distribution in 62 human GBM tumours (top), and after stratification by p53 mutation status (middle) and MGMT expression (bottom). D. Immunofluorescent staining for BCL6 in glioblastoma cell lines LN18, NZG10/03 and NZG09/06. Immunofluorescence data are representative of at least 3 independent experiments, and are similar to other glioblastoma cell lines. Adjustments to brightness and contrast were used to improve visibility upon printing, and were applied to the whole image.

Figure 2. BCL6 expression was induced by DNA-damaging therapy in glioblastoma. A. LN18 cells were untreated (U), or treated with 10 μM temozolomide every 2 days for 12 days (7 treatments total, upper left panel), 10 Gy of ionizing radiation (upper right) or increasing doses of doxorubicin as described (lower left). LN18 cells were treated with 1 μM doxorubicin for 24-72 hours (lower right panel). BCL6 and alpha tubulin (TUBA) were detected by western blot 24 h after treatment, with Raji cell lysate used as a positive control for BCL6 expression. B. Cell line T98G was treated with increasing doses of doxorubicin, or 10 Gy ionizing radiation for 24 h, and with 10μM TMZ every 2 days for 12 days (left panel.) NZG-1003, LN18 and NZG-0906 were treated with doxorubicin for 24 hours (centre panel), NZG-0906 was treated with 10 Gy ionizing radiation at 8, 16, 24 hours (right panel). BCL6 and alpha-tubulin were detected by western, and Raji used as a positive control. U, untreated cells. C. LN18 (left) and NZG-0906 (right) were grown on coverslips, left untreated (center panels) or treated with 3 μM (LN18) or 1 uM (NZG-0906) doxorubicin (lower panels), and BCL6 detected by immunofluorescence. An isotype antibody was used as a control on treated cells (upper panels). D. Brains from mice bearing intra-cranial GL261 tumours prior to (U), and 48 hours post irradiation (10 Gy) were collected and BCL6 expression in the tumor and the normal brain determined by

immunofluorescence microscopy using Alexa-488-labelled anti-BCL6 antibody. Nuclei were imaged with DAPI. All data shown are representative of at least 3 independent experiments. Cropped images retain all bands, immunofluorescence images were adjusted only for brightness and contrast, and were adjusted evenly over the entire image.

Figure 3. BCL6 is transcriptionally active in glioblastoma. A. Western blot for BCL6, alpha tubulin (TUBA), and beta actin (ACTB) of LN18 cells transfected with BCL6wt, GFP or non-transfected (N.T) with K562 and Raji cells as BCL6 negative and positive controls, respectively (left panel). Cells were harvested 48 hours after transfection. Luciferase assay of LN18 cells co-transfected with both $BCL6_4$-tkLUC and BCL6wt plasmids or PGL3 and BCL6wt plasmids and harvested 48 hours after transfection (right panel). The luciferase values were first normalized to cell number and then expressed as a proportion of their single transfected control (either $BCL6_4$-tkLUC or PGL3 alone). B. Luciferase assay of LN18 cells transfected with either $BCL6_4$-tkLUC or PGL3 plasmid and treated with either 50, 100, or 200 nM doxorubicin. C. Luciferase assay of LN18 cells transfected with either $BCL6_4$-tkLUC or PGL3 plasmid and treated with 10 Gy ionizing radiation. All assays were performed 48 hours after treatment.

Figure 4. BCL6 co-repressors are expressed in glioblastoma. A. q-RT-PCR of BCL6 co-repressors BCOR, NCOR1, and SMRT (NCOR2) in LN18 and U87-MG cells treated with 3 μM doxorubicin, 10 Gy ionizing radiation, or untreated. The value 1/DCt is shown (x-axis), with the DCt value calculated against HPRT Ct. B. Western Blot for BCOR, NCOR1, SMRT (NCOR2), alpha tubulin (TUBA), and beta actin (ACTB) in LN18 and U87-MG cells treated with 3 μM doxorubicin (Dox), 10 y ionizing radiation (IR), or untreated (Unt). All cells were harvested 48 hours after treatment.

Figure 5. Both over-expressed and drug-induced BCL6 can bind DNA. A. EMSA of LN18 nuclear lysate transfected with BCL6wt (lanes 2-7) or GFP (lanes 8 & 9). Complexes were formed with nuclear lysate and biotin labelled probe alone (lanes 2 and 8), with unlabelled competitor DNA (lanes 3 and 9), with BCL6 antibody (B1) (lane 4), with BCOR antibody (B2) (lane 5), with NCOR antibody (N) (lane 6), and with SMRT antibody (S) (lane 7). a, b, c indicate complexes formed with BCL6 and co-repressors. B. EMSA of LN18

nuclear lysate treated with 0.05, 0.1, 0.2 and 3 μM doxorubicin and harvested 48 hours after treatment (lanes 2-6). C. Relative binding to chromatin (fold change as compared to β-actin) of BCL6 in LN18 treated with 3 μM doxorubicin and harvested 8 or 48 hours after treatment, or left untreated. Genomic regions examined were BCL6 Exon 1, BCL6 Intron 9 and the TARS gene. Fold change was calculated using the $2^{-\Delta\Delta Ct}$ method.

Figure 6. Both loss of BCL6 and blockade of lateral groove increased apoptosis. A. NZG-1003, LN18 and T98G cells were transfected with control (left panel) or BCL6 (center panel) siRNA, and cells with active Caspase 3 determined by flow cytometric analysis (y-axis). Caspase-3 positive apoptotic cell gate was established from cells stained with a control antibody, and the percentage of cells in the apoptotic gate is given. BCL6 level was measured in parallel by intracellular staining (x-axis). In the center panel, BCL6 level was determined in the apoptotic population, and the control siRNA (light grey) compared to the BCL6 siRNA (dark grey). The median fluorescence intensity for each population is shown, data are representative of at least 3 independent experiments. B. NZG-1003 and LN18 cells were treated with the BCL6 peptide mimetic inhibitor RI-BPI, or a vehicle control, for 24 hours and annexin V/PI staining used to identify apoptotic and non-viable cells. Proportion of cells is given for each quadrant. All data are representative of multiple independent experiments.

Figure 7. Both BCL6 inhibition by dominant negative BCL6 and blockade of lateral groove decreased viability and clonogenic potential. A. LN18, NZG-1003 and NZG-0906 were transfected with either a control GFP construct (upper panels) or a DN-BCL6-GFP construct (lower panels). After 24 hours, GFP positive cells were gated and propidium iodide positivity analysed by flow cytometry as a measure of non-viability. Histogram gates were established on unstained cells, and the number of cells given for each gate. Hypoxia - LN18 cells were grown in 0.5% oxygen for 24 hours, transfected with either GFP or DN-BCL6-GFP, and replaced into 0.5% oxygen for 24 hours before analysis of GFP+ PI+ cells. B. GFP+ and GFP- cells were physically sorted from LN18 and T98G cells transfected with GFP, or DN-BCL6-GFP, then clonogenic plating efficiency determined for GFP+ and GFP- cells from each transfection. C. LN18 and T98G cells were treated with 25 uM FX1 for 24 hours, then clonogenic plating efficiency determined. All data shown are representative of at least 3 independent experiments.

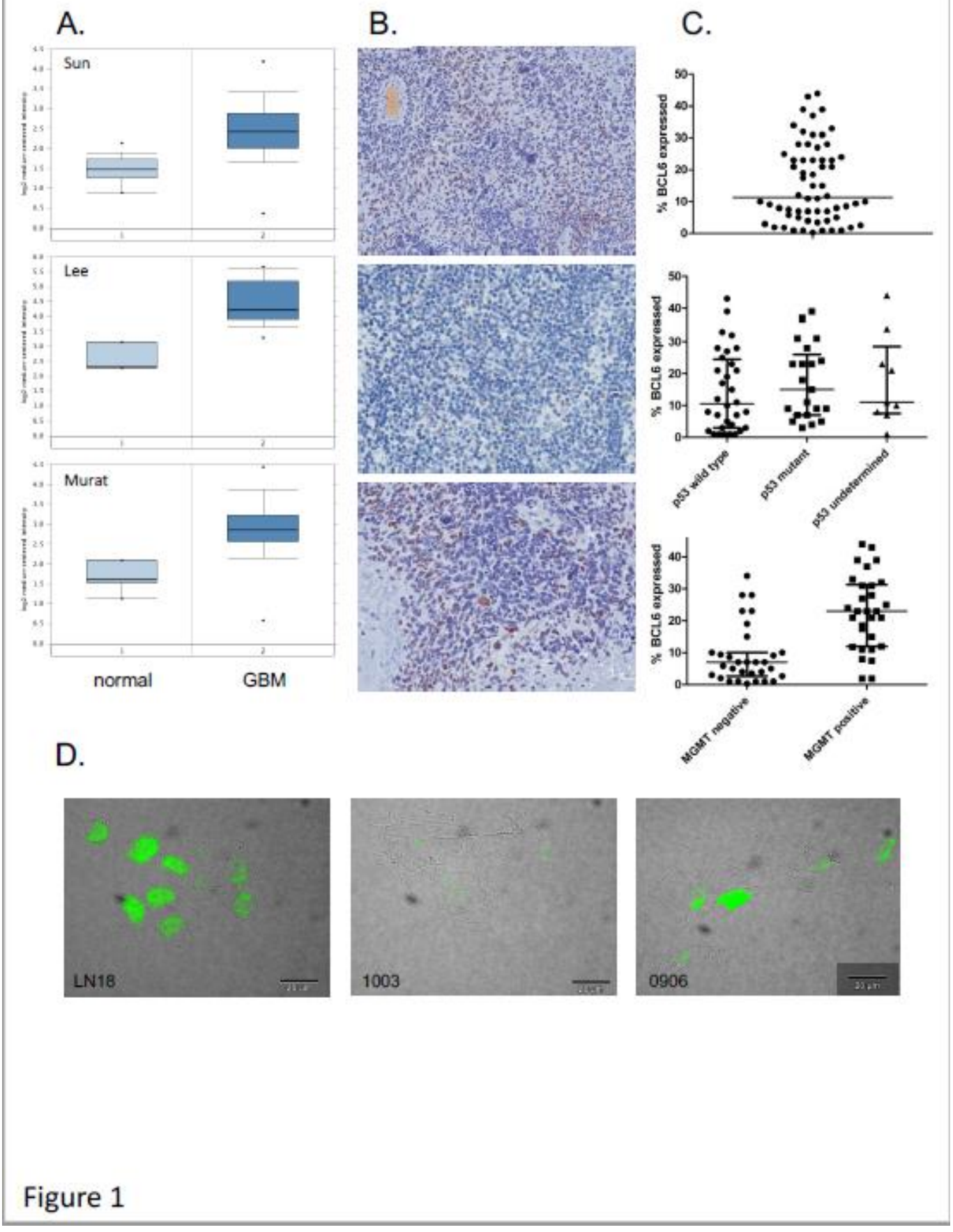
A.
B.
C.
Sun
Lee
Murat
normal
GBM
% BCL6 expressed
p53 wild type
p53 mutant
p53 undetermined
MGMT negative
MGMT positive
D.
LN18
1003
0906

Figure 1

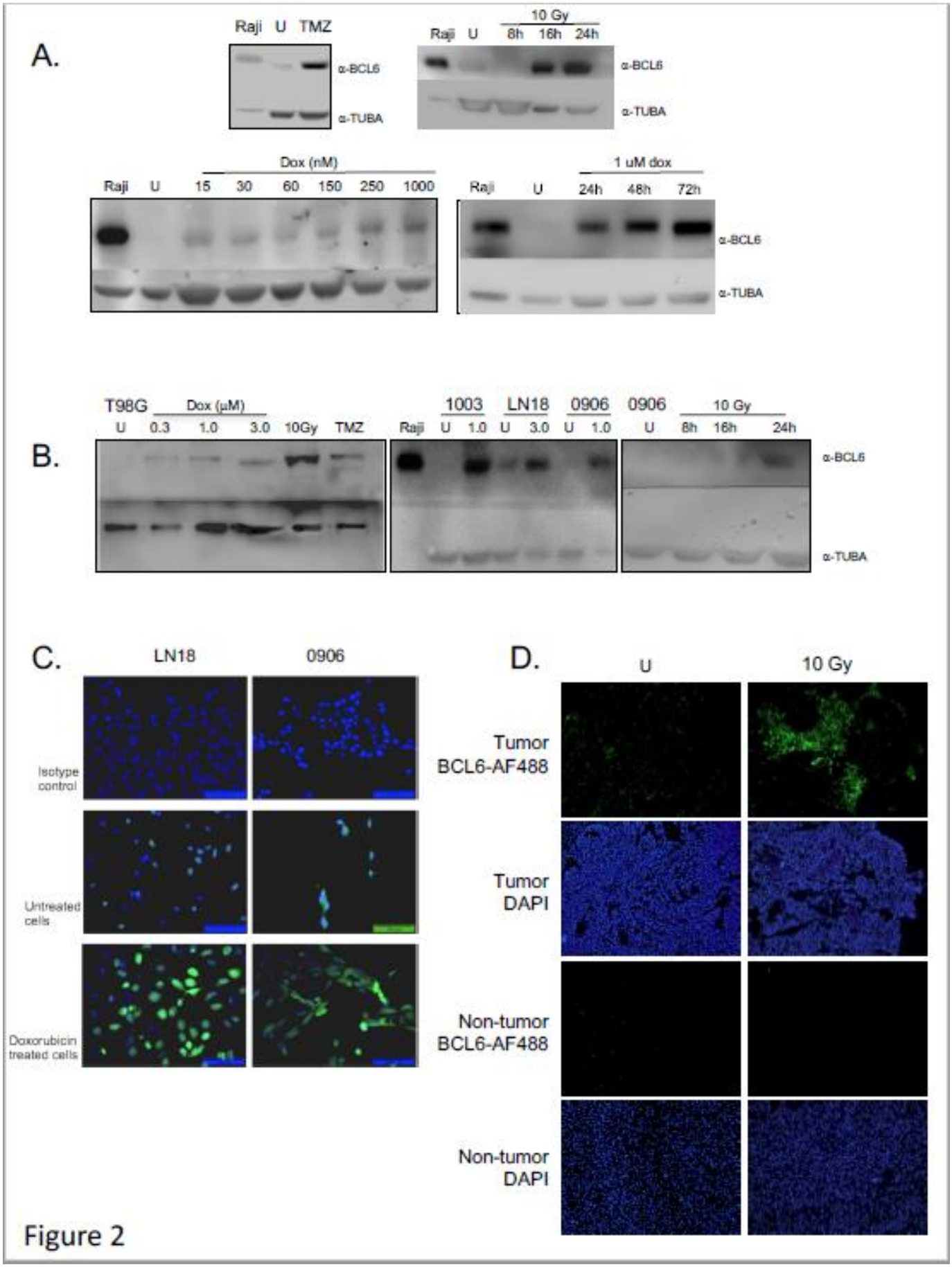
A.
Raji U TMZ
α-BCL6
α-TUBA
Raji U
10 Gy
8h 16h 24h
α-BCL6
α-TUBA
Raji U
Dox (nM)
15 30 60 150 250 1000
Raji U
1 uM dox
24h 48h 72h
α-BCL6
α-TUBA
B.
T98G
Dox (μM)
U 0.3 1.0 3.0 10Gy TMZ
Raji
1003
LN18
0906
0906
10 Gy
U 1.0 U 3.0 U 1.0 U 8h 16h 24h
α-BCL6
α-TUBA
C.
LN18
0906
Isotype control
Untreated cells
Doxorubicin treated cells
D.
U
10 Gy
Tumor BCL6-AF488
Tumor DAPI
Non-tumor BCL6-AF488
Non-tumor DAPI

Figure 2

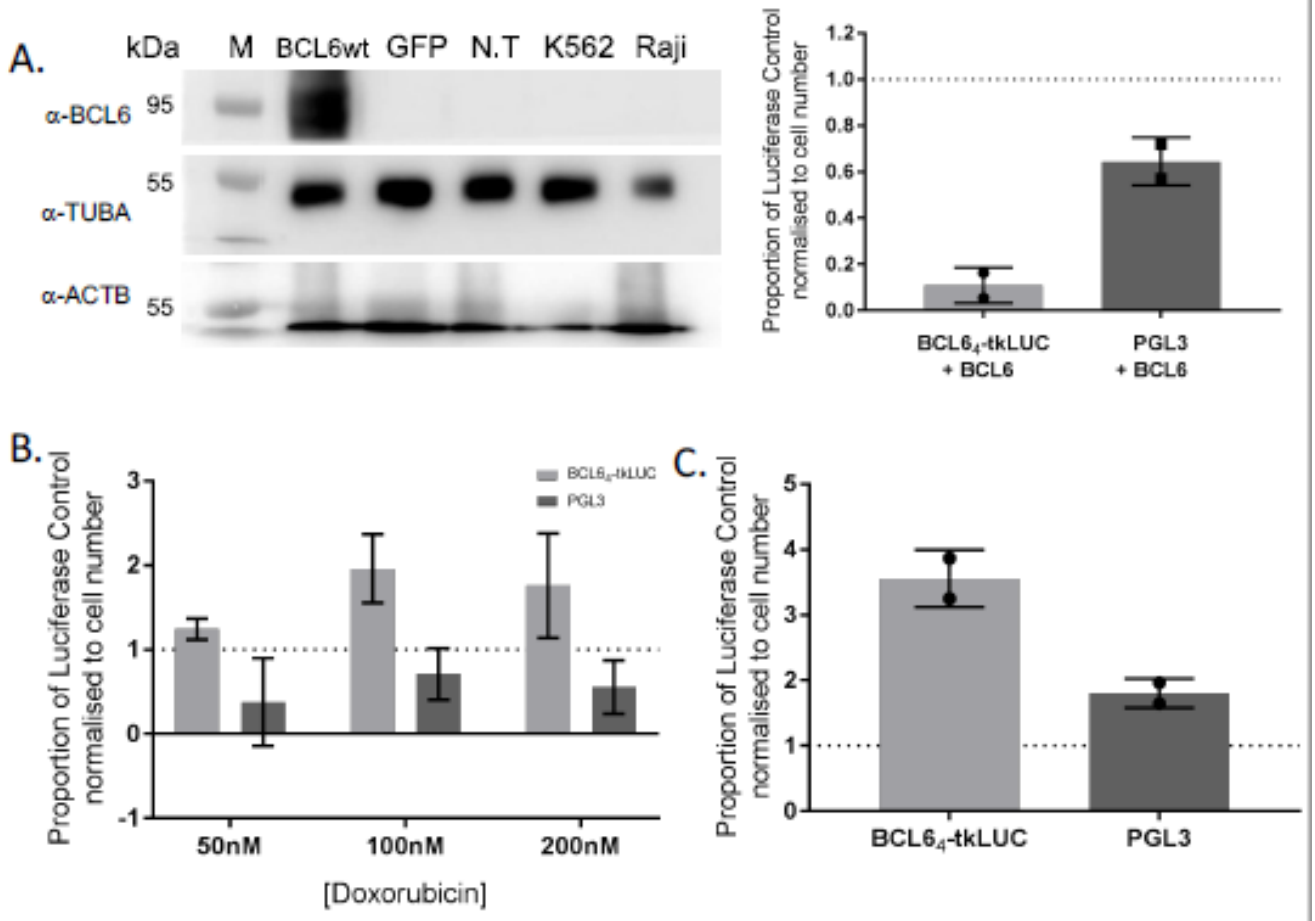
A.
kDa
M
BCL6wt
GFP
N.T
K562
Raji
α-BCL6
95
α-TUBA
55
α-ACTB
55
Proportion of Luciferase Control normalised to cell number
BCL6$_4$-tkLUC + BCL6
PGL3 + BCL6
B.
BCL6$_4$-tkLUC
PGL3
50nM
100nM
200nM
[Doxorubicin]
C.
BCL6$_4$-tkLUC
PGL3

Figure 3

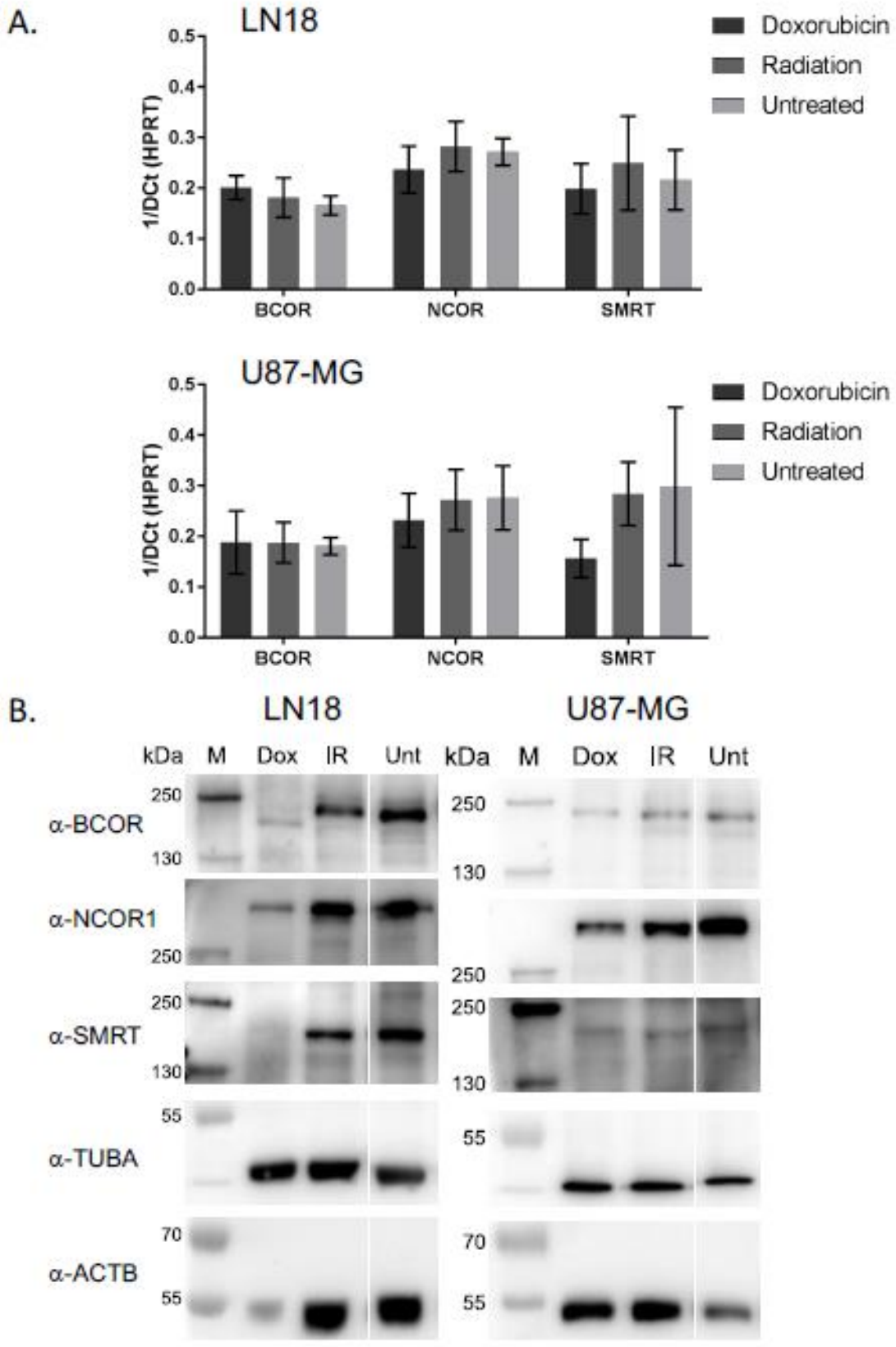
A.
LN18
1/DCt (HPRT)
0.5
0.4
0.3
0.2
0.1
0.0
BCOR
NCOR
SMRT
Doxorubicin
Radiation
Untreated
U87-MG
1/DCt (HPRT)
0.5
0.4
0.3
0.2
0.1
0.0
BCOR
NCOR
SMRT
Doxorubicin
Radiation
Untreated
B.
LN18
U87-MG
kDa
M
Dox
IR
Unt
kDa
M
Dox
IR
Unt
α-BCOR
250
130
α-NCOR1
250
α-SMRT
250
130
α-TUBA
55
α-ACTB
70
55
250
130
250
250
130
55
70
55

Figure 4

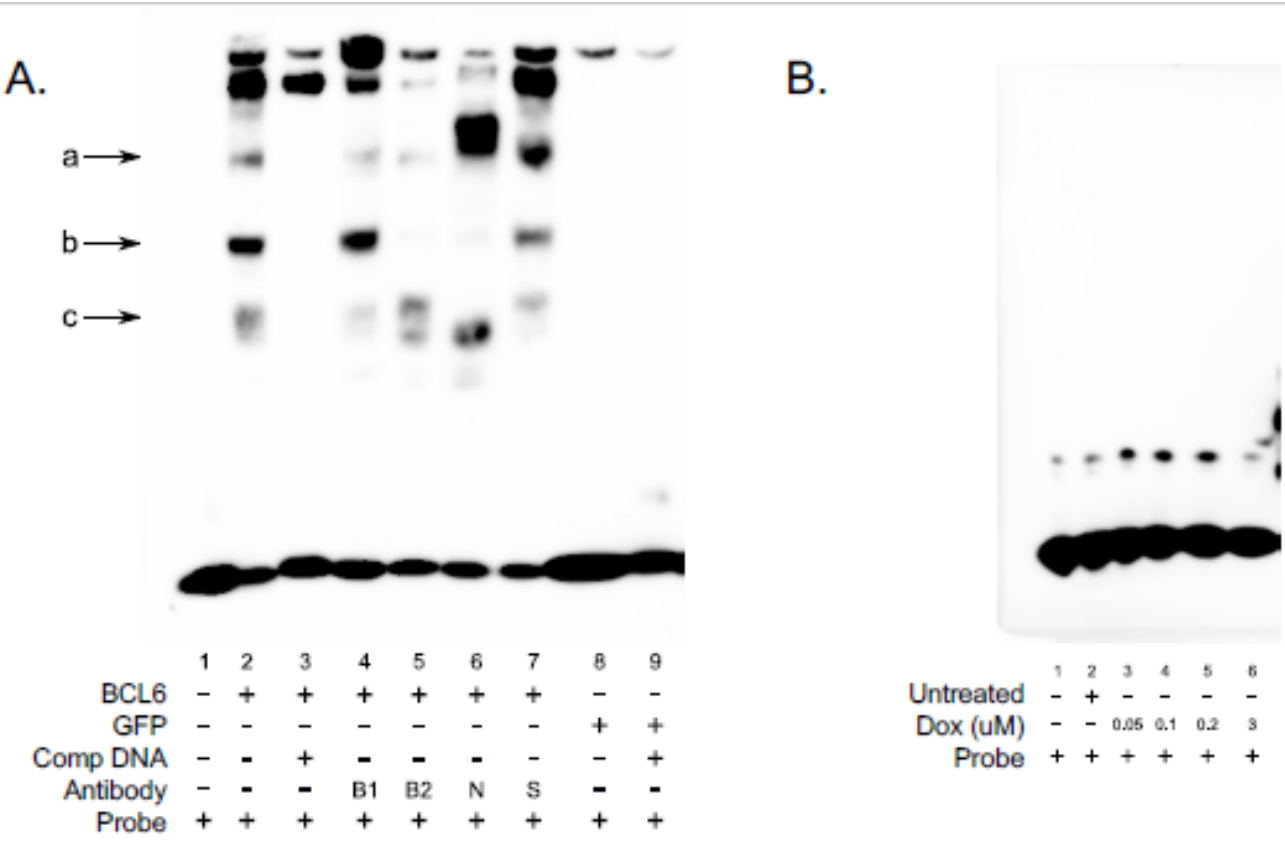
A.
a
b
c
1 2 3 4 5 6 7 8 9
BCL6 − + + + + + + − −
GFP − − − − − − − + +
Comp DNA − - + - - - − − +
Antibody − - - B1 B2 N S - -
Probe + + + + + + + + +
B.
1 2 3 4 5 6
Untreated − + − − − −
Dox (uM) − − 0.05 0.1 0.2 3
Probe + + + + + +

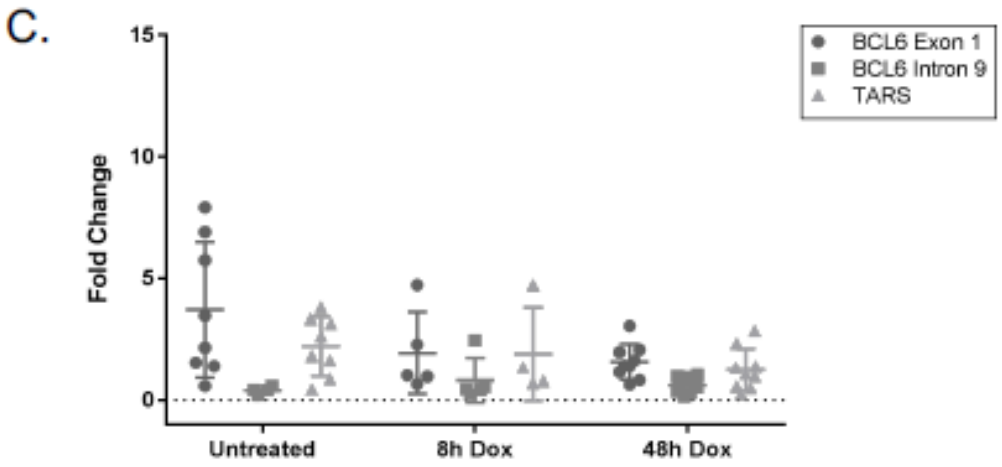
C.
BCL6 Exon 1
BCL6 Intron 9
TARS
Fold Change
15
10
5
0
Untreated
8h Dox
48h Dox

Figure 5

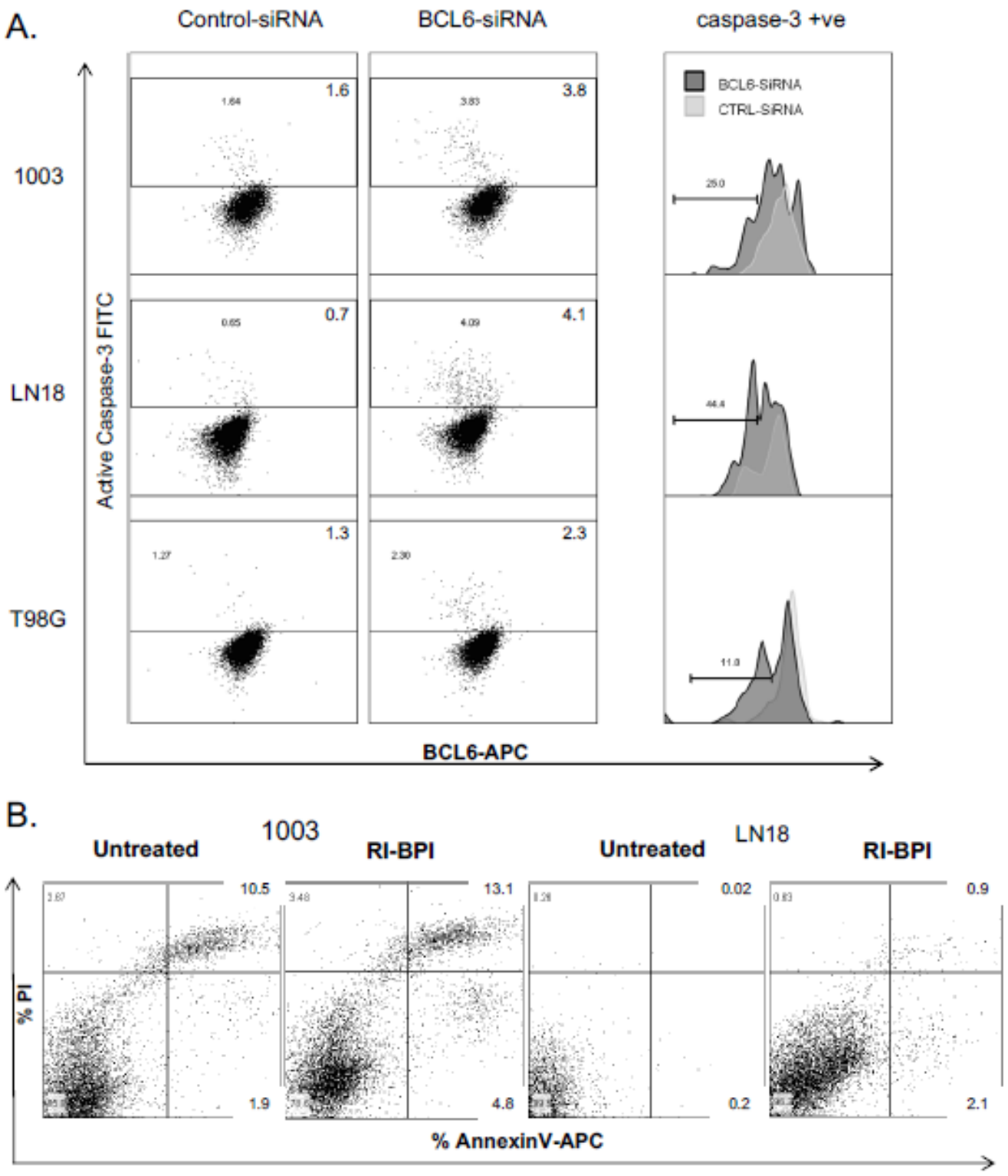
A.
Control-siRNA
BCL6-siRNA
caspase-3 +ve
1003
LN18
T98G
1.6
3.8
0.7
4.1
1.3
2.3
BCL6-SiRNA
CTRL-SiRNA
25.0
44.4
11.0
Active Caspase-3 FITC
BCL6-APC
B.
1003
LN18
Untreated
RI-BPI
Untreated
RI-BPI
10.5
13.1
0.02
0.9
1.9
4.8
0.2
2.1
% PI
% AnnexinV-APC

Figure 6

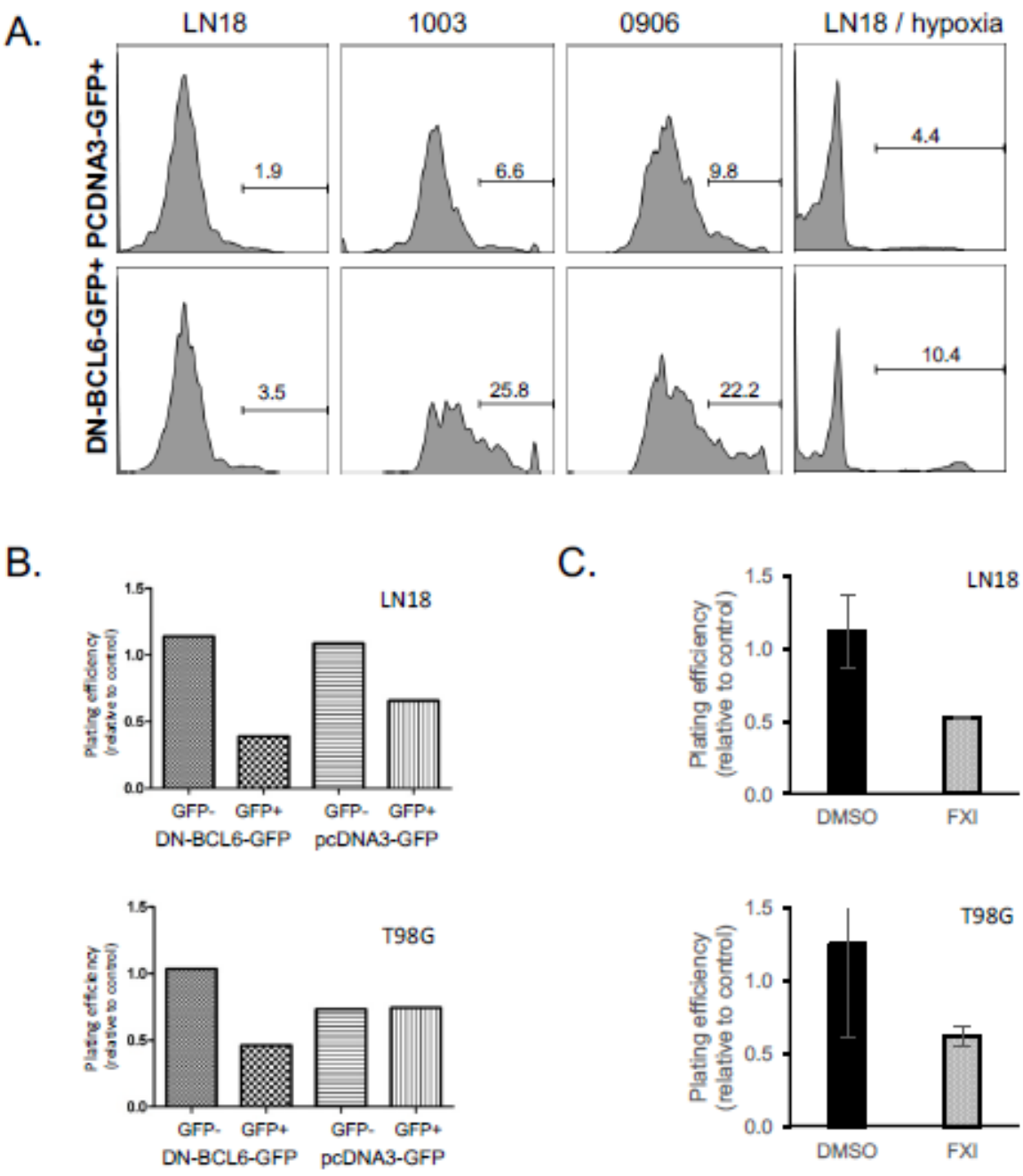
A.
LN18
1003
0906
LN18 / hypoxia
DN-BCL6-GFP+ PCDNA3-GFP+
1.9
6.6
9.8
4.4
3.5
25.8
22.2
10.4
B.
LN18
Plating efficiency (relative to control)
GFP-
GFP+
GFP-
GFP+
DN-BCL6-GFP
pcDNA3-GFP
T98G
C.
LN18
DMSO
FXI
T98G

Figure 7

9.3.RNA-seq data from FX1 treated cells

	baseMean	log2FoldCl	lfcSE	stat	pvalue	padj
WISP2	14.27834	-1.95935	0.428291	-4.57482	4.77E-06	9.63E-05
SOX9	361.749	-1.08563	0.141366	-7.67957	1.60E-14	2.65E-12
LBH	306.8257	-1.00718	0.25607	-3.93324	8.38E-05	0.001032
WNT9A	86.031	-0.98993	0.24532	-4.03527	5.45E-05	0.000733
WNT5B	250.2818	-0.94084	0.128014	-7.34953	1.99E-13	2.98E-11
CAMK1	132.6374	-0.93665	0.202404	-4.62765	3.70E-06	7.76E-05
L1CAM	4201.368	-0.62846	0.066683	-9.42452	4.32E-21	1.57E-18
DKK1	1038.024	-0.51977	0.098413	-5.28154	1.28E-07	4.38E-06
FST	7995.837	-0.49603	0.101504	-4.88684	1.02E-06	2.64E-05
WNT7B	250.026	-0.48164	0.188416	-2.55627	0.01058	0.049351
VEGFA	926.3281	-0.36577	0.123024	-2.97319	0.002947	0.01835
DKK3	2664.884	-0.20462	0.074592	-2.74317	0.006085	0.031917
PTTG1	1473.74	-0.19173	0.073031	-2.6253	0.008657	0.042077
JUN	1254.7	-0.18145	0.081027	-2.23931	0.025135	0.093178
MET	4373.197	0.159014	0.060832	2.613995	0.008949	0.043236
CCNA2	3341.02	0.194988	0.051348	3.797403	0.000146	0.001642
FZD7	574.7175	0.226659	0.085483	2.651499	0.008014	0.039605
PLAUR	739.2451	0.266713	0.112377	2.373387	0.017626	0.072153
PPARD	706.2775	0.279371	0.076632	3.645605	0.000267	0.002683
MMP2	2726.947	0.286193	0.079481	3.600768	0.000317	0.003105
VEGFC	927.5943	0.347004	0.073322	4.732608	2.22E-06	5.07E-05
VEGFC	927.5943	0.347004	0.073322	4.732608	2.22E-06	5.07E-05
LEF1	270.4387	0.428911	0.147469	2.908475	0.003632	0.02146
TNFRSF11I	167.4726	0.4488	0.17143	2.617987	0.008845	0.042808
CD44	11864.2	0.481494	0.04129	11.66135	2.01E-31	1.54E-28
BTRC	304.2225	0.485354	0.173107	2.803784	0.005051	0.027616
CACNA1G	243.5599	0.651775	0.27722	2.351114	0.018717	0.075392
IGF2	197.0119	0.72266	0.262663	2.751288	0.005936	0.031267
SNAI1	254.9513	0.746361	0.155887	4.787844	1.69E-06	4.05E-05
TCF7	279.6719	0.832998	0.134562	6.190448	6.00E-10	4.05E-08
EMP1	907.1133	0.916318	0.162719	5.631307	1.79E-08	8.05E-07
EPHB2	981.1168	1.013608	0.113551	8.926498	4.40E-19	1.35E-16
SALL4	11.82877	1.041748	0.434172	2.399389	0.016422	0.06853
ID2	505.5364	1.111374	0.188199	5.90532	3.52E-09	1.98E-07
WNT5A	1839.911	1.125761	0.12383	9.091165	9.80E-20	3.29E-17
IL6	90.45344	1.228416	0.335716	3.659088	0.000253	0.002582

Figure 44 RNA-seq data after treatment with FX1

RNA-seq data from Dox treated cells.

GENE	log2FoldCl	padj	GENE	log2FoldCl	padj	GENE	log2FoldCl	padj	GENE	log2FoldCl	padj	GENE	log2FoldCl	padj	GENE
INSM2	10.98473	3.42E-19	TMIE	5.805682	5.69E-05	MTRNR2L(	4.623333	2.07E-70	MYO15A	3.729278	2.94E-04	RP11-767I	3.185449	1.96E-04	C1QTN
CRTAC1	10.34776	3.21E-17	ISM2	5.803206	0.006905	GPR62	4.622509	0.001764	ACSBG1	3.724956	4.85E-11	SLFN5	3.184715	2.11E-112	CDS1
CXCR4	10.17191	1.19E-16	OPRL1	5.79908	9.51E-09	PRR18	4.621299	0.046832	IL17D	3.720924	3.75E-47	ALDH8A1	3.180064	0.011386	PDE2A
SOX3	10.01483	1.35E-15	MMP7	5.798952	0.009236	LINC00933	4.620395	2.69E-07	RASL11A	3.719171	7.13E-45	TMPRSS4	3.179547	0.008389	CYP4V2
GJB2	9.98198	1.56E-15	LIPH	5.798575	7.04E-05	TMEM108	4.618799	0.006432	RNF212	3.718278	0.018825	MDGA1	3.17817	1.29E-04	USP49
DIO3	9.90015	3.47E-15	RP11-12M	5.796705	0.022933	SIX2	4.617978	3.16E-05	ZNF603P	3.713524	0.0103	SYT5	3.177337	0.002013	FAM18
NME2P1	9.875479	3.98E-15	TMEM132	5.795898	1.63E-04	SLCO3A1	4.614127	2.64E-14	PRRX2	3.710597	2.42E-09	C19orf38	3.176974	0.00141	FOXD2
FOXJ1	9.839431	5.32E-15	ZFP69	5.795279	0.004076	XXbac-BPG	4.611526	0.026091	TPPP	3.710267	2.09E-22	APLF	3.173629	1.38E-15	ASIC3
PRIMA1	9.725212	1.62E-14	AGTR1	5.79398	6.78E-04	KIAA1683	4.610461	1.41E-10	FAM92B	3.70853	7.38E-04	TMC4	3.171116	2.24E-11	GFRA1
RGS16	9.68721	1.74E-14	CR1L	5.791907	5.37E-04	HIST1H2A	4.607917	4.58E-04	PTPRD	3.707843	0.007216	BEGAIN	3.170172	9.19E-05	FAM17
CHST8	9.62674	4.29E-14	EYA2	5.784721	1.85E-05	GCM1	4.60455	0.001353	BTG2	3.704968	1.57E-30	C11orf94	3.168935	2.63E-04	ZSWIM
SLC16A9	9.528901	5.75E-14	EFHD1	5.782873	9.02E-09	GPR12	4.590335	0.019997	CADM1	3.702774	4.33E-07	TMEM221	3.166625	0.011569	HCN3
MAF	9.505892	2.42E-14	ZBED6CL	5.778852	0.003926	SLC6A20	4.590231	4.78E-04	IRAK3	3.702715	0.03854	MMP3	3.166567	2.06E-15	PHF21I
SOX8	9.376042	2.72E-13	CNTN5	5.776057	5.27E-07	PLXDC2	4.585437	3.88E-12	FAT3	3.701774	0.004083	SORCS2	3.165164	0.020633	CCDC9
KIF26A	9.33409	3.19E-13	EHHADH	5.773823	4.75E-04	SLC25A27	4.58304	3.77E-12	TFPI2	3.700402	4.71E-72	TMEM74	3.16389	0.039885	ZNF385
PCSK5	9.241832	6.78E-132	KCNG2	5.771879	0.005115	FOXO4	4.58109	8.74E-156	AKAP3	3.700301	2.45E-04	IGSF9B	3.162549	4.35E-05	CTC-45
BMP6	9.235414	1.34E-13	NODAL	5.771753	0.00422	ARHGDIG	4.579663	0.007839	FBXW11P1	3.698957	6.45E-05	SLC22A23	3.161951	2.06E-18	ACO02
SOX11	9.21992	4.26E-26	RHCE	5.766546	5.22E-10	RNF151	4.578891	0.008169	COL11A2	3.697745	1.59E-68	FAM71E1	3.159048	2.51E-06	NMRK1
SFRP2	9.196029	1.16E-12	SEZ6	5.761983	4.12E-04	FAM71F2	4.572405	0.015289	ERO1B	3.694666	5.68E-55	VAMP1	3.156417	4.47E-38	NIPAL1
LMX1B	9.185604	1.75E-12	DDN	5.757067	7.71E-13	NUP62CL	4.570026	0.007546	FAM90A1	3.693756	0.017581	FAM78B	3.155407	2.15E-05	PYY
CCK	9.124571	2.65E-13	PRSS50	5.748621	0.008855	TBX10	4.567091	0.029818	CHST5	3.693295	4.14E-04	ANXA3	3.153995	1.35E-08	S1PR1
RET	9.117099	2.81E-12	SV2C	5.747346	0.006174	EPPK1	4.566472	3.31E-05	BEX4	3.68939	4.52E-04	LILRB5	3.152214	1.50E-04	PIK3R3
CADM3	9.072413	1.36E-12	AC006116	5.745231	0.025062	CYP26B1	4.565907	5.89E-36	GPR155	3.689309	7.94E-16	ETV7	3.151238	2.71E-20	SPTB
ALDH1A1	9.00383	1.80E-12	IHH	5.741899	0.026078	OR6E1P	4.565806	0.019717	TCF23	3.689244	0.015714	HSPA2	3.151052	3.31E-16	CDC42
FGF19	8.996119	3.14E-12	CTD-3088(	5.741684	0.011203	SMTNL1	4.565244	3.04E-05	GCH1	3.68649	8.15E-124	NKAIN1	3.149017	9.01E-06	MXD1
MAFB	8.994028	5.16E-17	SLC13A5	5.740873	3.22E-22	RSPH4A	4.559794	1.31E-06	SOX4	3.685868	6.10E-106	ARHGAP4	3.148609	9.10E-10	DNAH1
STAB1	8.94561	7.33E-10	LGI4	5.735746	2.74E-13	VTN	4.55408	5.85E-10	UQCRHL	3.685414	2.08E-05	HSPA12A	3.148336	1.83E-18	NR1I3
LY75-CD3(	8.923834	1.27E-09	KIF1A	5.734763	0.005657	NEUROG3	4.55174	0.028574	MEIG1	3.684854	6.20E-05	HSPB6	3.148271	5.88E-11	KCNJ12
TMEM200	8.898767	2.48E-11	MSLNL	5.734749	2.87E-04	SLAIN1	4.551686	0.001474	CYP26A1	3.684832	6.70E-07	KRTAP1-5	3.14782	0.026796	ZNF665
KCNA1	8.865436	2.25E-11	ZDHHC20F	5.734506	0.009793	CTD-2287(	4.548085	0.002053	NOS3	3.684764	0.038429	ABTB2	3.147269	5.22E-48	RP11-1
GCNT4	8.812171	1.01E-11	RAET1L	5.733746	0.028664	HIST1H2A(	4.546023	4.63E-25	PNPLA1	3.684505	0.010079	PRDM12	3.145737	0.005124	FAP
UNC5A	8.777091	4.14E-11	TDGF1P7	5.733702	5.23E-04	MYOM1	4.543954	1.63E-05	PPP4R4	3.681999	5.22E-07	NPIPB9	3.143147	2.93E-05	SKIDA1
LPL	8.746509	5.22E-11	ELOVL7	5.733617	1.87E-27	DLX3	4.542507	1.42E-09	TNRC18P1	3.681527	1.69E-04	RP11-278(	3.143121	0.003411	SLA
TPBGL	8.740308	6.46E-11	SYT7	5.729359	7.89E-09	APOBR	4.539994	1.25E-06	HIST1H2BI	3.678686	3.57E-07	TNXB	3.141578	7.15E-20	CRX
LRRN1	8.736893	1.09E-10	PCDHAC2	5.729153	1.42E-04	AC002310	4.537088	0.049794	C20orf144	3.676318	1.36E-10	NPB	3.141265	4.50E-04	KCNN3
SLC7A3	8.716295	6.85E-11	LRRC56	5.729034	2.27E-10	MCHR2	4.535299	0.01429	ZNF534	3.674778	0.029819	LTBP3	3.137516	2.75E-19	THBS2
POU3F1	8.681523	8.04E-11	PLCH2	5.727723	2.42E-04	PGPEP1L	4.533785	0.001908	FXYD3	3.673866	0.023889	CTRC	3.130952	0.021798	COL3A
FRG2B	8.6255	1.25E-10	LY75	5.7255	2.67E-09	CD5	4.532291	0.024203	TLR4	3.67199	3.15E-33	RP11-295K	3.129897	1.14E-08	HACD4
NRK	8.612652	1.57E-11	RSPO2	5.725138	0.029785	RP11-638I	4.529866	0.018486	SOX18	3.670909	3.72E-09	CILP2	3.126873	2.81E-05	CTD-22
ZCCHC12	8.609093	3.02E-37	ARHGAP2(	5.717756	7.98E-06	MOBP	4.529618	0.00653	TP53I11	3.666624	6.33E-59	HCST	3.126575	1.64E-04	HIST1H
NDUFB4P1	8.53866	5.49E-10	NF1P9	5.708334	9.67E-05	KCNJ10	4.528597	0.012176	ADAMTS9	3.665879	0.002695	NOVA2	3.120908	8.23E-04	IL17B
RP11-351I	8.525785	3.61E-10	TSSK1B	5.70451	0.001351	TRPS1	4.528044	2.52E-08	RP11-266L	3.664737	0.010352	GPR153	3.117807	1.56E-38	CXCL3
C6orf222	8.445534	7.05E-10	SAXO1	5.702414	0.004398	TMCC2	4.526973	8.75E-55	PARD6G	3.664066	2.64E-11	TNFRSF1B	3.117752	1.62E-18	SAMD1
ADAM23	8.441974	2.17E-10	SLC17A7	5.696602	1.75E-34	TCF3P1	4.524667	0.043969	CEBPA	3.66201	4.06E-96	C5AR1	3.117394	6.27E-07	POU4F
RORB	8.418784	1.66E-10	TMC5	5.694111	3.56E-08	PKNOX2	4.524451	0.044946	FGF14	3.659668	1.49E-06	RP11-168A	3.114651	5.63E-09	RP11-2
SHISA2	8.412953	4.95E-11	GPD1	5.693741	0.001907	TAF1L	4.522632	0.014765	HIST2H2BI	3.654877	5.73E-07	NKX3-2	3.112797	6.22E-24	INSR
CABP1	8.371233	1.99E-14	CDH5	5.689503	0.016199	LRRC55	4.522261	0.021092	HES7	3.65471	2.56E-22	VWCE	3.107626	3.34E-13	HSP90I

SALL3	7.860589	1.26E-06		ADGRF5P1	5.6371	0.002763		WNT16	4.457785	0.006418		COL5A3	3.609435	4.96E-06		KLHL29	3.065197	5.44E-112		CA11				
HAP1	7.832345	1.27E-26		ITIH2	5.634844	0.048652		CXorf57	4.455272	2.54E-16		TCAP	3.609075	2.42E-09		PDE3A	3.061359	5.22E-05		RASL11				
XKR7	7.790441	5.74E-07		HIST1H2B(	5.622535	4.64E-11		DEPTOR	4.452915	1.08E-09		GDF5	3.608833	4.77E-05		SLC5A5	3.058319	0.004723		PDCD4				
CCM2L	7.785121	1.85E-40		SLCO5A1	5.616706	7.01E-04		HHIPL1	4.452525	3.44E-12		NRARP	3.608333	1.62E-10		IQCF1	3.057046	0.031905		RP11-3				
PELI2	7.784267	1.34E-14		FFAR2	5.613603	0.004448		CPA2	4.452519	0.024509		WDR63	3.603889	2.93E-08		CTC-457E2	3.054319	0.044833		FAM19				
SOX2	7.782487	1.43E-07		ZAR1L	5.599401	4.19E-04		CASQ1	4.452517	0.02477		ADCY5	3.601872	8.72E-07		ZBTB10	3.052993	6.17E-47		ABC13				
CTTNBP2	7.774829	1.88E-07		MYT1	5.597535	0.037592		CHST15	4.450867	7.27E-12		PRAC2	3.601141	0.020052		THBD	3.052783	1.47E-08		ZNF75I				
LRRC32	7.769942	5.32E-07		CTB-50L17	5.59246	0.037942		SLC43A2	4.450833	1.43E-164		FGFR3	3.600921	3.57E-34		YWHABP2	3.048349	0.001495		TEKT4				
USP17L2	7.763464	1.56E-07		BTBD17	5.588531	0.03782		SH3GL3	4.448095	6.17E-20		DNAH12	3.6003	1.23E-05		DPYSL4	3.047628	2.29E-46		ANXA2				
SETBP1	7.736202	7.76E-09		RP11-824N	5.585195	0.001005		GBA3	4.445343	1.10E-04		CYP46A1	3.597581	6.41E-38		IFIT2	3.045692	2.65E-55		CD7				
RP4-764D2	7.731487	5.64E-07		GFY	5.583202	0.03822		NTRK3	4.444982	4.42E-18		JPH3	3.597508	3.02E-08		ANKS1B	3.045502	0.018412		OLFML				
PITX3	7.73048	4.79E-09		HIST1H3J	5.581255	8.01E-06		JSRP1	4.444796	3.23E-13		RP1-34B2(	2.924155	4.69E-18		HOXA3	3.045489	4.05E-18		NDST3				
CHRD	7.717345	1.62E-07		OVOL2	5.578991	0.046452		HIST1H3G	4.444627	2.15E-34		IL33	2.924081	0.014085		HIST1H2A(	3.04274	6.20E-65		ARL14E				
ATOH1	7.716166	1.99E-07		BMPR1B	5.576696	2.16E-04		MADCAM1	4.444057	9.94E-04		ITGA4	2.921898	1.48E-20		BTC	3.041978	9.00E-04		LINC01				
PCDH1	7.710677	5.45E-09		CCR2	5.576669	0.041246		CYB5R2	4.441986	0.010979		CYP21A1P	2.921767	0.039242		CCL27	3.040772	0.001726		INMT				
CDK5R2	7.704961	2.90E-09		ELFN1	5.575232	1.73E-16		SEMA3G	4.438274	1.92E-16		TFEC	2.915905	0.038904		GSX2	3.040638	3.76E-06		CFAP53				
ADGRG5	7.696973	7.48E-08		RBM22P3	5.573781	5.65E-04		HSPA6	4.430925	7.66E-19		FAM46A	2.915658	8.13E-108		RHBDL3	3.036069	1.20E-33		PFN4				
LEFTY1	7.696268	3.73E-07		CACNG7	5.572673	0.020275		OVGP1	4.430849	1.72E-11		ZC3H11B	2.915609	0.001499		FOS	3.035966	6.30E-14		MED15				
SLC25A47	7.693135	2.54E-07		CPSF1P1	5.57193	0.00422		DCAF4L2	4.427335	0.030951		RNF112	2.915369	7.90E-05		SERPINA6	3.034375	0.001239		HOXD1				
RP11-365F	7.693102	7.07E-08		ZNF467	5.567807	3.96E-10		MAST4	4.426106	6.65E-14		AGGF1P2	2.914348	0.022947		L3MBTL3	3.034032	2.53E-33		GABRA				
IGDCC3	7.686391	8.97E-08		DLL3	5.565067	1.49E-05		NPIPB6	4.42493	6.19E-05		IDO2	2.913678	0.01863		PPP1R32	3.032074	0.001375		ARPC4				
CFTR	7.681141	2.99E-06		RSAD2	5.55873	1.07E-04		ARC	4.423131	4.90E-06		FHOD3	2.911984	3.29E-05		GVQW1	3.029712	9.01E-07		NYAP1				
FZD10	7.67844	9.15E-07		ABCA12	5.554479	2.10E-04		TCAM1P	4.421868	0.014111		RP11-762I	2.91168	0.001004		AXIN2	3.028762	1.33E-45		CHST2				
OR2B6	7.67724	2.56E-08		FAM109B	5.554386	1.67E-04		CACNA1I	4.421758	0.002773		CA5A	2.909766	0.001312		CTD-2554(	3.026241	2.26E-05		SLC2A5				
HCN4	7.675515	5.70E-12		GDF7	5.552462	1.69E-11		KCNK15	4.42107	8.69E-05		GLTPD2	2.909633	6.83E-07		FAM117A	3.025802	2.84E-75		HS3ST3				
UNC5C	7.667632	4.26E-08		OTP	5.551402	0.019019		RP11-1035	4.420596	6.89E-13		DLX2	2.906171	9.26E-29		RP4-665N4	3.022432	0.014349		SLU7				
MSI1	7.665487	1.64E-08		ARID3C	5.541033	0.016247		C6orf141	4.420241	0.001813		TNFSF9	2.905395	6.66E-45		SNAI1	3.019067	1.39E-83		MAB21				
ZNF423	7.657002	3.01E-06		ITIH3	5.539226	0.001607		LDLRAD1	4.420128	0.041927		LA16c-380	2.904129	4.52E-04		RASGEF1B	3.016984	5.40E-07		RP11-3				
RAI2	7.655646	1.59E-07		CALN1	5.538609	0.008483		NKAIN1P1	4.41454	0.037214		PROC	2.904033	4.51E-10		ROS1	3.01601	3.04E-29		LSAMP				
SLC35D3	7.644038	1.10E-08		RHCG	5.537835	0.004107		SORBS1	4.414056	2.15E-30		YPEL2	2.902094	9.09E-15		ZNF844	3.015727	6.74E-52		ZNF517				
PCDH17	7.6439	1.33E-27		ZNF285B	5.534418	0.002215		AP002884.	4.41209	0.047857		ESRP2	2.901981	1.35E-04		ATRNL1	3.014682	6.21E-20		GATA2				
EGR3	7.638085	9.95E-17		NKAIN2	5.533309	0.002333		ATP1B2	4.412039	6.30E-22		HCAR1	2.899893	3.07E-05		FTCDNL1	3.011655	0.002969		FYN				
COL20A1	7.633251	1.93E-08		HGD	5.53301	0.02473		ST6GALNA	4.411672	0.042182		CACNB2	2.899524	9.35E-06		USP27X	3.010125	1.23E-21		FGFBP3				
LRRC10B	7.622737	2.38E-07		WNT8A	5.530118	0.043693		C15orf59	4.41141	3.03E-06		EPHB1	2.898104	9.60E-04		IPCEF1	3.009993	0.030319		GNG4				
TMEM98	7.607938	4.91E-09		ANO9	5.529556	0.001099		SPATA18	4.410938	0.004963		CHCHD7	2.897517	2.40E-101		NOTCH4	3.009942	6.69E-18		GRAMI				
NBEAP1	7.604316	3.04E-08		CNGB1	5.526769	2.21E-04		FAM187B2	4.410122	0.005642		CHST6	2.894814	5.68E-05		DNM3	3.008635	3.71E-06		FAM86				
LHX6	7.592147	2.73E-08		PAX1	5.523348	0.045275		GAPDHP27	4.409043	0.033752		ZNF575	2.890196	1.32E-08		ULBP1	3.005801	9.25E-30		ST8SIA				
BHLHE22	7.589598	2.53E-06		SLC5A10	5.521622	8.02E-06		RNF224	4.408913	0.039112		CDKN1A	2.889693	4.68E-88		MAGEB10	3.00462	1.34E-04		ZNF878				
BCL11A	7.569333	2.13E-09		KRT18P20	5.520672	0.046787		SCRG1	4.40484	0.009645		RHOF	2.886951	1.94E-32		SYCP2L	3.003775	0.046772		PBXIP1				
NKX1-2	7.567903	9.39E-07		CLCA2	5.502087	0.00455		FGD4	4.404313	2.38E-07		KIAA0825	2.885369	6.81E-08		TLR10	3.001382	0.042161		PTGDR				
CRHR1	7.551166	0.024701		LRRC4B	5.500484	2.77E-05		VSIG1	4.402295	0.015792		TBXA2R	2.884788	0.002745		C1QTNF9B	3.000708	0.010494		IL23A				
LEFTY2	7.536434	3.71E-06		RP11-296E	5.498198	6.18E-11		PRKCB	4.396063	1.63E-04		CCDC103	2.883361	3.78E-08		CHRNA1	2.997712	5.29E-04		PER2				
CUX2	7.52086	4.01E-06		SLC22A1	5.496106	2.14E-04		TRIM71	4.395642	0.010714		ADAMTS7	2.881154	6.59E-28		APOM	2.994598	8.03E-11		KIAA0(				
PAX3	7.51112	5.47E-08		HES1	5.495068	3.07E-15		CASKIN1	4.394301	1.63E-05		RAB37	2.881111	1.75E-05		ADRB1	2.994426	5.06E-05		KLHL25				
EFS	7.480911	6.02E-07		KIT	5.492877	0.009652		WNT10A	4.394173	0.014341		CITED4	2.876502	2.05E-10		SLC6A8	2.992232	8.24E-227		MEGF1				
KNDC1	7.457868	9.95E-06		ALDH3B2	5.490463	0.009171		RP5-1055(	4.392658	0.018381		NR2E1	2.872047	2.47E-04		CREBRF	2.989521	2.61E-21		ST14				
DISP3	7.44471	2.91E-05		ALOX15	5.489961	1.17E-04		IRF8	4.388194	0.031343		RHD	2.865231	9.93E-05		LGALS2	2.988792	0.035752		USP51				
EPS8L1	7.44168	1.11E-10		RP11-727F	5.488897	4.29E-07		MAPK8IP2	4.386583	4.13E-11		INHA	2.859071	0.004284		VIPR1	2.98868	0.001658		RAB43				
PGBD5	7.436537	2.73E-14		GRM4	5.488373	4.30E-05		GRM2	4.386461	0.017209		ICAM2	2.857095	0.047513		PPL	2.988037	0.014186		CYP2E1				

APCDD1	7.145135	1.62E-04		DNALI1	5.406513	1.60E-05		GTF2IRD1I	4.328582	0.042501		RP11-162F	2.825065	5.24E-04		SELPLG	2.953281	2.36E-26		LRP3
MXRA5	7.133297	4.40E-06		SCARA5	5.403986	0.031172		IGSF9	4.323679	2.48E-07		ANKRD55	2.818614	0.00526		SSPN	2.947915	2.59E-11		KRT8
TLL2	7.130073	4.36E-10		RIMS4	5.398658	3.12E-04		H2AFY2	4.318815	7.74E-04		KCNJ15	2.818366	8.16E-04		TENM4	2.946976	0.021911		HAMP
CCDC71L	7.127981	1.34E-18		ALX1	5.390631	1.09E-04		PLXDC1	4.313137	9.47E-11		SYN2	2.817513	0.025059		MBL1P	2.945779	0.048515		KCTD1
ARHGEF33	7.127401	1.97E-07		SASH3	5.390314	0.006009		CD300LG	4.311955	0.036681		ZNF503	2.817057	1.56E-29		NRTN	2.944369	1.30E-04		RUNDC
FLT3	7.101752	1.87E-04		SHBG	5.385052	2.08E-13		TMEM178	4.308153	2.59E-11		KBTBD11	2.816923	1.38E-08		ZMYND12	2.942505	0.021501		CLCN1
NTNG2	7.091627	6.95E-09		CNGB3	5.382442	0.002771		CDC20B	4.307509	1.18E-06		GFI1B	2.812308	6.75E-05		TMEM198	2.940667	2.06E-15		ACRBP
CFAP99	7.077108	5.02E-06		CSRNP3	5.37737	2.97E-04		CCDC173	4.306346	0.007601		C1orf228	2.811151	7.17E-04		ANKDD1B	2.936986	0.044193		STK26
EMX2	7.07313	6.92E-05		DUSP2	5.375303	2.81E-07		MCF2	4.306299	0.004824		TP53INP1	2.810915	3.53E-32		TTC9	2.935838	1.12E-18		VCAM1
FRG2	7.069882	2.69E-07		LRP2	5.375093	9.10E-11		VTCN1	4.306021	0.00681		GRIK5	2.810462	0.03306		LINC00672	2.932881	7.80E-04		HIST1H
ZNF280A	7.06883	2.74E-04		CX3CL1	5.371548	2.36E-07		NRG3	4.305009	0.018755		KATNAL2	2.809536	0.010697		NKX6-1	2.931757	4.17E-14		PTCH2
B4GALNT3	7.066191	0.006534		NTN1	5.365596	2.18E-27		AMBP	4.300251	0.038102		HES6	2.807907	3.16E-31		HIST1H2BI	2.931206	2.29E-08		FAM14
HRK	7.06556	1.08E-05		FTH1P1	5.364499	0.012629		PLXNA4	4.295724	0.003231		KDM4D	2.805139	1.13E-15		ABAT	2.928702	1.56E-16		THEGL
RP11-597A	7.058416	9.24E-06		SYBU	5.360739	0.011195		HIST1H3A	4.29488	3.91E-05		CHSY3	2.804802	6.80E-10		TMEFF2	2.927813	1.24E-18		MTSS1
COL26A1	7.055327	1.10E-09		C20orf202	5.357707	0.007136		BSN	4.293882	2.41E-19		ZNF80	2.802865	0.020896		SLC25A18	2.927727	1.67E-06		ROR1
PTPN5	7.049742	6.76E-06		MMP12	5.35586	0.026314		FLNC	4.29382	4.85E-09		ALDH1L2	2.802012	6.04E-04		PAIP2B	2.927166	3.26E-46		MSLN
NEFH	7.041327	2.44E-14		CDKN1C	5.354691	2.39E-43		ITGA8	4.286754	0.038297		RAPGEF5	2.800693	0.04194		DOC2B	2.92679	0.041696		ZNF862
FUT5	7.038805	3.57E-04		HCRTR1	5.354482	0.002462		RP11-565F	4.285816	0.048366		RP11-480I	2.79892	1.63E-06		MROH7	2.926583	5.05E-04		GBP5
AC130360	7.028892	3.63E-04		FAM189A2	5.35421	0.002786		TMPOP2	4.283659	4.90E-43		SMIM14	2.798424	4.85E-111		HIST1H2AC	2.924648	6.13E-42		RP11-3
JCHAIN	7.026405	8.34E-05		THEG	5.351289	0.031745		RP11-77K1	4.283261	2.45E-04		KCNH4	3.597464	4.31E-04		FBXO2	2.798249	0.037861		TMEM
COL2A1	7.025971	3.44E-04		ZMYND15	5.346614	2.48E-06		FAM110B	4.281973	9.69E-05		STOX2	3.59745	2.83E-04		DACH1	2.797822	4.26E-09		FAM12
NCAN	7.023824	1.25E-04		KCNJ2	5.345025	8.67E-09		CAPN3	4.279283	9.92E-06		AIM2	3.594938	4.67E-07		ZNF837	2.797753	9.14E-08		PCDHA
DPEP2	7.018005	8.81E-07		CYBA	5.343718	0.033752		DNAAF1	4.278941	7.88E-14		LGI1	3.594613	0.03543		CECR2	2.797384	2.82E-05		SP6
UGT1A10	7.011137	1.26E-06		C22orf15	5.339477	0.01616		MEIS3P2	4.277195	0.007345		POPDC2	3.593369	0.004817		SLC4A11	2.796953	4.03E-22		CAPN1
INSM1	7.000299	4.20E-04		SOX30	5.337453	2.84E-05		LBH	4.273866	2.18E-70		HIST1H4E	3.590013	1.27E-06		HEATR4	2.794532	0.008406		CASC1
KLHL40	6.997848	6.65E-05		IRF4	5.332255	0.007087		RGAG4	4.273067	9.01E-81		BTK	3.58782	1.58E-04		HIST2H4B	2.792198	0.038605		KLRD1
RP11-349C	6.98627	6.68E-05		NGFR	5.332074	3.28E-83		HIST2H2BI	4.271998	2.81E-54		TCP11L2	3.586024	1.62E-35		GLIPR2	2.792005	4.93E-47		CDH7
HAND1	6.982159	4.88E-04		PPIAL4G	5.329808	0.001246		PTGIS	4.271036	0.003293		CTRB2	3.585645	7.28E-09		GTF2IP6	2.79151	0.034738		UBN2
KDM4E	6.977266	5.43E-04		MYO15B	5.326613	2.25E-36		PAX5	4.266428	3.38E-06		C15orf48	3.585615	0.046452		RP11-347C	2.790828	0.002422		SIM2
PLA2G2A	6.975749	5.81E-04		WSCD1	5.322825	4.65E-14		NFATC1	4.264115	4.09E-07		FAM78A	3.584892	7.87E-14		HIST1H2BJ	2.79034	1.75E-18		IFI30
ADAMTS8	6.968111	1.10E-09		MGAT4A	5.322221	3.49E-12		NECTIN4	4.263534	6.10E-04		CNN2P9	3.583114	6.73E-04		LGR6	2.790128	0.026059		IFI6
CYP7A1	6.9671	5.92E-04		EPHA4	5.318917	3.08E-61		HNF1A	4.260801	0.03763		ESAM	3.580879	1.29E-23		ENO1P1	2.788613	0.005237		CSF3R
CILP	6.953971	1.01E-06		KCND2	5.318349	0.019834		PROM1	4.258347	1.24E-11		HBA1	3.580817	7.81E-08		LYPD1	2.787621	9.80E-20		PLGLB1
SBK1	6.947916	1.24E-09		AGGF1P1	5.317111	0.00474		FA2H	4.25399	5.22E-08		CFAP206	3.575339	0.004464		LTA	2.787575	0.042927		PCSK1
SULF2	6.944224	1.13E-09		RHOU	5.310617	1.23E-08		KCNH2	4.253	0.002431		RGMA	3.575263	2.78E-15		VCAN	2.782384	9.30E-26		TMEM
HELT	6.943987	6.69E-04		IGLON5	5.298656	0.016088		C1QTNF9B	4.25017	1.29E-08		LINC01314	3.572368	0.024583		CCR4	2.781246	0.017391		C2orf1
VGLL2	6.941128	2.65E-09		DES	5.297797	0.003466		NTRK1	4.241702	0.010015		SH2D3C	3.569887	2.18E-04		TPI1P2	2.781238	1.52E-14		HEXIM
FOSB	6.939989	2.19E-32		ZFR2	5.295625	0.001479		CIB2	4.238359	6.68E-08		FOXP3	3.565704	1.25E-04		YPEL5	2.780727	1.78E-97		FAM22
SHISA7	6.936477	1.09E-05		C17orf99	5.29468	0.002848		LRRC15	4.236454	0.010624		ZFHX2	3.563892	0.004445		HCAR2	2.780184	0.038835		SDHDP
MAFA	6.921296	2.53E-20		FES	5.293529	1.20E-09		PEG3	4.236085	4.62E-36		B3GNT5	3.563465	5.56E-18		MEF2C	2.779417	1.65E-08		ATCAY
CTD-2349I	6.916876	1.40E-05		C17orf47	5.291806	0.033689		FLT1	4.233316	9.75E-10		ART3	3.557842	0.005268		PDE4A	2.779367	1.17E-22		WHRN
CLCNKA	6.916319	6.57E-05		TSSK1A	5.290667	2.38E-09		NRCAM	4.23271	4.08E-11		NPIPB7	3.556663	0.013543		PLEKHD1	2.778106	0.004157		SLC25A
KLHL38	6.913164	3.90E-06		B3GAT1	5.290041	8.75E-08		SH3BGRL2	4.23098	1.05E-14		WFIKKN1	3.55519	1.77E-07		PPM1N	2.777581	2.04E-08		NF1P4
PTGER3	6.908022	1.43E-04		TLX1	5.2891	0.014045		SIRPA	4.223373	1.17E-43		ANGPT4	3.553451	0.002686		CKM	2.776916	0.003198		ADCY4
GPC4	6.903166	3.17E-09		LOC44046	5.287592	0.007267		CNR2	4.21489	2.25E-04		KIAA1456	3.553099	6.60E-11		POPDC3	2.774584	0.035201		NBR2
KLHL14	6.89964	1.15E-04		RP11-216L	5.287466	0.014009		CPLX1	4.210975	0.010588		CRABP2	3.550384	3.07E-43		RPSAP52	2.772165	7.37E-10		CCDC1
PNLDC1	6.890951	1.59E-06		PCP4L1	5.285461	7.58E-11		CNTNAP2	4.210377	3.29E-05		SLC6A12	3.548128	0.004632		GALNT16	2.771576	7.09E-04		SPRED3
EN1	6.876641	0.001037		CRB3	5.283928	0.038877		LHX2	4.209157	5.12E-15		CDH23	3.547016	0.014325		C3orf70	2.770974	9.50E-04		NXF1
FEV	6.876459	0.001004		ESRP1	5.282785	0.039501		IFI27	4.208485	1.05E-16		PRR5	3.54642	0.003128		RARB	2.770403	1.14E-05		MISP3
ESPNL	6.872188	2.39E-05		IMPA2	5.27728	8.48E-46		CARMIL3	4.206038	0.005092		SULF1	3.543004	2.03E-04		OVOL3	2.77025	0.004063		TCP10L

SLC32A1	6.693928	0.003033	RNF223	5.177711	1.35E-04	ATP6V1G1	4.152605	0.031658	KDR	3.508563	0.006811	PLCG2	2.734623	6.56E-11	USP32I
CCDC140	6.693382	0.003187	RP1-34B20	5.175819	1.94E-04	RAB33A	4.149587	2.78E-06	RP1-274L7	3.507843	0.017734	RBFOX3	2.729634	1.78E-04	FAM86
NPTX2	6.687988	5.95E-04	HSD11B2	5.172676	5.29E-15	ADGRG4	4.142962	0.003429	RP11-49C9	3.502674	0.007284	RBP4	2.729131	0.001545	TNFRSI
KLF1	6.680213	5.69E-06	CNTD2	5.163433	3.39E-07	POSTN	4.142725	1.25E-28	AQP1	3.501841	0.042854	TPH1	2.727667	0.025571	RPL3L
WSCD2	6.67783	7.06E-05	CXCL5	5.162666	0.011085	CACNG6	4.139355	0.004104	BMP8B	3.501712	0.001209	COX6B2	2.725579	1.38E-04	CAGE1
EGR4	6.671742	1.76E-08	PACRG	5.160815	0.028041	CTBP2P6	4.135452	0.039844	SOSTDC1	3.500744	0.016284	MYLK4	2.725251	2.83E-08	RP11-7
C1orf61	6.651089	7.99E-16	RP11-211(	5.160135	0.016476	GRASP	4.131947	4.47E-07	GRM6	3.500191	0.004142	FAM83H-A	2.723596	6.42E-04	PITX2
TBX4	6.637962	1.13E-04	GOLGA6A	5.157965	0.01771	LARGE1	4.131634	1.28E-19	C1orf162	3.499531	0.011325	MYO3B	2.720992	0.039072	SMOX
TMEM100	6.634332	1.80E-04	ZNF705E	5.157097	0.006154	MS4A6A	4.130789	0.033074	NATD1	3.498539	1.23E-49	SLC16A5	2.714509	0.017671	ZNRF2I
PTP4A3	6.617719	1.04E-04	CRYBA1	5.153916	0.012816	GPM6A	4.12696	5.49E-12	FNDC5	3.497063	5.43E-04	VCX	2.714195	3.97E-04	SIDT1
SHH	6.617685	8.17E-04	MUC7	5.153788	0.003704	NUTM2B	4.126759	1.10E-10	SLC35F1	3.495665	0.00277	SEL1L3	2.712663	1.93E-33	ABC7-4
VIL1	6.615768	8.16E-04	RPL23P2	5.150553	0.006064	CMTM2	4.126254	0.014325	KRTAP19-5	3.494481	0.003654	WI2-1896(	2.711397	9.82E-06	ACVR2
PSMB11	6.604032	9.72E-06	VN1R2	5.150207	7.73E-04	RP11-681L	4.126246	0.020536	GAS1	3.492792	4.31E-27	HIST1H1PS	2.710895	0.002779	UTP14(
LA16c-60G	6.59823	0.005291	A2ML1	5.149324	0.003911	PCDH20	4.125525	2.57E-06	ULBP2	3.490465	4.41E-53	ST8SIA6	2.708987	5.89E-04	WNK3
SCRT1	6.591361	1.28E-04	KCNK4-TE	5.145753	0.007032	RASAL1	4.121854	0.040082	OPRD1	3.48874	2.14E-07	C9orf50	2.708261	0.006807	ZNF415
CCDC177	6.590414	0.004995	UBD	5.145229	0.044737	CRB1	4.119318	4.48E-04	PLCXD3	3.488126	0.003339	FBXO32	2.705673	1.54E-50	FAM65
ADRA2A	6.587615	0.005205	ZDHHC11E	5.142983	0.001392	GALR3	4.118564	0.027373	CAPS	3.487784	4.40E-13	SYNPO2	2.705661	1.12E-12	GSDMI
HOXD12	6.584082	7.08E-06	CTC-559E9	5.139637	0.048588	MAP1A	4.117009	2.85E-71	HIST2H4A	3.480231	5.68E-48	NLGN4X	2.704963	0.011919	SPRY4
PXT1	6.578799	4.98E-04	CHRM4	5.130691	1.17E-66	UNC5D	4.11634	2.35E-06	SCARF1	3.480124	3.18E-07	DNAH2	2.704901	2.60E-06	SLC2A1
SLC8A2	6.573832	1.16E-05	JAKMIP3	5.125971	1.47E-09	INHBB	4.111376	4.07E-40	PLA2R1	3.479463	7.10E-06	TRAPPC6A	2.70303	6.94E-19	GPR85
ERICH3	6.570936	2.11E-04	BICDL1	5.123665	8.00E-27	FXYD6	4.11133	8.20E-04	CPNE9	3.477037	0.011383	RPL32P29	2.701519	5.52E-05	CCNG2
ACTN3	6.565618	1.03E-04	HIST1H2AI	5.117909	0.002173	ITGA9	4.111145	0.006451	LVRN	3.475581	3.37E-08	ZNF763	2.701147	1.96E-05	OSM
HOXD4	6.551369	1.17E-05	CYP17A1	5.116527	0.00565	SLC4A9	4.109982	0.042566	LONRF2	3.475298	2.38E-05	IL3RA	2.701141	1.93E-05	HR
OLIG2	6.549011	6.74E-11	PDIA2	5.115592	0.004532	GSG1L	4.10199	0.004564	ISL1	3.472691	7.53E-15	RNF144A	2.700128	0.00287	HIST1H
PPP1R14C	6.541268	0.00127	KCND3	5.114749	2.09E-07	GADD45G	4.099056	1.48E-06	LINC0095S	3.472369	9.40E-06	ID4	2.699909	2.40E-15	HLA-DI
FAM90A24	6.539059	2.38E-05	GPR35	5.11175	6.61E-10	HIST1H3H	4.098306	7.99E-64	ZNRF2P1	3.471269	1.24E-04	UNC79	2.698396	1.26E-04	NKX3-1
ZBTB32	6.53392	7.91E-08	NTN3	5.109552	9.14E-04	HIST1H2AI	4.097005	7.81E-04	MEFV	3.468219	0.011731	ADAM21	2.698097	1.06E-04	CLDN4
EIF4A1P9	6.532153	0.006807	HPX	5.101611	5.28E-11	RAB11FIP4	4.092579	2.12E-04	PGAM1P5	3.465656	0.009272	ITGB3	2.697989	8.21E-09	CCNI2
ANKRD65	6.523713	0.001776	RP11-680(	5.09217	0.005532	NXPH3	4.09111	5.45E-18	RP11-140L	3.4636	0.034537	STAT4	2.696234	1.72E-04	IRGM
ADGRB1	6.515926	0.00192	SLC25A1P3	5.08571	0.048366	RNF122	4.090403	1.03E-52	CD160	3.460815	0.009488	NEDD8-MI	2.695576	0.04948	WDR3
TAC3	6.51232	1.65E-05	TRIM26BP	5.085032	0.005723	SLC6A4	4.085933	6.87E-06	MEGF10	3.460031	0.001037	GAL3ST1	2.694383	0.00474	SLC19A
PKD2L1	6.510717	0.007317	RP4-800M	5.080349	0.005361	KLHL10	4.085026	1.30E-05	TACR2	3.458917	6.98E-05	ACPT	2.69317	0.044671	FAM21
FCGR1B	6.509355	0.00728	SMIM10L2	5.079994	1.90E-15	WNT3A	4.081204	0.012483	RP11-496H	3.457634	0.044614	RP11-456F	2.69184	0.047233	PLIN1
RAB3C	6.507858	0.002229	RP5-1056L	5.078513	0.008441	SLITRK3	4.078224	1.27E-21	SAG	3.457623	0.001119	IRF7	2.691703	1.23E-32	ADGRB
RP11-60C6	6.507134	0.007507	DNM1P34	5.078342	0.032777	TREH	4.077337	0.008341	RP11-694I	3.456831	0.001186	FAM174B	2.691183	3.79E-07	HIST1H
CA4	6.503999	1.53E-04	GFRA3	5.074546	0.013909	RP11-164J	4.075045	0.003009	CFAP52	3.456354	9.12E-05	NFATC4	2.689421	5.49E-43	VAV1
HS3ST6	6.499552	0.007822	VWA5B1	5.073757	0.00401	BCL2A1	4.074219	4.90E-04	COL4A3	3.456222	3.07E-04	RP11-616K	2.687981	0.024732	HMGN
AL590763.	6.479562	1.81E-04	FNDC7	5.073541	0.014411	CDH1	4.073201	2.56E-05	EBF4	3.45468	7.47E-09	KLHL35	2.687912	0.004449	GVINP
PCDHAC1	6.471007	5.31E-05	MAP2K4P1	5.073263	4.40E-04	MISP	4.071203	5.16E-05	PCSK6	3.454138	9.57E-06	HLA-DMB	2.684055	4.10E-05	CNNM
MYADML2	6.458624	4.11E-06	BARX1	5.071911	0.015954	NEUROD1	4.069106	0.019761	PCDH12	3.45399	9.11E-05	RP11-262H	2.682936	1.48E-04	PRSS35
AC008132	6.451936	6.64E-04	RP11-54D1	5.06993	1.08E-11	M1AP	4.065161	0.010081	DDX25	3.451157	1.68E-04	SNAP25	2.680671	3.99E-06	BACH2
SP7	6.446476	0.009569	SLC10A1	5.06679	0.008237	PDE9A	4.065059	1.23E-05	XAGE1B	3.445367	1.93E-09	SPX	2.680309	1.03E-05	EPOR
TUBG1P	6.444356	1.70E-04	RPLP1P6	5.053546	8.41E-20	HP	4.064225	0.021167	NPC1L1	3.445097	6.99E-04	ICAM4	2.680141	0.00887	MIB2
UPK2	6.439015	2.62E-11	LRRC4C	5.052066	0.012241	KCNK4	4.063843	0.006739	KMO	3.44397	3.27E-05	ATOH7	2.676915	0.02152	RP4-73
SEMA5B	6.423596	0.010681	MYCL	5.046985	2.01E-59	SSTR1	4.06104	1.51E-04	EOMES	3.443172	2.73E-14	AC003005	2.674944	0.023865	CRLF1
WNT1	6.419663	0.010759	RASAL3	5.044983	3.60E-04	LOXL4	4.057911	4.95E-11	NPR1	3.441885	8.93E-11	UGT2A1	2.674126	0.017945	ZNF487
ZNF536	6.382055	0.002493	SLC51B	5.043836	0.002919	NFIA	4.05134	9.25E-21	AC009950	3.441657	0.009874	LONRF1	2.67376	1.72E-45	ABHD1
SLC13A3	6.37522	0.003071	HIST2H3D	5.035662	0.002343	RP11-548K	4.050028	0.037535	GPR37	3.441437	2.87E-16	C8G	2.673277	6.91E-04	C8orf3
BEX2	6.367399	8.99E-05	TRPV6	5.032324	0.008398	TUBB2B	4.048037	9.93E-34	OR1F1	3.441028	0.01667	PRICKLE4	2.672627	3.03E-50	ACSL1

RFPL1	6.290466	0.0169		HIST1H3E	4.968103	1.67E-33		CH17-264E	3.999529	2.09E-04		GNAT2	3.378014	0.010793		LTB4R	2.639658
NPY1R	6.29023	6.96E-04		RTN4RL1	4.966399	4.25E-48		FAM83H	3.996721	7.28E-06		VMO1	3.374547	0.004437		LSR	2.638781
TNXA	6.288798	4.05E-04		VIPR2	4.965101	0.00946		RP11-74M	3.993102	6.26E-04		MN1	3.37354	2.17E-10		MYL12BP1	2.638267
FXYD1	6.284611	1.32E-04		SCN11A	4.963959	8.82E-06		VWA5B2	3.992799	5.58E-08		KIF26B	3.372521	5.38E-12		CLIC3	2.635637
NTN5	6.283568	2.18E-05		ADAD2	4.963843	0.003363		KIF19	3.991331	0.003343		SH3GL2	3.372174	2.05E-04		STRA6	2.635603
ATP2B2	6.28322	0.00446		SLC6A17	4.963307	0.043915		CHRM2	3.989101	0.011038		SLFN11	3.370464	0.038791		PGF	2.634618
INSRR	6.28092	6.89E-05		CHST1	4.962464	3.11E-21		NPTX1	3.987927	6.40E-46		BIK	3.370288	5.76E-07		SUCNR1	2.634039
MUC22	6.261506	4.06E-04		OLR1	4.96124	1.63E-36		MYO1A	3.987765	3.10E-05		FOXO1	3.368466	3.26E-22		NAT16	2.630405
OLIG1	6.25832	1.10E-06		FRAS1	4.960776	5.46E-21		MTRNR2L1	3.986099	0		HSD17B13	3.367506	0.006946		KCNMB4	2.629451
HUNK	6.251746	1.06E-24		ADAM11	4.950439	2.04E-86		PAGE1	3.985976	0.0487		ESPN	3.365651	7.90E-05		MLXIPL	2.629184
TEX14	6.245912	2.08E-21		PLEK	4.944466	1.34E-04		RNF207	3.985372	4.29E-09		ANO1	3.365131	0.038072		ZNF821	2.629107
COL25A1	6.244536	0.001818		TFP1	4.941178	8.27E-05		APOE	3.970339	1.00E-05		MAN1C1	3.362816	3.04E-14		TSPYL2	2.627114
MT1G	6.226996	0.021328		HIST2H3A	4.939201	2.65E-13		DIO1	3.968416	0.03979		ARHGAP44	3.361651	0.003236		ESR2	2.627109
MYH6	6.22548	0.020915		HIST2H3C	4.939201	2.65E-13		NAPSA	3.968241	1.50E-04		JAG1	3.361327	2.32E-39		COLGALT2	2.626707
C2orf27AF	6.223845	0.007278		ALOXE3	4.939132	9.06E-22		RP11-353N	3.968138	0.042671		ACTA2	3.35931	1.99E-27		MST1L	2.625484
ZBTB7C	6.213123	3.65E-05		TRIM58	4.937976	2.93E-05		ID2	3.967312	1.70E-95		GNAL	3.358753	1.73E-11		CTSZ	2.625423
PRLHR	6.20891	8.35E-04		SLCO2B1	4.937447	0.00488		SLC10A4	3.964471	7.70E-04		ITGAM	3.35798	0.001383		DNAAF3	2.623895
ATP4A	6.202181	0.002126		MYLPF	4.932112	6.25E-11		CELP	3.964447	0.001188		FAM182B	3.356889	3.99E-04		SPTBN5	2.621806
SP9	6.199083	4.19E-07		RP11-488L	4.928748	0.034097		TNNC2	3.962712	0.028075		HIF3A	3.356203	0.002067		VDR	2.620735
TG	6.195972	2.12E-04		STAR	4.927287	0.005757		LLNLR-271	3.962478	0.036042		MMP23B	3.356047	9.52E-05		ERN1	2.619685
GABRA4	6.19521	0.009295		ADPRH	4.92513	0.00359		SLC6A15	3.962271	0.013637		GUCY1A3	3.35521	2.14E-06		AMTN	2.618276
MFAP3L	6.188319	1.25E-31		AC026954.	4.924566	0.008103		BCL11B	3.961523	0.001186		EFCAB12	3.352633	3.66E-24		RAB9B	2.618228
CADM2	6.187736	0.003727		MLC1	4.922781	0.031944		RP11-266L	3.958819	1.30E-04		FRZB	3.348445	4.03E-08		MBLAC1	2.61748
DNAI1	6.186307	3.22E-04		P2RY1	4.922766	6.35E-25		GLDC	3.958408	2.47E-04		RPL9P29	3.346798	3.09E-05		CTHRC1	2.617038
FRG2EP	6.180689	0.006669		FOXA3	4.922631	2.38E-09		VWA3B	3.955324	0.011502		AC003002.	3.346785	4.45E-04		SYNE4	2.616275
VSTM2L	6.171099	4.65E-37		YPEL1	4.918287	1.62E-36		AC255361.	3.955239	1.15E-06		PPM1L	3.345448	3.00E-19		GTF2B	2.614476
ANKUB1	6.169882	2.16E-04		RP11-84C1	4.91694	0.01931		SAA2	3.954138	0.033601		RNF125	3.342884	6.15E-07		FAM201B	2.61151
ULK4P1	6.166386	4.09E-04		NOTO	4.91489	0.018895		HIPK4	3.952146	0.018264		PRKY	3.342696	0.024727		C1orf54	2.608469
CYP26C1	6.164943	0.00287		SLC34A2	4.914283	0.008818		FAM26F	3.948119	0.030137		DCST2	3.339348	9.66E-08		CTC-398G3	2.604604
PPP2R2C	6.163187	0.001969		FAM19A3	4.912518	0.002577		NKX2-3	3.947693	0.003952		AC064850.	3.337395	0.041321		PHOSPHO	2.603797
RPS27P25	6.162643	0.026054		ACTL8	4.909062	0.018983		HSPB9	3.937358	9.20E-06		RAET1G	3.336291	9.98E-07		PRRG2	2.603709
ACAN	6.160855	1.75E-04		TRIM54	4.904825	2.18E-09		EXOC3L2	3.93702	3.15E-06		RANBP3L	3.332819	0.011531		MRO	2.603699
NCF1C	6.154438	0.02755		DTX1	4.902421	0.02456		TMEM52	3.935694	1.25E-05		PIGZ	3.331712	3.93E-09		PIPOX	2.598121
TPO	6.151373	2.08E-04		FAIM	4.887724	1.26E-11		ST18	3.934343	0.0085		CCDC114	3.330951	0.007528		NUTM2D	2.59802
NES	6.137725	7.90E-07		AGT	4.879697	0.032131		CACNG4	3.933342	2.82E-18		PHYHIP	3.329859	0.002398		FAM229A	2.597487
CCDC154	6.121793	9.12E-07		GPRC5C	4.878649	1.41E-31		TNFAIP8L3	3.932528	1.36E-07		BAMBI	3.329565	1.22E-62		C1orf226	2.594224
IMPDH1P1	6.119254	0.010021		HAND2	4.877844	2.88E-12		FOXC1	3.931889	3.30E-106		HIST1H4H	3.327109	1.75E-14		EXOC3L1	2.591562
SYT3	6.119253	0.002961		LRMP	4.873009	0.003127		FITM1	3.93133	0.02449		PAPPA2	3.327069	0.03726		BMP4	2.590428
ATP12A	6.116421	0.00236		HCK	4.870615	0.037501		GGN	3.923058	6.11E-11		LINC00431	3.325748	8.69E-08		LMNTD2	2.590025
RARRES2P	6.11441	2.92E-04		MUC4	4.861786	0.007861		PPIAP3	3.919318	0.010499		CYP27A1	3.325288	0.026793		PCDHA3	2.589864
CLDN6	6.097661	2.66E-06		GPR150	4.847391	5.89E-17		GRIN2C	3.916603	3.41E-08		SLC37A1	3.319463	3.31E-06		ZC3H12D	2.589646
FAM198B	6.093862	0.004298		CTBP2P4	4.84411	0.019387		NPW	3.911984	5.20E-05		CD84	3.316856	0.013455		ANGPTL4	2.589386
DSC1	6.092961	0.001108		SALL1	4.843249	4.06E-50		C7orf57	3.911483	7.22E-04		STOX1	3.316597	7.88E-27		SLC7A7	2.589018
SLPI	6.089069	2.21E-05		COL10A1	4.842404	5.67E-08		DUX4L26	3.909761	0.031795		LMF1	3.316431	0.026459		NEU1	2.588037
KCNJ9	6.087005	0.033109		SEC1P	4.842256	0.018961		CCDC116	3.906233	0.003446		FCGRT	3.311908	3.59E-05		HHLA2	2.58781
PPP1R16B	6.085366	1.33E-04		PAG1	4.841642	2.10E-04		CATSPERG	3.904706	1.29E-18		RPL24P4	3.3078	0.016864		IQUB	2.586768
RP11-185N	6.081048	0.008677		MIP	4.84055	6.62E-08		WNK2	3.901352	6.69E-04		NKX2-1	3.307657	3.86E-09		PITPNC1	2.586278
TSPEAR	6.080551	0.003932		KIAA1210	4.84021	0.020157		TGFB3	3.899568	1.61E-11		SPOCK2	3.306814	0.001598		FUCA1	2.585403

CCNA1	5.97305	1.13E-20		TBX20	4.769133	0.0053		SDCBP2	3.852148	4.37E-21		MYO1D	3.268272	7.24E-13		RADIL	2.545498
AMER2	5.972506	2.19E-04		TIMM8AP	4.763805	0.023467		KLK4	3.851684	0.00582		CLDN5	3.267919	1.41E-05		RTN1	2.537621
ADCY10	5.968534	2.81E-04		CES4A	4.752958	3.74E-05		CTD-3088(	3.850992	6.88E-09		LRRC37A1	3.267527	0.00924		UST	2.537543
FAM90A1	5.967301	0.044916		OASL	4.752897	5.50E-114		CLEC18B	3.848301	9.76E-04		BCAS1	3.266563	2.02E-04		SCUBE3	2.535106
MMP28	5.962269	0.002228		PPIEL	4.752395	0.030179		SMIM10L2	3.84647	0.001666		FLRT1	3.266203	2.17E-06		TIGD4	2.534835
UNCX	5.961327	0.043981		LHFPL4	4.749609	0.026382		PRODH	3.844825	5.33E-04		RFPL2	3.264232	0.007089		TSPAN18	2.534089
P2RX2	5.959167	2.42E-04		ASPRV1	4.748761	2.12E-10		ST6GAL1	3.837321	5.99E-07		ADAMTS1	3.261004	7.50E-05		SPATA17	2.533148
TRIM63	5.958245	0.044593		ATP1B4	4.747947	0.018996		A1CF	3.836654	0.02527		SPDYE18	3.255356	0.021674		MAP1LC3E	2.532714
FEZF2	5.957331	0.044874		CEL	4.746702	1.00E-11		FOXD4L1	3.833797	3.57E-04		ZBED9	3.252524	5.46E-09		TMEM130	2.531706
GALR2	5.956527	7.34E-11		INSL3	4.744003	0.022445		MT3	3.83335	2.24E-04		GPR61	3.252465	5.82E-06		HIST1H2BI	2.529622
ASIC4	5.955414	5.84E-05		RP11-364E	4.742076	3.82E-05		CTC-435M	3.830867	0.026525		DFNB59	3.252311	3.06E-04		MATN1	2.528364
TAS1R1	5.955028	4.28E-04		DFFBP1	4.739119	0.010011		FOXP2	3.8308	0.005521		SLC6A13	3.251473	5.62E-04		SLC37A2	2.527786
CTC-512J1	5.953769	0.005444		PAPPA	4.737502	7.33E-04		COL6A6	3.822882	0.010079		CEACAM2	3.250692	3.46E-04		PCYOX1L	2.526419
MUC3A	5.952058	0.046702		CXCL14	4.736056	0.004864		ADGRG2	3.820546	1.69E-06		GDF9	3.247761	2.96E-09		EFCC1	2.525164
ANKRD35	5.951766	0.002917		UNC45B	4.734926	0.043523		SPANXN1	3.819472	0.011906		VASN	3.247477	2.94E-122		MAP2	2.524764
LRRN2	5.951093	6.97E-07		TUBA4B	4.731557	0.041733		SMAD9	3.81573	1.93E-30		SERINC5	3.245774	4.03E-137		MFSD2A	2.524277
NEURL3	5.931557	0.001229		SNRPN	4.731221	0.006149		RP11-540I	3.812917	3.37E-04		SIRT4	3.245234	4.49E-07		RHOH	2.524194
PDZRN3	5.924808	5.13E-04		MCC	4.729399	7.17E-19		LKAAEAR1	3.810283	2.65E-04		XXbac-B44	3.243842	0.012283		TTC21A	2.522557
ADAMTS1	5.919084	2.24E-15		IMPDH1P6	4.729055	0.007726		ENPEP	3.809955	0.030241		SPOCK3	3.242928	0.03971		TUB	2.522502
DPP4	5.918527	1.13E-31		CR1	4.72627	0.024822		NR4A2	3.809213	3.40E-18		EFNB2	3.242504	3.73E-56		NRN1L	2.522169
PLPPR5	5.914505	0.049784		MGP	4.724183	0.005043		SMPD3	3.807522	2.85E-40		TMEM45B	3.241188	1.38E-04		GBX2	2.520164
CHRM1	5.911075	0.020002		PKD1L3	4.720646	0.023388		MAP4K1	3.806072	2.35E-10		LRRC43	3.23722	0.04984		RASA4CP	2.52004
GFRA2	5.909378	0.020816		SERPINB5	4.716637	0.01091		EXO5	3.805876	0.023615		DDIT4L	3.236228	0.002472		RGS2	2.519652
BTBD7P1	5.909375	0.021087		DCDC1	4.711157	0.002441		GHR	3.804588	8.28E-05		GAS7	3.235344	0.003582		FANK1	2.519441
CYP21A2	5.90617	0.010759		SLC26A8	4.710472	8.98E-05		KLHL24	3.803933	6.81E-26		COLEC12	3.234914	5.60E-18		TRAF3IP3	2.517954
AP3B2	5.900982	5.91E-70		STRCP1	4.707045	0.006277		LRRC19	3.802629	0.001587		GRB7	3.234063	5.24E-04		EFCAB3	2.517397
DLL1	5.892792	1.85E-32		C11orf96	4.700878	4.44E-17		PLA2G10	3.802023	0.017734		FAM43A	3.233745	1.45E-31		RANP4	2.516028
IGF2	5.887243	1.87E-103		ACHE	4.695658	2.26E-15		HIST1H2AI	3.793848	7.30E-05		GAL3ST4	3.23371	1.40E-04		TUBB2A	2.515914
CYP39A1	5.885906	2.99E-04		DPCR1	4.695139	0.002861		SHC3	3.789012	0.00721		ANKRD24	3.229938	9.08E-05		NCF1	2.513107
BTN1A1	5.881993	9.38E-04		DCHS2	4.690174	8.39E-07		SLC34A3	3.785451	0.032169		TNFRSF19	3.22832	5.60E-06		NUTM2A	2.51181
CLVS2	5.87917	0.004151		SGCG	4.690141	1.92E-05		AUTS2	3.784465	3.38E-18		CHRNA7	3.226978	1.33E-07		KRT18P41	2.510335
KRT18P55	5.877147	2.68E-04		HLA-DOA	4.685705	0.002477		FAM86B2	3.782466	5.09E-11		LDLRAD2	3.226771	0.007791		VANGL1	2.509039
FOXD4	5.876157	0.021535		AKAIN1	4.678941	0.002164		ZNF843	3.781942	2.07E-09		ACSL6	3.225123	5.65E-04		RARRES3	2.507906
KIAA1211l	5.875852	0.003718		PLIN4	4.675633	2.49E-12		AC000095	3.78041	0.03142		VSIG10L	3.224134	3.41E-13		PTHLH	2.50784
TOX3	5.873836	0.003062		KSR2	4.675405	0.00858		CELF5	3.780381	0.004417		ARL14	3.223035	1.53E-05		GRB10	2.505959
PGA4	5.868302	0.008703		SERPINI1	4.674738	1.58E-29		MYBPC3	3.775899	0.035806		PLEKHG1	3.222872	7.45E-19		TMEM200	2.504913
NLRP9	5.86742	0.018648		PIK3R5	4.673509	0.023456		AC010980	3.774196	3.56E-05		CD247	3.221558	4.79E-05		ACOXL	2.503669
ATP1A4	5.866834	0.001526		CNTN4	4.672957	0.043085		TNFAIP6	3.773568	0.049916		GPR132	3.219065	0.006515		RDH10	2.503379
PDE3B	5.862047	1.95E-08		RND1	4.672621	3.35E-31		EPHB6	3.772974	3.63E-05		MMP9	3.215492	5.04E-07		LGALS9	2.501963
SORCS1	5.860989	0.006626		CACNA2D2	4.66436	1.35E-14		HMX3	3.771582	1.90E-04		DRAXIN	3.214708	1.97E-05		HPCAL4	2.501094
AVPR1A	5.859495	0.002106		VRTN	4.663244	9.90E-04		HEY1	3.768352	1.32E-14		SOD3	3.214119	1.95E-07		FAM122C	2.500242